STELLINGEN

behorende bij het proefschrift:

'Wind wave propagation in tidal seas'

Hendrik Lieuwe Tolman
Januari 1990

1 Getijden en stormvloeden in randzeeën moeten voor de voortplanting van windgolven als een instationair medium worden beschouwd.

2 In instationaire en inhomogene stromingsvelden kan de grootte van effecten van golf-stromingsinteracties op golven niet bepaald worden aan de hand van de lokale diepte en stroomsnelheid. Dit maakt het in rekening brengen van de interacties over het gehele domein noodzakelijk.

3 Het gebruik van één wrijvingsfactor voor de beschrijving van de bodemgrenslaag bij aanwezigheid van golven en een gemiddelde stroming is misleidend wanneer de effecten van een gemiddelde stroming op de lokale golfenergie-dissipatie beschouwd worden.

4 Bij het analyseren van effecten van een gemiddelde stroming op golfhoogtes in ondiep water is het te beperkt om alleen de effecten van de stroming op de lokale golf-energiedissipatie t.g.v. bodemwrijving te beschouwen.

Hasselmann et al., 1973
Weber, 1989

5 In de onwikkeling van (derde generatie) golfmodellen rechtvaardigde de beperkte kennis van de golf-fysica het gebruik van eenvoudige en onnauwkeurige numerieke (voortplantings-) schema's. In studies waar kwalitatief goede windvelden beschikbaar zijn, dreigen door het voortschrijdend begrip van de fysica deze numerieke fouten bepalend te worden voor de voorspellingskracht van de modellen.

6 Vanuit numeriek oogpunt is bij golfvoorspelling in vele practische situaties de grootste winst in modelnauwkeurigheid te behalen uit een selectieve verfijning van het ruimtelijk rekenrooster.

7 Aangezien universiteiten in Nederland zelf geen invloed hebben op het beleid van toelating van studenten, maar wel gefinancierd worden naar studierendement, is het voor universiteiten moeilijk om zelf aan kwaliteitsbeheersing van het onderwijs te doen.

8 Menige stelling bij proefschriften aan de TU Delft verwoordt een persoonlijke mening i.p.v. een wetenschappelijk verdedigbaar standpunt, waardoor niet voldaan wordt aan het promotiereglement. De TU Delft zou zich daarom moeten herbezinnen op dit reglement of de naleving ervan.

Promotiereglement
TU Delft art. 5.2

9 Een (commercieel) bedrijf met een uitgebreide en ondoorzichtige bestuurs- en beheersstructuur zoals die van de TU Delft is geen lang leven beschoren.

10 Het gebruik van computerprogrammatuur voor het rekenen aan complexe problemen leidt vaak tot het uitschakelen van het gezonde verstand.

11 De gehele mensheid is voortdurend bezig met de bestrijding van de gevolgen van de vooruitgang van de westerse wereld.

Wind wave propagation in tidal seas

Wind wave propagation in tidal seas

Proefschrift
ter verkrijging van de graad van doctor aan
de Technische Universiteit Delft,
op gezag van de Rector Magnificus, prof. drs. P.A. Schenck,
in het openbaar te verdedigen ten overstaan van een
Commissie aangewezen door het College van Dekanen
op donderdag 15 februari 1990 te 16.00 uur

door

Hendrik Lieuwe Tolman
geboren 16 januari 1961 te Leeuwarden
civiel ingenieur

1990

Dit proefschrift is goedgekeurd door de promotor
prof. dr. ir. J.A. Battjes

Dr. ir. L.H. Holthuijsen heeft als toegevoegd promotor
in hoge mate bijgedragen aan de totstandkoming van het
proefschrift

Vergissen is menselijk, maar om de boel echt in het honderd te laten lopen heb je een computer nodig.

(A. Bloch, Murphy's Law blz. 63)

SAMENVATTING

In deze studie zijn de effecten van getijden en stormvloeden op windgolven in randzeeën onderzocht. Dit onderwerp is bestudeerd met analytische en numerieke beschouwingen voor een aantal academische gevallen en met zogenaamde "hindcasts" (d.w.z. voorspellingen achteraf) voor drie stormen op de Noordzee. De resultaten van deze hindcasts zijn bovendien vergeleken met waargenomen golfgegevens. Voor deze studie is een derde generatie golfmodel ontwikkeld (WAVEWATCH), waarin alle relevante effecten van getijden en stormvloeden op windgolven in rekening worden gebracht.

De resultaten van de studie laten zien dat getijden en stormvloeden als een instationair medium moeten worden beschouwd voor de voortplanting van windgolven in randzeeën. Voor zulke omstandigheden kan de gebruikelijke quasi-stationaire benadering van golf-stromingsinteracties niet gebruikt worden. Voorts blijken de interacties in hoofdzaak door stromingen veroorzaakt te worden; effecten van veranderingen van de gemiddelde waterspiegel leveren alleen een significante bijdrage aan de interacties bij het optreden van stormvloeden.

De hindcasts voor de Noordzee laten een relatief kleine getij- en stormvloedsmodulatie van gemiddelde golfparameters zoals de significante golfhoogte en de gemiddelde golf periode zien (5% tot 10%). De (relatieve) grootte van deze modulaties neemt af bij toenemende windkracht en golfhoogte. Modulaties van de spectrale dichtheden van het golfspectrum kunnen van de orde van grootte 50% zijn. Voor de stormen die hier beschouwd zijn, zijn waargenomen modulaties van gemiddelde golfparameters voor het grootste deel veroorzaakt door variaties van de windsnelheid.

ABSTRACT

In the present study the effects of tides and storm surges on wind waves in shelf seas are assessed. The subject is studied using analytical and numerical approaches for several academic cases and by hindcasting three storm cases on the North Sea. The results of the hindcast are furthermore compared with observed wave data. For this study a third generation wave model (WAVEWATCH) has been developed, which incorporates all relevant effects of tides and surges on wind waves.

It is shown that tides and storm surges should be considered as an instationary medium for wind wave propagation in shelf seas. For such conditions the commonly applied quasi-stationary approximation to wave-current interactions cannot be used. Furthermore it is shown that interactions are predominantly caused by currents; effects of mean surface level variations contribute significantly in storm surge conditions only.

The hindcasts for the North Sea show relatively small tide and surge induced modulations of mean wave parameters such as the significant wave height or the mean wave period (typically 5% to 10%). The magnitude of these modulations decreases with increasing severity of wind and wave conditions. Modulations of the spectral density of the wave spectrum can be of the order of 50%. Observed modulations of mean wave parameters in the storm cases considered here appear to be for the most part wind-induced.

CONTENTS

APPENDICES:

1 INTRODUCTION

1.1 BACKGROUND

Waves and currents in oceans and seas have been the subject of many studies, in particular in the second half of this century. In the last few decades many operational models were developed for the separate prediction or hindcasting of both wind waves and currents, ignoring interactions between the two types of motion. This separate treatment of waves and currents contrasts with theoretical knowledge on wave-current interactions and with the simultaneous occurrence of waves and current in storm surges in shelf seas. The close relation between storm surges and extreme wave conditions is known to most people living in low countries, whereas in more detail the effects of currents on waves have been recognized by sailors for centuries (e.g. the existence of tidal races, i.e. current-induced severe wave breaking, near inlets and headlands).

Wave-current interactions, in particular the influences of currents on waves, have been the subject of several theoretical investigations in the last decades. After some pioneering papers by Unna (1941, 1942, 1947) and Barber (1949), the theory for wave-current interaction was developed by Longuet-Higgins and Stewart (1960, 1961, 1962), who introduced the concept of radiation stress, and by Whitham (1965) and Bretherthon and Garrett (1968), who introduced the concept of action conservation. The theory is now well established and treated in numerous textbooks, review papers and reports (e.g. Whitham, 1974; Peregrine, 1976; Phillips, 1977; Mei, 1983; Peregrine and Jonsson, 1983). Recent research has mainly been concentrated on the numerical modelling of waves on currents and on the description of the bottom boundary layer for a combined wave-current system.

Wave-current interactions are for a major part governed by depth and current induced changes of wavenumber and wave frequency. Such changes depend on the character of the variations of depth and current:

variations of depth and current in space result in changes of the wavenumber, whereas variation in time result in changes of the absolute frequency (i.e. the frequency as observed from fixed locations) (e.g. Mei, 1983, page 96). The literature on wave-current interactions is mostly concerned with small scale areas for which the depth and current field are assumed to be quasi-stationary with respect to the propagation time of wind waves. In such an approach the absolute frequency is assumed to remain constant during propagation. To the knowledge of the author, only a few applications for large scale areas and/or instationary depths and currents are available. Interactions in such cases are (properly) treated by Unna (1941), Longuet-Higgins and Stewart (1960) and Barber (1949). In several recent papers, however, effects of instationarity are not accounted for, but a quasi-stationary approach is used even for explicitly instationary currents (e.g. Chen and Wang, 1983).

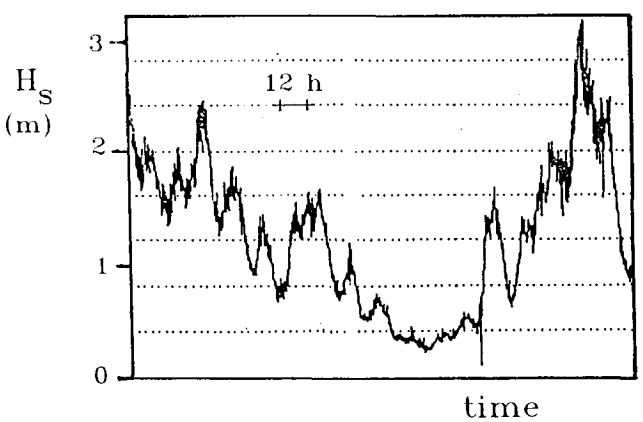

Fig. 1 Measured significant wave heights H_s at the southern North Sea, platform Euro-0, 50 km west of the entrance to the port of Rotterdam.

The fact that the effects of wave-current interactions are potentially important in large scale areas is illustrated here with measurements acquired in the southern North Sea, approximately 50 km west of the entrance to the port of Rotterdam (figure 1). Currents and mean water level variations in this area are dominated by a semi-diurnal tide.

The data given in figure 1, which are not unusual for the location considered, show wave height modulations of up to 50%, with a period of approximately 12 h, suggesting a tidal influence. Since the tidal range in the measurement area is locally only about 5%, current variations rather than depth variations are expected to be responsible for the observed wave height modulations.

1.2 AIM AND SCOPE OF THE PRESENT STUDY

Considering the above, the subject of wave-current interactions for large scale, instationary depths and currents seems to be poorly investigated. Tides and surges on shelf seas represent such instationary depth and current conditions, because the typical travel time of wind waves through shelf seas (order of magnitude of a few days) is much larger than the time scale of current and depth variations (typically 12 h). Thus this study deals with the interactions between effects of tides and storm surges and wind waves in shelf seas (away from the coast). Figure 1 suggests that effects of currents on waves can be significant, whereas studies of wave-driven currents suggest that significant effects of waves on currents mainly occur in the surfzone. Therefore only effects of tides and surges on wind waves (and not vice versa) will be considered here.

From a theoretical point of view wave-tide interactions in shelf seas are interesting due to the effects of instationarity of depth and current. From a practical point of view wave-tide interactions in shelf seas are interesting considering the magnitude of wave-tide interactions (see figure 1). Therefore this study has two main objectives :

- To establish the nature of the effects of depth and current instationarity on wave-current interactions, in particular for waves on tides in shelf seas.

- To assess the magnitude of the effects of wave-tide interactions in natural shelf sea conditions.

1.3 APPROACH IN THE PRESENT STUDY

In general research of wave-current interactions can be performed using analytical or numerical approaches, physical models and observations in nature. However, physical scale models cannot be used to investigate wind waves on tides and storm surges due to the large differences in scales considered (e.g. 10 s and 100 m for a typical wind wave versus 12 h and from 100 km to 1000 km for a typical tide). Observations in nature are also not sufficient, since tidal effects on waves are difficult to isolate in measured data, as will be shown in chapter 5. Such observations can at best be used in combination with other approaches. Consequently the present investigation of the effects of tides and storm surges on wind waves is primarily performed using analytical and numerical approaches, but a comparison with field observations is included as well.

Analytical approaches can be used only for highly idealized cases. For this study academic cases can be useful to help understand the effects of depth and current instationarity. For this purpose one-dimensional waves on a one-dimensional tide in a sea with a constant bottom level are considered in chapter 4.

With a numerical wave model (which is discussed below) propagation of irregular waves on a two-dimensional tide in an academic shelf sea is considered (chapter 4). In geometry and latitude this sea is somewhat similar the North Sea. This case serves the same purpose as the above one-dimensional academic case.

The numerical model is used in chapter 5 to hindcast historic storms in the North Sea. By using several versions of the wave model the following influences of tides (and storm surges) on wind waves have been isolated: (a) the total wave-tide interactions; (b) depth and current instationarity; (c) depth and current refraction (d) currents and (e) (tidal) surface level variations. For two of these storms the hindcast waves are compared with measured data (chapter 5).

The numerical wave model was developed as part of this study (see chapter 3) for the calculation of wind wave propagation, generation and dissipation in an area where depth and current vary in space and

time. The model incorporates state-of-the-art formulations for the wave generation, dissipation and wave-wave interactions as well as all major effects of temporal and spatial variations in depth and current on wind waves. The currents and water levels used in the numerical calculations are calculated with a previously available numerical tide and storm surge model (DUCHESS), which solves the two-dimensional shallow water equations (e.g. Wang, 1989). This model is driven by both astronomical boundary conditions and by wind forcing.

The layout of this thesis is as follows. The governing equations are discussed in chapter 2; the numerical model is presented and discussed in chapter 3; academic cases are considered in chapter 4, using both analytical and numerical approaches; the North Sea hindcasts are presented and discussed in chapter 5. Finally the overall results are discussed in chapter 6 and conclusions and recommendations are presented in chapter 7.

2 GOVERNING EQUATIONS

2.1 INTRODUCTION

Water motion in shelf seas such as the North Sea is here divided in long wave motion, short wave motion and turbulence, where the long wave motion incorporates the largest time scales including the mean circulation and turbulence incorporates the smallest time scales. For the three types of motion different (analytical) models are used.

The short wave model describes wind waves, which are the main subject of this study. The description of wind waves will be discussed in the following sections.

The long wave model describes tides and storm surges. In general the water depth is several orders of magnitude smaller than the horizontal scale of the long waves and, in particular in the southern North Sea, tidal current velocities show only small variations over the vertical. It is therefore sufficient to describe the long wave motion using a depth-averaged horizontal current velocity $\underline{U}$ and the depth d, which is determined by the (stationary) bottom level and the (instationary) surface level. Both the velocity $\underline{U}$ and the depth d represent average values over time scales which are small compared to the long wave time scale, but large compared to the short wave time scale. This study deals with influences of tides and storm surges on wind waves, and not vice versa, for which reason the depth d and current $\underline{U}$ are treated as known parameters.

Turbulence has a time scale smaller than that of the short wave motion. For the short wave motion, turbulence is only of significance in the bottom boundary layer where wave energy is dissipated. Other aspects of turbulence are beyond the scope of this study.

For short waves the time and space scales of the local description of wave motion (typically of the order of 10 s and 100 m) are much smaller than the time and space scales of propagation and generation. The scales of propagation are determined by (a) the size of the sea

basin considered (e.g. 100 km to 1000 km) and (b) the travel time of short waves over the entire basin (e.g. 10 h to 100 h). The scales of generation are mainly determined by the scales of the wind field (often comparable to the scales for wave propagation).

For long waves the time and space scales are typically 10 h and 1000 km (tidal period and wave length).

An intercomparison of the space and time scales of short and long waves indicates that the long wave motion can be considered as *(quasi-) stationary* and *(quasi-) homogeneous* in the *local* description of short waves, but that it is essentially *instationary* and *inhomogeneous* on the scales of short wave *propagation* and *generation*.

In the following the short waves (i.e. wind waves) are denoted simply as waves, whereas the long waves (i.e. tides and storm surges) are denoted as tides and/or (depths and) currents.

2.2 DESCRIPTION OF WIND WAVES

2.2.1 Deterministic description of monochromatic waves

In the uniform-wave theory for periodic surface gravity waves without currents (e.g. LeBlond and Mysak, 1978; Phillips, 1977; Whitham, 1974), a monochromatic unidirectional harmonic wave is described with an amplitude a, wavenumber k and (intrinsic) frequency σ. The phase parameters k and σ are interrelated in the dispersion relation (surface tension neglected)

$$\sigma^2 = gk \tanh kd \qquad (2\text{-}1)$$

where g is the acceleration of gravity. The phase velocity c of the waves, i.e. the propagation velocity of the wave crests, is given by :

$$c = \frac{\sigma}{k} \qquad (2\text{-}2)$$

The wave energy travels with the group velocity c_g:

$$c_g = n\,c \qquad (2\text{-}3)$$

$$n = \frac{1}{2} + \frac{kd}{\sinh 2kd} \qquad (2\text{-}4)$$

The group velocity vector $\underline{c}_g$ has an absolute value c_g and a direction θ, which is perpendicular to the wave crest. The average wave energy E (per unit horizontal area) is given as :

$$E = \tfrac{1}{2}\rho g a^2 \qquad (2\text{-}5)$$

where ρ is the mass density of water.

When a situation with a mean current $\underline{U}$ is considered, a distinction can be made between a frame of reference which is fixed to the bottom (denoted as the fixed frame) and a frame of reference which moves with the local mean current velocity $\underline{U}$ (i.e. ignoring the wave orbital velocity, denoted as the moving frame). If the length and time scales of current (and depth) variations are large compared to the length and time scales of a single wave, the current and depth are (quasi-) stationary and (quasi-) homogeneous with respect to the local description of the waves. Consequently the uniform-wave theory is locally applicable in the moving frame. The above defined intrinsic frequency σ is then observed in the moving frame (in situations with currents σ is also called the relative frequency). The frequency as observed in the fixed frame is the absolute frequency ω, which is related to the relative frequency σ and the wavenumber k by the following Doppler-type equation :

$$\omega = \sigma + \underline{k}\cdot\underline{U} \qquad (2\text{-}6)$$

where $\underline{k}$ is the wavenumber vector with absolute value k and direction θ. If the relative frequency σ or the wavenumber k and the direction θ are known, the absolute frequency ω is uniquely determined by equations (2-1) and (2-6). If, however, the absolute frequency ω and direction θ are known, several solutions for k (and σ) are available as discussed by Peregrine (1976) (see figure 2, taken from Peregrine). Point E in figure 2 represents a situation without currents where $\omega = \sigma$, so that only equation (2-1) has to be solved. Point A represents a case with a following current and point B represents a case with an opposing current. The solutions at points C and D have no

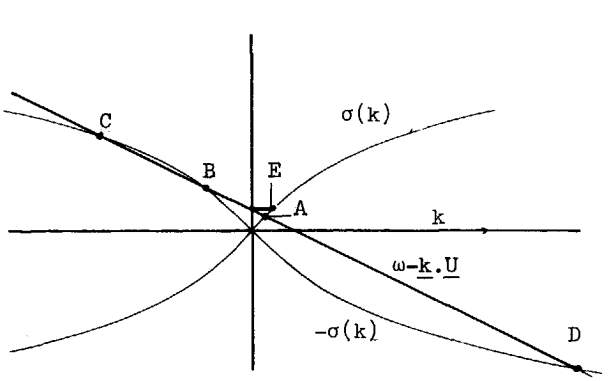

Fig. 2 Multiple solutions for dispersion relation (2-1) and Doppler equation (2-6) for giver absolute frequencies ω and directions θ (Peregrine, 1976).

significance for wind waves on shelf seas (see Peregrine, 1976). For some (opposing) current $\underline{U}$ and direction θ the solutions at points B and C will coincide. In such a case the energy propagation velocity c_g equals the component of the current velocity in the propagation direction of the waves, so that the wave energy cannot propagate against the current (stopping velocity, wave blocking). This obviously also occurs for stronger opposing currents, for which no solution to equations (2-1) and (2-6) is available.

2.2.2 Spectral description

At the scale of a few hundred wave periods the (wind) wave surface elevation η relative to the mean water level is assumed to be a Gaussian stationary and homogeneous zero-mean random process. Its statistics can be described with the three-dimensional covariance function C :

$$C(\underline{r},t_1) = < \eta(\underline{x},t)\ \eta(\underline{x}+\underline{r},t+t_1) > \qquad (2\text{-}7)$$

where $\underline{r}$ is the displacement vector, t_1 is the time lag, and $< >$ denotes ensemble average. The three-dimensional variance density spectrum G is defined as the Fourier transform of this covariance function :

$$G(\underline{k},\omega) = \iiint_{-\infty}^{+\infty} C(\underline{r},t_1)\, e^{-i(\underline{k}\cdot\underline{r}+\omega t)}\, d\underline{r}\, dt \qquad (2\text{-}8)$$

The variance density spectrum is closely related to the energy density spectrum, the difference being a constant factor ρg.

In a first order approximation the spectral components satisfy the linear theory for uniform surface gravity waves. In that case a one-to-one relationship exists between the wavenumber k and frequency ω so that the spectrum (2-8) essentially becomes two-dimensional. One is free to choose the two independent spectral variables. Commonly used are the wavenumber vector, the wavenumber and the direction or the wavenumber and the (relative or absolute) frequency and the direction ($F(\underline{k})$, $F(k,\theta)$, $F(\omega,\theta)$ or $F(\sigma,\theta)$ respectively). In this thesis the following two-dimensional variance density spectrum will mainly be used :

$$F(\omega,\theta) \quad , \quad 0 < \omega < \infty \quad , \quad 0 < \theta < 2\pi \qquad (2\text{-}9)$$

where

$$\mathrm{var}(\eta) = \int_0^{\infty}\int_0^{2\pi} F(\omega,\theta)\, d\omega\, d\theta \qquad (2\text{-}10)$$

Note that on the larger time and space scales of wave propagation, the spectrum also becomes a function of location $\underline{x}$ and time t, so that (2-9) essentially becomes five-dimensional (i.e. $F(\omega,\theta;\underline{x},t)$).

2.3 PROPAGATION

2.3.1 Introduction

If waves propagate over slowly varying depths and currents, the uniform-wave theory remains (locally) applicable, as indicated in section 2.2.1. Changes of the wavenumber k, frequencies σ and ω and direction θ as occur during propagation over instationary and inhomogeneous depths and currents are determined from the kinematics of wave trains. The change of amplitude during propagation can be

determined using energy or action conservation equations, ignoring generation and dissipation of wave energy for the moment.

2.3.2 Kinematics

As indicated in section 2.2.1 basic properties of a harmonic wave or of a component of an irregular wave field travel with the propagation velocity $\underline{c}_g$ of the energy of the waves (equation (2-3)). In cases with currents, the propagation velocity of the wave energy becomes :

$$\frac{d\underline{x}}{dt} = \underline{c}_g + \underline{U} \tag{2-11}$$

The rates of change of absolute frequency ω, wavenumber k, relative frequency σ and direction θ while moving with this velocity $\underline{c}_g+\underline{U}$, denoted as $d\omega/dt$, dk/dt, $d\sigma/dt$ and $d\theta/dt$ respectively, can be determined by differentiating equations (2-1) and (2-6) and using the following kinematic consistency relation (e.g. Whitham, 1974, his equation 1.31; Phillips, 1977, his equation 2.6.2), which is a conservation equation for the number density of the waves (∇_x is the differential operator in the $\underline{x}$ space) :

$$\frac{\partial \underline{k}}{\partial t} + \nabla_x \omega = 0 \tag{2-12}$$

The equations for these rates of change are (e.g. Christoffersen, 1982; Mei, 1983, page 96) :

$$\frac{d\omega}{dt} = \frac{\partial \sigma}{\partial d}\frac{\partial d}{\partial t} + \underline{k}\cdot\frac{\partial \underline{U}}{\partial t} \tag{2-13}$$

$$\frac{dk}{dt} = -\frac{\partial \sigma}{\partial d}\frac{\partial d}{\partial s} - \underline{k}\cdot\frac{\partial \underline{U}}{\partial s} \tag{2-14}$$

$$\frac{d\sigma}{dt} = \frac{\partial \sigma}{\partial d}\left[\frac{\partial d}{\partial t} + \underline{U}\cdot\nabla_x d\right] - c_g \underline{k}\cdot\frac{\partial \underline{U}}{\partial s} \tag{2-15}$$

$$\frac{d\theta}{dt} = -\frac{1}{k}\left[\frac{\partial \sigma}{\partial d}\frac{\partial d}{\partial m} + \underline{k}\cdot\frac{\partial \underline{U}}{\partial m}\right] \tag{2-16}$$

in which s is the space coordinate in the direction θ and m is a coordinate perpendicular to s. The operator d/dt is defined as

$$\frac{d}{dt} = \frac{\partial}{\partial t} + (\underline{c}_g+\underline{U})\cdot\nabla_x \tag{2-17}$$

Note that since equations (2-1) and (2-6) provide a local relation between the wavenumber and the frequencies, only one of the equations (2-13) through (2-15) has to be integrated to obtain solutions for ω, σ and k.

2.3.3 Dynamics

In cases without currents the change of wave height during propagation is determined using an energy conservation equation (Whitham, 1974; Phillips, 1977; Mei, 1983). A spectral form of such an energy balance equation was first used by Gelci et al. (1956), and has been used in many wave models since then (e.g. SWAMP group, 1985). For energy or variance spectra with arbitrary independent spectral variables the conservation equation can be written as :

$$\frac{\partial F(\underline{\iota},\underline{x},t)}{\partial t} + \nabla_x \cdot \left[\underline{c}_g F(\underline{\iota},\underline{x},t)\right] + \nabla_{\iota} \cdot \left[\underline{c}_{\iota} F(\underline{\iota},\underline{x},t)\right] = 0 \qquad (2\text{-}18)$$

where $F(\underline{\iota},\underline{x},t)$ is the essentially five-dimensional variance density spectrum, $\underline{\iota}$ are the independent spectral variables (e.g. $\underline{\iota} = \underline{k}$ or $\underline{\iota} = (\omega,\theta)$), ∇_{ι} is the two-dimensional differential operator in the $\underline{\iota}$ space and $\underline{c}_{\iota}$ is the two-dimensional propagation velocity in the $\underline{\iota}$ space, given by the equations (2-13) through (2-16). The first term in equation (2-18) describes the local rate of change of the variance density. The second term describes propagation in the $\underline{x}$ space. The third term describes the redistribution of energy density over the spectrum. This redistribution corresponds to the change of phase parameters (ω, σ, k) and direction (θ) of monochromatic, unidirectional waves.

In cases with nonuniform currents, the wave energy is not conserved, since the mean horizontal momentum transport of the waves (i.e. the radiation stress) causes an exchange of energy with the mean current (Longuet-Higgins and Stewart, 1961, 1962). Unlike the total wave energy E, the total action $A = E/\sigma$ is conserved during propagation (e.g. Whitham, 1965; Bretherthon and Garrett, 1968). The corresponding action conservation equation for irregular waves is given as (e.g. Hasselmann et al., 1973, page 72) :

$$\frac{\partial N(\underline{k},\underline{x},t)}{\partial t} + \nabla_x \cdot \left[(\underline{c}_g+\underline{U})\ N(\underline{k},\underline{x},t)\right] + \nabla_k \cdot \left[\underline{c}_k N(\underline{k},\underline{x},t)\right] = 0 \qquad (2\text{-}19)$$

where $N(\underline{k},\underline{x},t)$ is the action density defined as $F(\underline{k},\underline{x},t)/\sigma$. This equation has a similar structure as equation (2-18); the separate terms describe the local rate of change of the action density, the propagation in the $\underline{x}$ space and the redistribution of action density over the spectrum.

2.4 GENERATION AND DISSIPATION

2.4.1 Introduction

In a conventional approach without currents, the generation and dissipation of (spectral) wave energy density are represented as source terms S at the right hand side of the spectral energy balance equation (2-18) :

$$\frac{\partial F(\underline{k},\underline{x},t)}{\partial t} + \nabla_x \cdot \left[\underline{c}_g F(\underline{k},\underline{x},t)\right] + \nabla_k \cdot \left[\underline{c}_k F(\underline{k},\underline{x},t)\right] = S(\underline{k};\underline{x},t) \qquad (2\text{-}20)$$

For brevity of notation the dependence F and S on $\underline{x}$ and t is omitted in equations in the following. A review of source terms is given by e.g. Hasselmann (1968), Phillips (1977), LeBlond and Mysak (1978) and Sobey (1986). The source term $S(\underline{k})$ is commonly divided in three separate terms, i.e. the wind input $S_{in}(\underline{k})$, the nonlinear interactions $S_{nl}(\underline{k})$ and the dissipation $S_{ds}(\underline{k})$:

$$S(\underline{k}) = S_{in}(\underline{k}) + S_{nl}(\underline{k}) + S_{ds}(\underline{k}) \qquad (2\text{-}21)$$

The terms will be discussed separately in the following, first for cases without currents.

Compared to propagation, for which reliable theoretical expressions can be derived, the processes of generation and dissipation are poorly understood. The presently most sound approaches (physical and numerical) for source terms are gathered in the WAM model (WAMDI group, 1988). All formulations for source terms used in this study are taken directly from the WAM model, except for a part of the dissipation term.

2.4.2 Wind input

After a pioneering paper by Jeffreys (1925), extensive research on wave growth mechanisms started with theoretical papers of Phillips (1957) and Miles (1957). A distinction is commonly made between linear growth ($S_{in,l}$; Phillips, 1957), due to resonant interaction between air turbulence and waves, and exponential growth ($S_{in,e}$; Miles 1957, 1959 a and b, 1960, 1962), due to wave-wind interactions (feed-back mechanism) :

$$S_{in} = S_{in,l} + S_{in,e} \tag{2-22}$$

Phillips (1966) gives a single expression for the wind input which incorporates both linear and exponential growth. The linear growth term is only relevant in the first stage of the wave growth. If some wave energy is present, as in nearly all practical situations, the exponential growth soon becomes dominant. In the WAM model the linear growth term is therefore neglected altogether.

An expression for the exponential growth term based on theory and on observations is given by Snyder et al. (1981). Rescaled with the wind friction velocity U^* (Charnock, 1955; Komen et al., 1984) their expression becomes (Komen et al., 1984, WAMDI group, 1988) :

$$S_{in,e}(\underline{k}) = \max\left[0, \left[0.25\ \rho_r \left[\frac{28\ U^*}{\sigma/k}\cos(\theta-\theta_w) - 1\right]\right]\right] \sigma\ F(\underline{k}) \tag{2-23}$$

with

$$U^* = U_{10}\left[(0.8 + 0.065\ U_{10})10^{-3}\right]^{\frac{1}{2}} \tag{2-24}$$

where ρ_r is the relative density, i.e. density of air divided by density of water ρ_a/ρ_w, θ_w is the wind direction and U_{10} is the wind speed in m/s at ten meters above the mean sea surface.

2.4.3 Nonlinear interactions

In the process of wave generation, several nonlinear effects are of importance. In a review paper, Hasselmann (1968) distinguishes three

types of nonlinear interactions, i.e. resonant wave-wave interactions, nonlinear corrections to the exponential growth term $S_{in,e}$ and nonlinear wave-wind interactions (which also can be interpreted as a correction to $S_{in,e}$). In particular the nonlinear wave-wave interactions are important since they result in a universal spectral shape and since they are material for the growth of the energy of spectral components with frequencies lower than the spectral peak frequency (e.g. Hasselmann et al., 1973).

The existence of nonlinear wave-wave interactions was first recognized by Hasselmann (1960) and Phillips (1960). Such wave-wave interactions describe the resonant exchange of energy between wave components (e.g. Hasselmann 1961, 1962, 1963a and b; Phillips 1966, 1977). For deep water at least four wave components are needed to satisfy resonance conditions. These resonance conditions are given as:

$$\left.\begin{aligned} \underline{k}_1 + \underline{k}_2 - \underline{k}_3 &= \underline{k}_4 \\ \sigma_1 + \sigma_2 - \sigma_3 &= \sigma_4 \end{aligned}\right\} \qquad (2\text{-}25)$$

where the components 1, 2 and 3 exchange energy with component 4. Expressions for the exchange of energy due to this mechanism will not be given here (see e.g. Hasselmann, 1968; Sell and Hasselmann, 1972; WAMDI group, 1988).

2.4.4 Dissipation

In the source term for wave energy dissipation three different mechanisms can be distinguished, i.e. whitecapping, ($S_{ds,w}$), surf breaking ($S_{ds,s}$) and energy dissipation due to wave-bottom interactions ($S_{ds,b}$). Surf breaking only occurs in extremely shallow water where water depth and wave height are of the same order of magnitude (e.g. Battjes and Janssen, 1978). For shelf seas as considered in this study, this mechanism is not relevant. Thus the dissipation source term becomes (away from the coast) :

$$S_{ds} = S_{ds,w} + S_{ds,b} \qquad (2\text{-}26)$$

Whitecapping :

Expressions for the whitecapping source term ($S_{ds,w}$) have been proposed by Hasselmann (1974) and by Komen et al. (1984), both for deep water. For application in intermediate water depths, the expression of Komen et al. was reformulated by the WAMDI group (1988), resulting in :

$$S_{ds,w}(\underline{\iota}) = - 2.36\ 10^{-5}\ \hat{\sigma}\ \frac{k}{\hat{k}} \left[\frac{\alpha}{\alpha_{PM}}\right]^2 F(\underline{\iota}) \qquad (2\text{-}27)$$

with

$$\alpha = \hat{k}^2 \iint F(\underline{\iota})\ d\underline{\iota} \qquad (2\text{-}28)$$

$$\hat{\sigma} = \left[\ \overline{1/\sigma}\ \right]^{-1} \qquad (2\text{-}29)$$

$$\hat{k} = \left[\ \overline{1/\sqrt{k}}\ \right]^{-2} \qquad (2\text{-}30)$$

where α is an average steepness parameter, α_{PM} is the value of α for a Pierson-Moskowitz spectrum ($\alpha_{PM} = 3.02\ 10^{-3}$) and $\hat{\sigma}$ and $\hat{k}$ are an average relative frequency and wavenumber respectively. The overbar notation denotes straightforward averaging over the spectrum, e.g.

$$\overline{k} = \iint k\ F(\underline{\iota})\ d\underline{\iota}\ \left[\ \iint F(\underline{\iota})\ d\underline{\iota}\ \right]^{-1} \qquad (2\text{-}31)$$

In equation (2-27) $\hat{\sigma}$ and $\hat{k}$ are used instead of the straightforward average values $\overline{\sigma}$ and $\overline{k}$ to enhance the numerical stability when the above expression for the whitecapping source term is applied in a numerical model (WAMDI group, 1988).

Wave energy dissipation at the bottom :

Dissipation of wave energy due to wave-bottom interactions can occur due to many mechanisms. A review of mechanisms is given by e.g. Shemdin et al. (1978), who consider percolation, bottom motion (soft mud, vegetation) and bottom friction. For relatively fine sands as found in the North Sea, only bottom friction is important (Shemdin et.

al., 1978; Weber et al., 1988). Wave energy dissipation due to bottom friction is still poorly understood, in particular when (irregular) waves on currents are considered. A review of the available literature is given in appendix A. The selection of the formulation for the bottom friction source term is also discussed in appendix A. The selection is strongly influenced by the capability of the available formulations to describe current influences on these source functions. In this section only a brief description of the governing mechanisms and available formulations is given.

In the WAM model the bottom friction source term is described using a semi-empirical expression derived from the JONSWAP results for swell dissipation (Hasselmann et al, 1973). However, the energy dissipation as calculated using this JONSWAP formulation is found to be too small for relatively shallow water conditions (e.g. Bouws and Komen, 1983; Cavaleri et al., 1989). Several more sophisticated expressions for the bottom friction source term are available (e.g. Hasselmann and Collins, 1968; Collins, 1972; Madsen et al., 1988a,b; Weber, 1989). Such expressions have been used successfully in recent versions of the WAM model (Weber et al., 1988; Cavaleri et al., 1989; Weber, 1989) or other wave models (e.g. Graber and Madsen, 1988). For this study the formulation of Madsen et al. (1988a) has been selected (see appendix A); it can be written as

$$S_{ds,b}(\underline{\iota}) = - \frac{8}{3\pi} f_w \frac{1}{d} \left[n - \frac{1}{2} \right] u_{b,r} F(\underline{\iota}) \qquad (2\text{-}32)$$

with

$$u_{b,r}^2 = 2 \iint \frac{\sigma^2}{\sinh^2 kd} F(\underline{\iota}) \, d\underline{\iota}$$

where f_w is a non-dimensional friction factor and $u_{b,r}$ is a representative near-bottom current velocity. The friction factor f_w is estimated using the formulation of Jonsson (1963, 1966a) :

$$\frac{1}{4\sqrt{f_w}} + \log_{10}\left[\frac{1}{4\sqrt{f_w}} \right] = m_f + \log_{10}\left[\frac{a_{b,r}}{k_N} \right] \qquad (2\text{-}33)$$

with

$$a_{b,r}^2 = 2 \iint \frac{1}{\sinh^2 kd} F(\underline{\iota}) \, d\underline{\iota}$$

where $a_{b,r}$ is the representative near-bottom excursion amplitude, k_N is the equivalent roughness length scale of bottom and m_f is constant (m_f = -0.08 as determined experimentally by Jonsson and Carlssen, 1976). Equation (2-33) is valid for $a_{b,r}/k_N$ larger than approximately 1. For smaller values of $a_{b,r}/k_N$ a constant value of f_w is used (f_w = 0.30 for $a_{b,r}/k_N < 1.57$, e.g. Jonsson, 1978, 1980).

The major problem in estimating the wave friction factor of equation (2-33) is the estimation of the bottom roughness k_N. When sandy bottoms are considered, such as that of the North Sea, ripple formation can change the bottom roughness dramatically. For the southern North Sea this implies that the bottom roughness can range from sand grain roughness (with values as low as k_N = 200 μm) to ripple roughness (with values as large as k_N = 20 cm, e.g. Weber et. al, 1988). Grant and Madsen (1982) have proposed a formulation for the calculation of ripple geometry and corresponding bottom roughness length scales k_N from sand grain roughness. This formulation shows a strong discontinuity in bottom roughness for wave conditions at which the first ripples are formed (monochromatic waves). Numerical experiments have shown that the generation of the first ripples strongly influences depth and time limited growth curves for homogeneous conditions. As a result small changes in the selected grain diameter can lead to either no differences or large differences in e.g. the calculated evolution of the wave height. This is not realistic because of (a) the non-uniform grain size, (b) depth variations in the area for which the spatial grid point is representative and (c) the randomness of the waves. Since moreover grain diameters of shelf sea sediment and their spatial distribution in general are not well known and since the process of ripple formation under combined wave-current conditions is still poorly understood, the ripple geometry in the corresponding bottom roughness will not be calculated explicitly. Instead the roughness length k_N in equation (2-33) is taken to be constant in space and time. This constant roughness length is estimated by tuning the wave model to fit available measurements (chapter 3 and appendix B).

2.4.5 Source terms for waves on currents

If situations with waves on currents are considered, wave propagation is more conveniently described with an action balance equation than with an energy balance equation (section 2.3.3). Generation and dissipation of wave action then are represented as source terms T at the right hand side of equation (2-19).

$$\frac{\partial N(\underline{k})}{\partial t} + \nabla_x \cdot \left[(\underline{c}_g + \underline{U})\, N(\underline{k})\right] + \nabla_k \cdot \left[\underline{c}_k N(\underline{k})\right] = T(\underline{k}) \qquad (2\text{-}34)$$

Deriving a spectral energy balance equation from this spectral action balance equation (cf. Phillips, 1977, sections 2.7 and 3.8 for monochromatic waves), it follows that $T(\underline{k})$ equals $S(\underline{k})/\sigma$. Since depth and current are quasi-stationary and quasi-homogeneous with respect to the local description of the waves (and thus with respect to the local magnitude of the source terms), formulations for the source terms for situations without currents can be applied directly in the moving frame of reference when situations with currents are considered. Explicit current influences then only enter the formulations through parameters which are used to describe the air or bottom boundary. In the expressions for the whitecapping and nonlinear interaction terms such parameters do not occur. In the input source term $S_{in,e}$ the wind speed is such a parameter. In situations with currents the wind speed U_{10} consequently becomes the relative wind speed U_{10_r} (i.e. the wind speed in the moving frame). Finally the current is expected to influence the bottom friction term. However, of all investigated available models (appendix A), a model in which effects of currents on the wave boundary layer is simply neglected (i.e. the application of equations (2-32) and (2-33) in a moving frame) showed the best agreement with the available data. The low-intensity turbulence of the mean current apparently has only a small effect on the highly turbulent wave boundary layer. Consequently the presently best way to incorporate effects of currents on the wave energy dissipation due to bottom friction is simply to use equations (2-32) and (2-33), ignoring effects of the currents on the formulation for the friction factor (as concluded in appendix A). Thus the source terms for the action balance equation (2-34) become :

$$\sigma\, T(\underline{\iota}) = S'_{in,e}(\underline{\iota}) + S_{nl}(\underline{\iota}) + S_{ds,w}(\underline{\iota}) + S_{ds,b}(\underline{\iota}) \qquad (2\text{-}35)$$

where $S'_{in,e}$ is given by equations (2-23) and (2-24), replacing U_{10} by U_{10_r}, and where the other (energy density) source terms are given as in sections 2.4.3 and 2.4.4. Note that all source terms are expressed in terms of relative frequencies, since they are essentially defined in the moving frame.

2.5 DISCUSSION

In the previous sections of this chapter effects of currents (and corresponding large scale surface level variations) on waves have been considered. During propagation, instationary and inhomogeneous depths and currents result directly in changes of the phase parameters of the waves (ω, k and σ) as follows from the kinematics of wave trains. Effects of depth and current instationarity occur explicitly in the change of absolute frequency (equation (2-13)), whereas effects of depth and current inhomogeneity occur explicitly in the change of wavenumber and direction (equation (2-14) and (2-16)). The changes of phase parameters implicitly result in changes of the wave amplitude, either due to the conservation of action during propagation, or due to their effects on the magnitude of source terms. In the source terms for generation and dissipation of wave action or energy, no explicit influences of the currents other than the application of a relative wind speed occur. However, the source terms include implicit wave-current interactions since the wavenumber and the relative frequency of the waves are influenced by currents during propagation.

Obviously the change of wave phase parameters ω, σ and k during propagation is the key to wave-current interactions. Errors in calculated current-induced changes of wave phase parameters directly influence current-induced wave height variations due to either the conservation of action or the magnitude of the source terms. Therefore the calculation of current influences on wave phase parameters has to be performed with care, and the validity of either quasi-stationary or quasi-homogeneous approximations has to be checked thoroughly, before such approximations can be used.

3 THE NUMERICAL MODEL

3.1 INTRODUCTION

For the investigation of wave-current interactions at the scales of shelf seas, a numerical model seems the most suitable approach (see chapter 1). Such a model should incorporate all relevant (large scale) wave-current interactions which are discussed in chapter 2, as well as all known effects of wave generation, dissipation and nonlinear wave-wave interactions.

Several numerical wave models have been developed to describe waves on currents (e.g. Tayfun et al., 1976; Radder, 1979; Sakai et al., 1983; Holthuijsen et al., 1988; Mathiesen, 1984). Some models (or combinations of models) even incorporate a feedback; i.e. the effects of wind waves on currents (Skovgaard and Jonsson, 1976; extended by Christoffersen, 1982; Dingemans et al., 1986). However, these models all consider (quasi-) stationary depths and currents, so that they cannot be used for this study. Furthermore, wave generation, dissipation and nonlinear wave-wave interactions are highly parameterized, if considered at all in such models.

The description of source terms is much further developed in ocean wave models. After the pioneering work of Gelci et al. (1956, 1957), many such models have been developed (see e.g. SWAMP group, 1985; SWIM group, 1985). These models are denoted as first, second or third generation wave models, depending on the level of parameterization of generation and dissipation (see e.g. WAMDI group, 1988, section 1). The highest stage of development for such models is presently reached in the third-generation WAM model (WAMDI group, 1988). In this model the source terms which represent wave generation and dissipation are calculated using an explicit representation of state-of-the-art theories. With the WAM model, which was a joint effort of many scientists, wave modelling has reached a fairly high level of development. In fact the present quality of the model results is limited mostly by the quality of the input wind fields rather than by the physics incorporated in the model. Wave-tide interactions, however, are not

incorporated in these models, so that these models also cannot be used for this study.

Since a model which could be used for this study was not available, a numerical model (WAVEWATCH) has been developed (Tolman, 1989). WAVEWATCH is a full spectral grid model, utilizing the third generation approach of the WAM model for the calculation and integration of the source terms (WAMDI group, 1988). The selection of numerical schemes, the testing and the calibration of WAVEWATCH are described by Tolman (1989). The description and discussion of WAVEWATCH in this thesis is limited to the selection of the model equations (section 3.2), a description of the numerical algorithms and schemes (section 3.3), a presentation of selected test results (appendix B), and a discussion of the features of the model (section 3.4).

3.2 MODEL EQUATIONS

As is shown in chapter 2, effects of wave-current interactions mainly occur during the propagation of waves, and are most elegantly described using the action balance equation (2-34). In WAVEWATCH the action balance equation is solved for the absolute frequency spectrum $N(\omega,\theta)$. If such a spectrum is used, the change of absolute frequency is described by a separate term in the action balance equation. By switching this term on and off, the effects of depth and current instationarity are easily investigated, for which reason this specific formulation of the action balance equation was selected. To be able to utilize concepts of the WAM model with respect to the calculation of S_{nl} and the integration of the source terms, the action density source terms are defined on the relative frequency $f_r = \sigma/2\pi$ instead of the absolute frequency ω, which introduces a Jacobean transformation at the right hand side of equation (2-34). The basic equation to be solved in WAVEWATCH thus becomes :

$$\frac{\partial N}{\partial t} + \nabla_x \cdot \left[(\underline{c}_g + \underline{U})N\right] + \frac{\partial}{\partial \omega}\left[c_\omega N\right] + \frac{\partial}{\partial \theta}\left[c_\theta N\right] = J\,T \qquad (3\text{-}1)$$

with :

$$N = N(\omega,\theta,\underline{x},t) \quad , \quad T = T(f_r,\theta;\underline{x},t)$$

$$J = 2\pi^{-1}\left[1 + \frac{\underline{U}\cdot\underline{e}_s}{c_g}\right]^{-1} \qquad (3\text{-}2)$$

where $\underline{e}_s$ is the unit vector in the direction θ, c_ω is the propagation velocity in ω space ($d\omega/dt$, equation (2-13), representing a change of absolute frequency due to the depth and current instationarity) and c_θ is the propagation velocity in the θ space ($d\theta/dt$, equation (2-16), representing refraction).

Note that the choice of the spectrum $N(\omega,\theta)$ is purely based on research considerations. As will be shown in section 3.4, this description is not the most elegant one with respect to the physics involved or with respect to numerical economy.

3.3 NUMERICAL ALGORITHMS

3.3.1 Introduction

To integrate the five-dimensional action balance equation (3-1) economically, a fractional step method is used (e.g. Yanenko, 1971). Using such a method wave propagation and wave generation are treated in separate numerical modules where output of the first module is used as input for the second module (see figure 3). The propagation module,

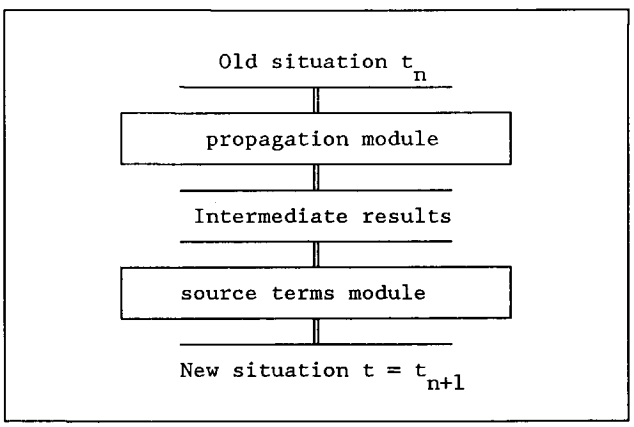

Fig. 3 Flow chart for the wave model

which uses explicit, basically second order accurate numerical schemes is described in section 3.3.2. The source terms module, which is based on the WAM model (WAMDI group, 1988), is described in section 3.3.3.

3.3.2 The propagation module

In the propagation module the action conservation equation, i.e. the action balance equation (3-1) without the source terms, is integrated. Replacing ∇_x by $(\partial/\partial x_1, \partial/\partial x_2)$ and $d\underline{x}/dt = \underline{c}_g + \underline{U}$ by (c_{x_1}, c_{x_2}) the action conservation equation can be written as :

$$\frac{\partial N}{\partial t} = - \frac{\partial}{\partial x_1}\left[c_{x_1} N\right] - \frac{\partial}{\partial x_2}\left[c_{x_2} N\right] - \frac{\partial}{\partial \omega}\left[c_\omega N\right] - \frac{\partial}{\partial \theta}\left[c_\theta N\right] \qquad (3\text{-}3)$$

The basic numerical scheme used to integrate this equation is an explicit predictor-corrector scheme that can be considered as an iterative approximation of the Crank-Nicholson scheme (e.g. Abbott, 1979). This scheme is denoted here as the ICN scheme. For propagation in the x_1 space only (i.e. dropping the second and following terms on the right hand side of equation (3-3) for convenience of notation only) this scheme can be written as :

Predictor $N^{n'}$:

$$\frac{N^{n'} - N^n}{\Delta t} = \frac{\left[c_{x_1} N^n\right]_{i-1} - \left[c_{x_1} N^n\right]_{i+1}}{2\Delta x_1} \qquad (3\text{-}4)a$$

Half time value $N^{n''}$:

$$N^{n''} = 0.5 \left[N^n + N^{n'} \right] \qquad (3\text{-}4)b$$

Corrector N^{n+1} :

$$\frac{N^{n+1} - N^n}{\Delta t} = \frac{\left[c_{x_1} N^{n''}\right]_{i-1} - \left[c_{x_1} N^{n''}\right]_{i+1}}{2\Delta x_1} \qquad (3\text{-}4)c$$

where n and i are discrete time and space counters respectively. The main advantages of this scheme are the lack of numerical diffusion and

the simple way in which it can be used for multi-dimensional problems. The main disadvantage is the unconditionally unstable behaviour for linear problems, which, however, can be solved with minor adaptations to the scheme. The selection of this scheme is discussed by Tolman (1989).

If the above ICN scheme is used without adaptations, the basically unstable behaviour of the scheme results in (purely numerical) oscillating solutions in all four spaces ($\underline{x}$, ω and θ). They mainly occur when the action density distribution is badly resolved in the space considered (e.g. section B.2.2; Van Stijn et al., 1987) and are strongly related to the occurrence of negative action (Tolman, 1989). Such oscillating solutions can be eliminated or suppressed in many ways (see e.g. Van Stijn et al., 1987). To solve these problems here, WAVEWATCH integrates equation (3-3) using a four-dimensional version

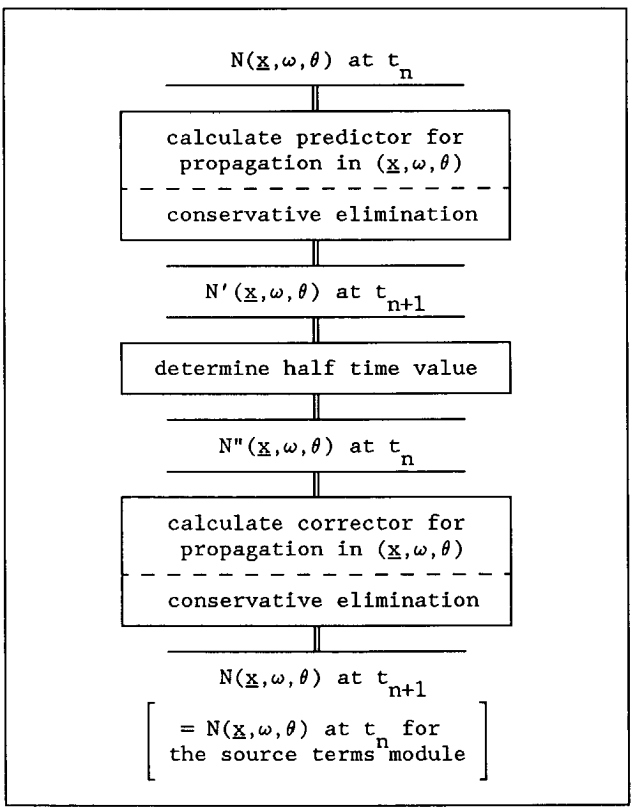

Fig. 4 Flow chart for wave propagation module

of the ICN scheme with several adaptation, the flow chart of which is given in figure 4. Before discussing the adaptations the predictor of the scheme is presented as

$$\left[\frac{N^{n'} - N^{n}}{\Delta t}\right]_{i_1,i_2,i_3,i_4} =$$

$$\left[\frac{(1+\alpha)\left[c_{x_1} N\right]_{i_1-1} - 2\alpha\left[c_{x_1} N\right]_{i_1} - (1-\alpha)\left[c_{x_1} N\right]_{i_1+1}}{2\Delta x_1}\right]^{n}_{i_2,i_3,i_4} +$$

$$\left[\frac{(1+\alpha)\left[c_{x_2} N\right]_{i_2-1} - 2\alpha\left[c_{x_2} N\right]_{i_2} - (1-\alpha)\left[c_{x_2} N\right]_{i_2+1}}{2\Delta x_2}\right]^{n}_{i_1,i_3,i_4} +$$

$$\left[\frac{M_{i_3-1,i_3} - M_{i_3,i_3+1}}{\Delta\omega}\right]^{n}_{i_1,i_2,i_4} +$$

$$\left[\frac{\left[c_\theta N\right]_{i_4-1} - \left[c_\theta N\right]_{i_4+1}}{2\Delta\theta}\right]^{n}_{i_1,i_2,i_3} \qquad (3\text{-}5)$$

with

$$\left.\begin{aligned} M_{i_3,i_3+1} &= \pm \max\left[\, (N\Delta\omega)_u/\Delta t \;,\; |M'_{i_3,i_3+1}| \,\right] \\ M'_{i_3,i_3+1} &= 0.5\left[\, (c_\omega N)_{i_3} + (c_\omega N)_{i_3+1} \,\right]_{i_1,i_2,i_4} \end{aligned}\right\} \qquad (3\text{-}6)$$

where α is the upstream fraction ($0 \le \alpha \le 1$ for $c_{x_1} > 0$ and $-1 \le \alpha \le 0$ for $c_{x_1} < 0$), n is the discrete time counter and i_1 through i_4 are grid counters in x_1, x_2, ω and θ space respectively. Finally u is a suffix, indicating the "upstream" bin in ω-space. The sign of M in equation (3-6) equals the sign of M'. The corrector is obtained by replacing the counter n' in the left hand side of this equation by the counter n+1, and by replacing the counters n at the right hand side by n". Note that the above adaptations stabilize the ICN scheme if α is chosen as discussed below.

The first two terms at the right hand side of equation (3-5) represent the propagation in the $\underline{x}$ space and consist of a combination of the ICN

scheme and a first order upstream scheme. The partial upstream character of this scheme is needed to assure stable behaviour of the propagation module in situations where source terms are dominant, or where the spatial resolution of the considered action density distribution is poor. The upstream fraction α is dynamically adjusted to assure that it remains small in cases where propagation is dominant (since high values of the upstream fraction bring down the accuracy of the propagation module) and to assure that α is large enough to stabilize the propagation scheme if source terms dominate. Based on numerical experiments, Tolman (1989) suggests the following expression for the upstream fraction :

$$\left.\begin{aligned} |\alpha| &= \max\left[\alpha_c \ , \ \alpha_{min}\right] \\ \alpha_c &= \min\left[1 \ , \ 0.10 + 3.75 \ \frac{B\Delta x}{c_g}\right] \end{aligned}\right] \qquad (3\text{-}7)$$

where

$$B = S'_{in,e}(\sigma,\theta) \ / \ F(\sigma,\theta) \qquad (3\text{-}8)$$

In this equation $S'_{in,e}$ is given by equation (2-23), replacing U_{10} by U_{10_r}. The value of α_{min} depends on the spatial resolution of the model (see appendix B).

The third term at the right hand side of equation (3-5) represents the propagation in the frequency space (i.e. the change of absolute frequency due to the instationarity of depth and current). The limitation of the flux M' in equation (3-6) represents an upstream Courant criterion. If M equals M', which should be the case for nearly all spectral bins and spatial grid points in the model, this term in equation (3-5) reduces to the original formulation of the ICN scheme (equation (3-4)).

The fourth term at the right hand side of equation (3-5) (which is identical to the original ICN scheme of equation (3-4)) represents the propagation in the directions space (refraction). The conservative elimination algorithm, introduced in figure 4, is used to stabilize the propagation in the directions space. This algorithm removes all

negative action from the two-dimensional spectrum $N(\omega,\theta)$, while conserving the total action density $N(\omega)$ at the given frequency :

$$N(\omega) = \int_0^{2\pi} N(\omega,\theta)\, d\theta \qquad (3\text{-}9)$$

In this algorithm all negative action for a given frequency ω (and location $\underline{x}$) is removed first, after which the action density for all directions is multiplied by a constant factor to conserve $N(\omega)$.

For boundary points in the $\underline{x}$ space, i.e. grid points on sea for which at least one of the eight surrounding points is located on land, an angle derivative upstream scheme is used (for the propagation in $\underline{x}$ space only). This scheme replaces the first two terms on the right hand side of equation (3-5) by :

$$\left[\frac{[c_{xs}N]_{int} - [c_{xs}N]_{i_1,i_2}}{\Delta s} \right]^{n}_{i_3,i_4} \qquad (3\text{-}10)$$

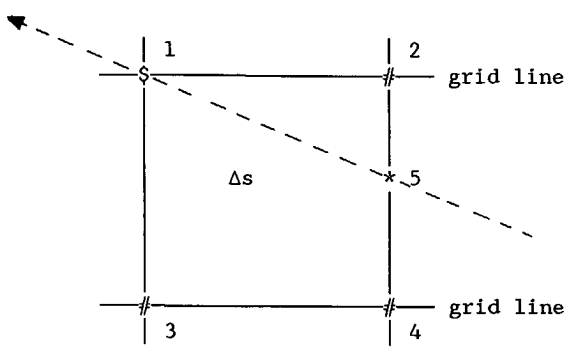

Fig. 5 Interpolation point in the angle derivative upstream scheme for boundary points in the x_1-x_2 space. Waves propagate from interpolation point 5 to prediction point 1. Flux in point 5 calculated using linear interpolation between points 2 and 4.

where Δs is the distance between the spatial grid point and the interpolation point (see figure 5), c_{xs} is the propagation velocity in the s direction ($c_{xs} = (\underline{c}_g + \underline{U}) \cdot \underline{e}_s$) and int is a suffix denoting the interpolation point.

This scheme introduces an interpolation point as is shown in figure 5 (point 5). The change of action density in point 1 is calculated from the action fluxes $c_{xs}N$ in points 1 and 5. Point 5 is located at the first upstream intersection of the wave propagation line and a grid line in either x_1 or x_2 direction. In determining the location of point 5 influences of the currents are neglected. The flux at point 5 is determined by linear interpolation from the fluxes at points 2 and 4. Point 2, 3 and 4 can either be sea or land points. In land points the action fluxes are assumed to be zero.

At the boundaries in the frequency space a zero flux is assumed. For low frequencies this is allowed since $c_\omega = d\omega/dt$ (equation (2-13)) approaches zero for ω approaching zero. For high frequencies such an assumption is allowed since $N(\omega)$ is expected to be proportional to ω^{-5} or ω^{-6} at the high frequency tail of the (action) spectrum (e.g. Phillips, 1977, 1985), so that the flux $c_\omega N$ goes to zero for increasing frequencies. Details on the effects of such closed boundaries can be found in Tolman (1989).

Since the directions space is a closed (circular) space no boundary points exist and no special boundary treatment is needed.

3.3.3 The source terms module

In the source terms module the following reduced version of the action balance equation (3-1) is integrated :

$$\frac{\partial N}{\partial t} = \frac{S}{\sigma} \qquad (3\text{-}11)$$

In integrating this equation two problems occur, i.e. the calculation of the nonlinear interactions S_{nl} and the numerical stability at the high frequency flank of the spectrum for economical time steps (e.g. 15 min., see WAMDI group, 1988). To solve these problems, concepts of the WAM model (WAMDI group, 1988) have been used. To use the concepts

of the WAM model with respect to the economic calculation of the nonlinear interactions, an exponential (relative) frequency distribution is used, which is given as :

$$f_{r,i_\xi+1} = \xi \, f_{r,i_\xi} \quad , \quad \xi > 1 \tag{3-12}$$

where i_ξ is the counter for the discrete frequencies. Following the WAM model, $\xi = 1.1$ is used. Furthermore the WAM model is expressed in terms of variance spectra $F(f_r,\theta)$. To use the concepts of the WAM model with as little adaptations as possible, action density spectra $N(\omega,\theta)$ are converted to variance density spectra $F(f_r,\theta)$ (instead of action density spectra $N(f_r,\theta)$ as in equation (3-3)) before calculating and integrating the source terms. The thus calculated changes in the variance spectra $\Delta F(f_r,\theta)$ in turn are converted to changes in the action density spectra $\Delta N(\omega,\theta)$ and added to the action density spectra as calculated using the propagation module. The corresponding flow chart of the source terms module is shown in figure 6. The separate parts are discussed below.

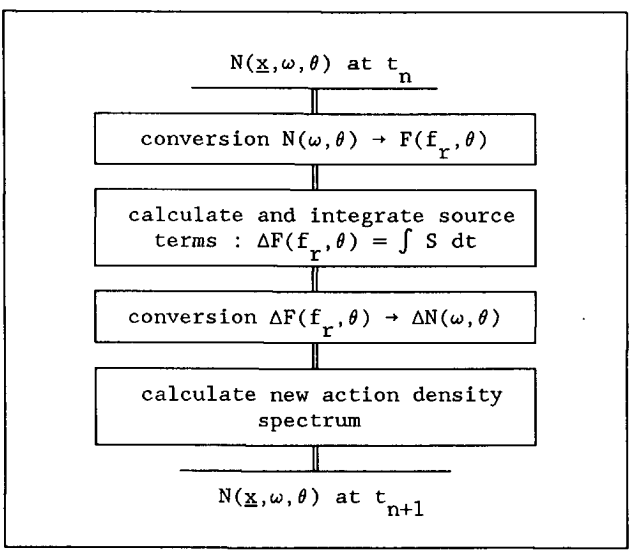

Fig. 6 Flow chart for source terms module

Conversions:

The calculation of $F(f_r,\theta)$ from $N(\omega,\theta)$ is performed using a Jacobean transformation and the definition of wave action (i.e. $N(\omega,\theta) = F(\omega,\theta)/\sigma$) :

$$F(f_r,\theta) = \sigma\, J^{-1}\, N(\omega,\theta) \qquad (3\text{-}13)$$

where the Jacobean J is given by equation (3-2). The numerical treatment of this conversion incorporates an interpolation between the fixed absolute frequency grid of the propagation module and the fixed relative frequency grid of the source terms module, since both frequency grids in general do not coincide for arbitrary current velocities. The interpolation is performed using a simple linear interpolation technique.

A similar conversion is performed to calculate the change of action density $\Delta N(\omega,\theta)$ from the change in variance density $\Delta F(f_r,\theta)$:

$$\Delta N(\omega,\theta) = \sigma^{-1}\, J\, \Delta F(f_r,\theta) \qquad (3\text{-}14)$$

Such a conversion again incorporates a linear interpolation between fixed ω and f_r grids. The conversion is performed on the change of variance density instead of the new variance density itself. Thus errors introduced by the linear interpolation are limited to the effects of the source terms, so that errors introduced by this interpolation do not influence propagation for cases with propagation only.

N.B. The equations (3-15) and (3-17) of Tolman (1989) also describe the above conversions. In these equations the Jacobean $J_{\sigma\omega}$ (Tolman, 1989, equation (2-12)) is erroneously replaced by $J_{\sigma\omega}^{-1}$.

Calculation of source terms:

The calculation of source terms for wind input and dissipation (equations (2-23) replacing U_{10} by U_{10_r}, (2-27) and (2-32)) is straightforward algebra. The calculation of the nonlinear interactions is much more complicated and involves integration over a five-dimensional

continuum of resonant quadruplets. Following the WAM model, this is reduced to a two-dimensional continuum by considering a mirror symmetrical pair of quadruplets of the following form only ($\lambda = 0.25$) :

$$\left.\begin{aligned} \sigma_2 &= \sigma_1 \\ \sigma_3 &= (1+\lambda)\ \sigma_1 \\ \sigma_4 &= (1-\lambda)\ \sigma_1 \end{aligned}\right] \qquad (3\text{-}15)$$

An economic integration method for such pairs of quadruplets was developed by Hasselmann and Hasselmann (1985a) (expressions not given here). For application in shallow water the expression for S_{nl} is simply scaled with the following factor (WAMDI group, 1988) :

$$R = 1 + \frac{5.5}{x}\left[1 - \frac{5}{6}x\right] e^{-1.25\ x}\ ,\ x = k_p d \approx 0.75\ \hat{k}d \qquad (3\text{-}16)$$

Integration of source terms:

For the integration of the source terms a simple Euler method is used, in which the change of the variance density spectrum in a single time step is given by :

$$\Delta F(f_r,\theta) = S\ \Delta t \qquad (3\text{-}17)$$

This integration method is much simpler and cheaper than the semi-implicit method used in the WAM model (WAMDI group, 1988), and it gives similar results when combined with the stability precautions as given below (e.g. Tolman, 1989, page 24).

Since high-frequency spectral components react fast to changes in wind conditions, an explicit integration method generally needs relatively small time steps to assure numerical stability (order of 1 min). Using such time steps, a third generation model is not economically feasible. To assure numerical stability for reasonable time steps (e.g. Δt = 20 min, as used in the WAM model), the high frequency tail of the spectrum is parameterized. Furthermore the maximum change of variance for every single spectral bin in every time step is limited. Both precautions are taken directly from the WAM model.

For frequencies beyond the high-frequency limit $f_{r,hf}$ the following shape of the tail is applied (the suffix hf indicates values at $f_r = f_{r,hf}$) :

$$F(f_r,\theta) = \frac{c_{g,hf}}{c_g}\left[\frac{k_{hf}}{k}\right]^{2.5} F(f_{r,hf},\theta) \quad , \quad f_r > f_{r,hf} \tag{3-18}$$

which corresponds to a f_r^{-4} tail in deep water. As in the WAM model, the high-frequency limit $f_{r,hf}$ is calculated as

$$f_{r,hf} = \max\,(4f_{r,PM} \, , \, 2.5\bar{f}_r) \tag{3-19}$$

where $f_{r,PM}$ is the Pierson Moskowitz frequency for fully developed spectra and $\bar{f}_r$ is the straightforward mean frequency (comparable to $\bar{k}$ of equation (2-31)).

The maximum change of the variance density of every spectral bin in each time step is 10 % of the highest spectral level that can be reached, which is estimated as the PM equilibrium level (cf. the WAM model).

$$\max\left[\left|\Delta F(f_r,\theta)\right|\right] = 0.1\,\frac{0.081\,\pi}{c_g}\,k^{-3} \tag{3-20}$$

Note that only the maximum variation in a single time step is related to some equilibrium range, but not the shape of the spectrum itself.

New action density:

The new action density after one time step is calculated by adding the change of action density in one time step to the old action density (as calculated by the propagation module) :

$$N(\omega,\theta)^{n+1} = N(\omega,\theta)^{n} + \Delta N(\omega,\theta) \tag{3-21}$$

Resulting negative action is eliminated by setting the action density of such bins to zero without further corrections. This elimination of negative action only deals with negative action as generated by the

source terms module, since $N(\omega,\theta)^n$ as calculated by the propagation module cannot become negative. Thus the above non-conservative elimination of action does not influence propagation.

3.4 DISCUSSION

In this section numerical features of WAVEWATCH will be discussed using the test results as presented in appendix B. Both general features of the model and features as expected in the North Sea hindcasts (chapter 5) are discussed. Furthermore values of the minimum upstream fraction α_{min} and of the bottom roughness length scale k_N will be selected for use in the North Sea hindcasts. Finally some remarks will be made on the action density spectra and the corresponding formulation of the action balance equation as selected for WAVEWATCH.

3.4.1 Numerical features of WAVEWATCH

In the discussion of the numerical features a distinction will be made between the propagation and generation properties of WAVEWATCH.

The quality of the numerical description of wave propagation is governed by the resolution of action density distributions (appendix B, section B.2.2). In particular the propagation in the $\underline{x}$ space is sensitive to the resolution in this space (and to the value of α_{min}). This is illustrated in the figures B-1, B-4 and B-7, which show energy or variance density distributions in the x_1, θ and ω space respectively, which are all described by approximately 5 grid points. For this relatively poor resolution, numerical errors of the propagation in the ω and θ space are still small (figures B-4 and B-7), whereas errors for the propagation in the x_1 space (figure B-1b) are considerable. Note that the numerical scheme for propagation in the $\underline{x}$ space as used in WAVEWATCH is significantly more accurate than the first order upstream scheme as used in e.g. the WAM model.

In the North Sea hindcast studies of chapter 5 the discretizations as gathered in table 1 are used. Since the hindcast studies consider wind

seas without isolated swell, the spectral resolution (i.e. the resolution in the ω and θ spaces) is expected to be comparable to or better than the resolution as used in the corresponding tests (e.g. figures B-7 and B-4). Consequently the propagation in the frequency and directions space is expected to be described excellently in the North Sea hindcasts. Using a spatial increment of 24 km, the spatial resolution in the southern North Sea becomes comparable to the resolution as is shown in figure B-1b. However, since propagation in the southern North Sea takes place over a few grids only, errors as large as in figure B-1b cannot develop. For other parts of the North Sea the spatial resolution is expected to be much better.

Table 1 Discretization and constants as used in WAVEWATCH for the North Sea hindcasts

24 angles	:	$\Delta\theta$	= 15 °
26 frequencies	:	f_1	= 0.041 Hz
		f_{26}	= 0.453 Hz
		ξ	= 1.1
spatial increment ($\Delta x_1 = \Delta x_2 = \Delta x$)	:	Δx	= 24 km
time step	:	Δt	= 15 min
constants	:	α_{min}	= 0.25
		k_N	= 0.04 m

The results of WAVEWATCH with respect to the reproduction of growth curves are comparable to those of other third generation models available (WAM, WAMDI group, 1988; EXACT-NL, Hasselmann and Hasselmann, 1985a), both with respect to time-limited growth in homogeneous conditions (Tolman, 1989), and with respect to fetch-limited growth in stationary conditions (appendix B; Tolman, 1989). However, differences between WAVEWATCH and e.g. WAM in the fetch-limited cases seem to be much larger than can be explained by the differences in the propaga-

tion schemes only. The reasons for this difference should be investigated further. Such an investigation, however, is beyond the scope of this study.

3.4.2 Choice of coefficients

Minimum upstream fraction (α_{min})

The value of the minimum upstream fraction α_{min} depends largely on the feasible (spatial) resolution for the geographical area under consideration, as shown in appendix B, section B.2.2. Due to the available computer memory on the IBM 3083 computer, on which WAVEWATCH has been implemented, the smallest feasible spatial increment for the North Sea calculations was 24 km. Such a grid increment leads to a relatively poor spatial resolution in particular to describe the southern North Sea. This spatial resolution is comparable to the resolution as obtained in figure B-1b. Based on the results of this figure an upstream fraction α_{min}= 0.25 was selected for the North Sea hindcasts. In the North Sea hindcasts this upstream fraction showed good results, in which no signs of numerical instability could be recognized.

Bottom roughness length scale (k_N)

A bottom roughness length scale k_N= 0.04 m has been used for the North Sea calculations of chapter 5. This is in close agreement with the results of Weber et. al. (1988) and Weber (1989), who consider depth-limited wave conditions on the southern North Sea. Furthermore the depth-limited growth curves as calculated using k_N= 0.04 m show good agreement with both measurements and recent analytical formulations for depth-limited growth curves (appendix B, section B.3.3). The above value of k_N is therefore fairly realistic for a (North Sea) research model. For the application in an operational hindcast or forecast model k_N could be calibrated further using observational data to obtain the best possible model results.

3.4.3 Model formulation

The action density spectrum $N(\omega,\theta)$ is used as the basic spectrum in the (propagation module of the) numerical model WAVEWATCH to enable research into the effects of depth and current instationarity on waves (see section 3.1). For models in which the research into the effects of depth and current instationarity is not one of the main subjects, the use of the action spectrum defined on the wavenumber and direction $N(k,\theta)$ and the corresponding formulation of the action balance equation (2-34) is more convenient for both theoretical reasons and reasons of numerical economy.

From a theoretical point of view a wavenumber spectrum is more satisfactory than a frequency spectrum, since wavenumber spectra are invariant with respect to changes of frame of reference (fixed or moving). Furthermore many concepts used in wave modeling (e.g. the use of standard spectral shapes) are invariant with respect to depth, when wavenumber spectra are used. Finally the basic formulations for the nonlinear source term, which is a key concept in third generation wave models, are basically derived for action wavenumber spectra. Note that the source term module of a model like WAVEWATCH is easily reformulated in terms of the spectrum $N(k,\theta)$, since all source terms are easily reformulated in terms of $N(k,\theta)$ and since all concepts of the WAM model are directly applicable to source terms in a wavenumber spectrum formulation. This is not the case if $N(\omega,\theta)$ is replaced by $N(\underline{k})$, since the economic algorithm for the calculation of the nonlinear interactions is not easily reformulated in terms of $N(\underline{k})$.

Furthermore the wavenumber spectrum $N(k,\theta)$ is more convenient than the frequency spectrum $N(\omega,\theta)$ with respect to numerical economy. First the conversions between absolute and relative frequency spectra are not needed when a the spectrum $N(k,\theta)$ is used instead of $N(\omega,\theta)$, since the wavenumber spectrum is invariant with respect to the chosen frame of reference. Furthermore the computing time needed for the calculation of relative frequencies σ and group velocities c_g (needed for the calculation of propagation velocities and source terms) will reduce by an order of magnitude, as shown below. Using the frequency spectrum $N(\omega,\theta)$, σ and c_g are calculated using an implicit equation for both

spectral dimensions. Changing to wavenumber spectra, relative frequencies and group velocities (needed for the calculation of propagation velocities and source terms) are calculated using an explicit equation for one spectral dimension (k) only, which reduces the calculational effort by more than an order of magnitude. In the present form of WAVEWATCH, implemented on an IBM 3083, the above calculations take 10 to 20 % of the of the (total) calculational effort.

Although the wavenumber spectrum formulation is more convenient for operational models than a frequency spectrum formulation, it is not likely that such a wavenumber spectrum formulation will lead to better model results. From a numerical point of view, the main advantage of the wavenumber spectrum formulation would be the elimination of the spectral interpolation and the corresponding numerical diffusion in the spectral conversions. This diffusion, however, has no significant effect on the results of the model, as shown by Tolman (1988, his section 4.3.2).

4 PROPAGATION IN IDEALIZED CASES

4.1 INTRODUCTION

In chapter 2 it is shown that wave-current interactions mainly occur due to depth and current induced variations of the wave phase parameters (absolute and relative frequency ω and σ, wavenumber k). To get some insight in such variations, in particular for instationary depth and current conditions, two academic cases are considered for which changes in phase parameters are assessed.

In the first case monochromatic unidirectional waves propagate at an arbitrary angle relative to a one-dimensional tide in water with a constant bottom level. For this case approximate analytical solutions for depth and current induced variations of ω, σ and k are obtained.

In the second case short-crested irregular waves propagate on a two-dimensional tide in an academic shelf sea. For this case changes in the phase parameters are determined using the propagation module of WAVEWATCH.

4.2 MONOCHROMATIC UNIDIRECTIONAL WAVES ON A ONE-DIMENSIONAL TIDE

4.2.1 Introduction

To illustrate the influence of (space and) time derivatives of tidal depths and currents on phase parameters of (wind) waves, consider a one-dimensional tide in water with a constant bottom level. The tide is represented by a one-dimensional long wave, propagating in the positive x_1-direction :

$$d(x_1,t) = d_o + A_d \sin \chi(x_1,t) \qquad (4\text{-}1)$$

$$U(x_1,t) = A_U \sin \chi(x_1,t) \qquad (4\text{-}2)$$

$$\chi(x_1,t) = Kx_1 - \Omega t \qquad (4\text{-}3)$$

$$c_t = \Omega/K = \sqrt{gd_o} \tag{4-4}$$

$$A_U/A_d = \sqrt{g/d_o} \tag{4-5}$$

In these equations χ is the tidal phase, c_t is the tidal propagation velocity, K and Ω are the wavenumber and frequency of the tide and A_U and A_d are the velocity and depth amplitude respectively (the current velocity is assumed to be constant over the depth and has a component in the x_1 direction only).

To isolate the effects of space and time derivatives of the tidal depths and currents, changes in wave phase parameters have been determined using three different approximations. The first is a quasi-stationary approximation in which time derivatives of depth and current are neglected. This is the conventional approximation for taking current influences into account. The second is a quasi-homogeneous approximation in which space derivatives of depth and current are neglected. The third is an instationary and inhomogeneous approach using a small perturbation approximation in which both time and space derivatives of depth and current are accounted for. The resulting frequencies and wavenumbers of the first two approximations will be marked with the suffices s and h for stationary and homogeneous respectively. Results without suffix relate to the instationary and inhomogeneous approximation (i.e. the reference approximation).

To determine changes of wave parameters a method of characteristics is used in which the waves are followed with the propagation velocity of the wave energy $\underline{c}_g+\underline{U}$. The analysis starts at a location and time where $\chi = 0$, which implies that in the initial situation the depth equals d_o and that there is initially no current. The wave parameters in this initial situation are indicated with suffix o (e.g. ω_o). In the following, changes of the phase parameters ω, σ and k are determined and discussed for all three approximations separately. Changes are expressed as absolute changes from the initial situation, e.g. $\Delta\omega = \omega - \omega_o$.

4.2.2 Quasi-stationary approximation

In a quasi-stationary approximation all partial time derivatives of depth and current are assumed to be zero, so that also $d\omega/dt$ in equation (2-13) is zero. However, U and d are varying in time and space as in equations (4-1) through (4-5). The absolute frequency ω ($= \omega_s$ in this approximation) therefore remains constant and equal to the initial frequency ω_o. Using the dispersion equations (2-6) and (2-1), the local wavenumber (k_s) can be determined at any location (time) along ray paths from ω_o, the (local) depth d, the (local) current velocity U and the direction θ. The changes of absolute frequency and wavenumber are :

$$\Delta\omega_s = 0 \tag{4-6}$$

$$\Delta k_s = k_s - k_o \tag{4-7}$$

Since the absolute frequency remains constant, the change of relative frequency $\Delta\sigma_s$ is opposite to the Doppler shift kU_p (equation (2-6)), where U_p is the current velocity in the propagation direction of the waves ($U_p = U \cos\theta$). If $U_p \ll c = \sigma/k$, the variation in wavenumber is relatively small ($\Delta k/k_o \ll 1$), so that the change of relative frequency becomes :

$$\Delta\sigma_s = -(k_o+\Delta k)U_p \approx - k_o U_p \tag{4-8}$$

Consequently the effects of currents remain relatively simple when a quasi-stationary approximation is used : the absolute frequency remains unchanged by the currents and the variation of the relative frequency is opposite to the local Doppler shift (which directly determines the magnitude of variations of the wavenumber due to the dispersion relation (2-1)).

4.2.3 Quasi-homogeneous approximation

In a quasi-homogeneous approximation partial space derivatives rather than time derivatives of depth and current are assumed to be zero. It then follows from equation (2-14) that wavenumber k ($= k_h$ in this

approximation) rather than absolute frequency ω remains constant. The local frequency can be determined at any time (location) along the ray path from k_o, the (local) depth d and the (local) current velocity U. Using equations (2-1) and (2-6) the changes of absolute frequency and wavenumber are :

$$\Delta k_h = 0 \tag{4-9}$$

$$\begin{aligned} \Delta\omega_h &= \sqrt{gk_o \tanh k_o d} - \omega_o + k_o U_p \\ &= \Delta\sigma_h + k_o U_p \end{aligned} \tag{4-10}$$

The change of absolute frequency $\Delta\omega_h$ consists of the Doppler shift $k_o U_p$, due to current variations only, and the change of relative frequency $\Delta\sigma_h$, due to depth variations only. For arbitrary depth and current variations the ratio between these two contributions to $\Delta\omega_h$ is determined using equation (2-1) and a truncated Taylor series expansion for $\sqrt{\tanh k_o d}$ (assuming $\Delta d/d_o \ll 1$) :

$$\frac{\Delta\sigma_h}{k_o U_p} = \frac{\Delta d/d_o}{U/\sqrt{gd_o}} (\cos\theta)^{-1} \frac{\sqrt{k_o d_o}}{2\sqrt{\tanh k_o d_o}\cosh^2 k_o d_o} \tag{4-11}$$

For the depth and current field considered here, Δd and U (= ΔU since U = 0 initially) are interrelated (equations (4-1) through (4-5)), so that this ratio becomes a function of $k_o d_o$ and θ only :

$$\frac{\Delta\sigma_h}{k_o U_p} = (\cos\theta)^{-1} \frac{\sqrt{k_o d_o}}{2\sqrt{\tanh k_o d_o}\cosh^2 k_o d_o} \tag{4-12}$$

In figure 7 this ratio is plotted as a function of $k_o d_o$ for several angles θ. This figure shows that the depth-induced variation of absolute frequency ($\Delta\sigma_h$) is only relevant compared to the current-induced variation of the absolute frequency ($k_o U_p$) for relatively shallow water (e.g. $k_o d_o < 1$), and for waves traveling in directions almost perpendicular to the propagation direction of the tide (e.g. $80° < |\theta| < 110°$). In the latter case, however, Doppler shifts become negligible since $\cos\theta$ approaches 0, so that the entire change of

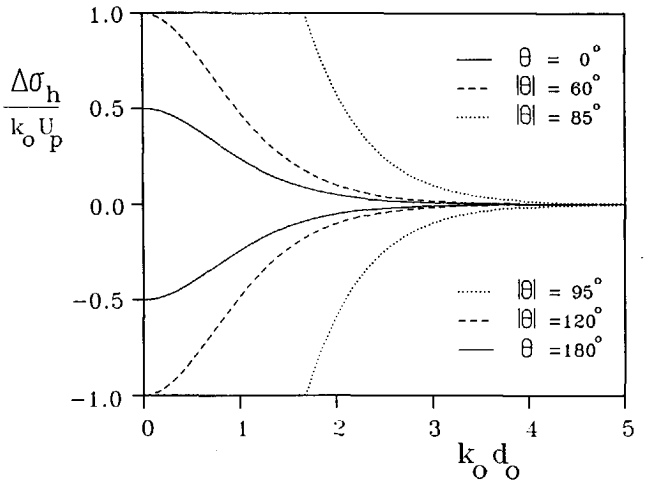

Fig. 7 The ratio between the depth-induced and current-induced contributions to the change of absolute frequency in quasi-homogeneous approximation $\Delta\omega_h$ ($\Delta\sigma_h$ and $k_o U_p$ respectively) for a one-dimensional tide.

absolute frequency becomes small. For shelf seas away from the coast, where relative water depths $k_o d_o$ are usually not very small, the changes of frequencies for the quasi-homogeneous approximation thus become :

$$\Delta\omega_h \approx k_o U_p \qquad (4\text{-}13)$$

$$\Delta\sigma_h \approx 0 \qquad (4\text{-}14)$$

As in the quasi-stationary approximation, the effects of currents in the quasi-homogeneous approximation remain relatively simple : the relative frequency and wavenumber remain unchanged by the current and the variation of the absolute frequency equals the local Doppler shift.

4.2.4 Instationary and inhomogeneous approximation

If both space and time derivatives of depth and current are accounted for in the basic equations of chapter 2, both the wavenumber k and the

absolute frequency ω will change. To obtain the change of phase parameters (e.g. ω), one would have to integrate equations (2-11), (2-16) and one of the three equations (2-13) through (2-15) (in time). To simplify the derivation of analytical solutions, a small-perturbation approximation is used in which :

a) the current velocity is assumed to be relatively small ($U \ll c_g$), so that $c_g+U \approx c_g$,
b) changes in k, ω and σ are assumed to be relatively small ($|\Delta k/k_o| \ll 1$ etc.),
c) effects of depth variations are neglected (which away from the coast are negligible in the two previous approximations), and
d) the change $\Delta\theta$ of direction is neglected (i.e. tide-induced refraction is neglected), so that $\theta = \theta_o$ in the following.

Using such an approximation equation (2-13) becomes :

$$\frac{d\omega}{dt} = \left.\frac{\partial\sigma}{\partial d}\right|_{k=k_o} \frac{\partial d}{\partial t} + k_o \cos\theta_o \frac{\partial U}{\partial t} \qquad (4\text{-}15)$$

Since $\partial d/\partial t$ and $\partial U/\partial t$ are periodic functions of the tidal phase χ, $d\omega/dt$ and ω vary with χ only. It is therefore convenient to integrate the rate of change $d\omega/d\chi$ in χ (instead of $d\omega/dt$ and $d\underline{x}/dt$ in t). Since

$$\frac{d\omega}{d\chi} = \frac{1}{-\Omega + c_{g,o}\cos\theta_o K} \frac{d\omega}{dt} \qquad (4\text{-}16)$$

(from equations (2-17) and (4-3)), the change of absolute frequency becomes :

$$\Delta\omega(\chi) = \frac{1}{-\Omega + c_{g,o}\cos\theta_o K} \int_0^{\chi} F(\chi')\, d\chi' \qquad (4\text{-}17)$$

where $F(\chi)$ is the rate of change $d\omega/dt$ of equation (4-15). This equation holds for any Ω and K, not only for K and Ω related as in equation (4-4). Thus expressions for the integral at the right hand side can be obtained by considering combinations of Ω and K for which $\Delta\omega(\chi)$ is known (i.e. a quasi-stationary or a quasi-homogeneous situations). In a quasi-homogeneous situation $c_{g,o}(\cos\theta_o)K/\Omega$ approaches 0

and $\Delta\omega(\chi)$ approaches $\Delta\omega_h(\chi)$ (equation (4-13)), so that the integral at the right hand side of the above equation equals $-\Omega\ \Delta\omega_h(\chi)$. Using equations (4-4) and (4-13), the above equation becomes :

$$\Delta\omega = \frac{1}{1 - c^* \cos\theta_o}\ k_o U_p \qquad (4\text{-}18)$$

in which the propagation ratio c^* is defined as :

$$c^* = \frac{c_{g,o}}{c_t} = n_o \left[\frac{\tanh k_o d_o}{k_o d_o}\right]^{\frac{1}{2}} \qquad (4\text{-}19)$$

Since c^* is a function of $k_o d_o$ only, it can be interpreted as an alternative relative depth parameter (instead of $k_o d_o$).

In figure 8 the change of absolute frequency $\Delta\omega$, normalized with the local Doppler shift $k_o U_p$, is presented as a function of the relative depth $k_o d_o$ for several angles θ_o. This figure shows that the change of absolute frequency is of the same order of magnitude as (but not equal

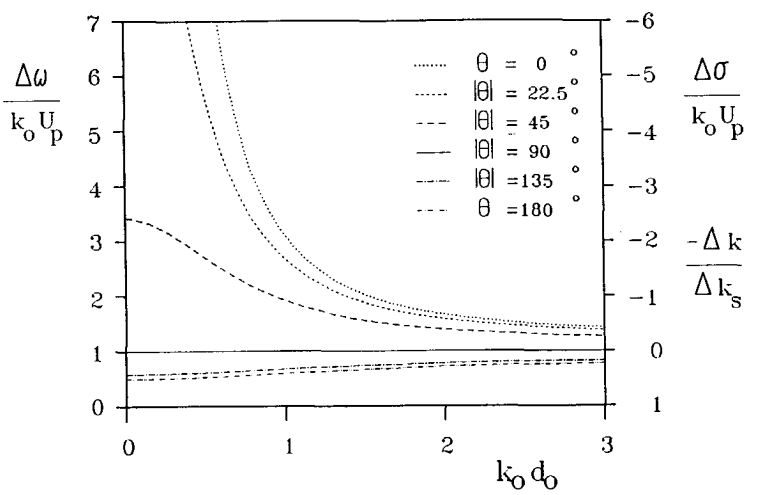

Fig. 8 Normalized change of absolute frequency ($\Delta\omega$), relative frequency ($\Delta\sigma$) and wavenumber (Δk) as a function of the relative depth $k_o d_o$ for waves traveling on a one-dimensional tide at angle $\theta^o = {}^o\theta_o$

to) the Doppler shift $k_o U_p$ for most directions and relative depths. For waves traveling in directions opposite to the tide (i.e. $90° < \theta_o < 270°$), $\Delta\omega$ is smaller than the Doppler shift, with a minimum of $0.5\ k_o U_p$, whereas for waves traveling in the same direction as the tide ($-90° < \theta_o < 90°$), $\Delta\omega$ is larger than the Doppler shift. For waves in shallow water, traveling in approximately the same direction as the tide (e.g. $k_o d_o < 1$ and $|\theta_o| < 20°$), the change of absolute frequency even becomes an order of magnitude larger than the Doppler shift.

An expression for the change of relative frequency is simply found by subtracting $\omega_o = \sigma_o$ from equation (2-6) and by using equation (4-18) :

$$\Delta\sigma = \frac{c^* \cos\theta_o}{1 - c^* \cos\theta_o} k_o U_p \qquad (4\text{-}20)$$

Since $\Delta\omega$-$\Delta\sigma$ equals the Doppler shift $k_o U_p$ (equation (2-6)), changes in the relative frequency are strongly related to changes in the absolute frequency, so that $\Delta\sigma$ (also shown in figure 8) need not be discussed separately.

An expression for the change of wavenumber can be obtained from equation (2-14) using an approximation similar to that of the above derivation for $\Delta\omega$ (now invoking a quasi-stationary situation where $c_w(\cos\theta_o)K/\Omega$ approaches infinity instead of zero). The result is :

$$\Delta k = \frac{-c^* \cos\theta_o}{1 - c^* \cos\theta_o} \Delta k_s \qquad (4\text{-}21)$$

The change of wavenumber (see figure 8) is directly related to the change of relative frequency (equation (2-1)), so that Δk need not be discussed separately.

4.2.5 Discussion

For all three approximations for the case considered here, a current velocity $\underline{U}$ causes a local difference between the absolute frequency ω and the relative frequency σ, which equals the Doppler shift $k_o U_p$. In

the quasi-stationary approximation the absolute frequency remains unchanged, so that current-induced changes of the relative frequency equal the Doppler shift, whereas in a quasi-homogeneous approximation changes of the absolute frequency equal the Doppler shift. In the more realistic instationary inhomogeneous approximation neither changes of the absolute frequency nor changes of the relative frequency equal the Doppler shift, but in general both $\Delta\omega$ and $\Delta\sigma$ are of the same order of magnitude as the Doppler shift, as is illustrated in figure 8.

For increasing water depths $k_o d_o$ the change of phase parameters of the instationary and inhomogeneous approximation (see figure 8) approach the results of the quasi-homogeneous approximation, i.e. no changes in relative frequency and wavenumber and $\Delta\omega$ approaches $k_o U_p$. Such behaviour is to be expected since the short wave propagation velocity c_g then becomes negligible compared to $c_t = \sqrt{gd_o}$, so that variations of the current velocity as observed when moving with c_g are mainly variations in time (i.e. $\partial U/\partial x$ can be neglected). The solution for the instationary and inhomogeneous approximation never approaches the results of the quasi-stationary approximation. This is explained since quasi-stationary conditions can only occur for (propagating) tides if the propagation velocity c_t of the tide is much smaller than the propagation velocity of the waves c_g, which is physically impossible. Note, however, that in this case spatial gradients of depth and current are minimal due to the constant bottom level and the one-dimensional structure of the tide. In more realistic situations both bottom level variations and the two-dimensional structure of the tide are expected to increase the relative importance of the inhomogeneity.

4.3 IRREGULAR WAVES ON A TWO-DIMENSIONAL TIDE

4.3.1 Introduction

To illustrate the influence of (space and) time derivatives of tidal depths and currents on phase parameters of waves in a more realistic situation, the academic sea as shown in figure 9 is considered. Dimensions, depths and latitude of this sea roughly correspond to the dimensions, depths and latitude of the North Sea. Current and depth induced variations of wave phase parameters at this sea are assessed

using the propagation module of WAVEWATCH, for which the sea is described on a 25 km × 25 km grid. Tidal depth and current fields where calculated using the numerical model DUCHESS (see appendix C) by applying a harmonic surface level variation with a 12 h period and an amplitude of 0.25 m at the open boundary (phase constant along boundary). due to the rotation of the earth, the resulting tide travels cyclonically through the sea; maximum current velocities are shown in figure 10. In the following the solutions for the three approximations are described separately, after which the results are discussed together.

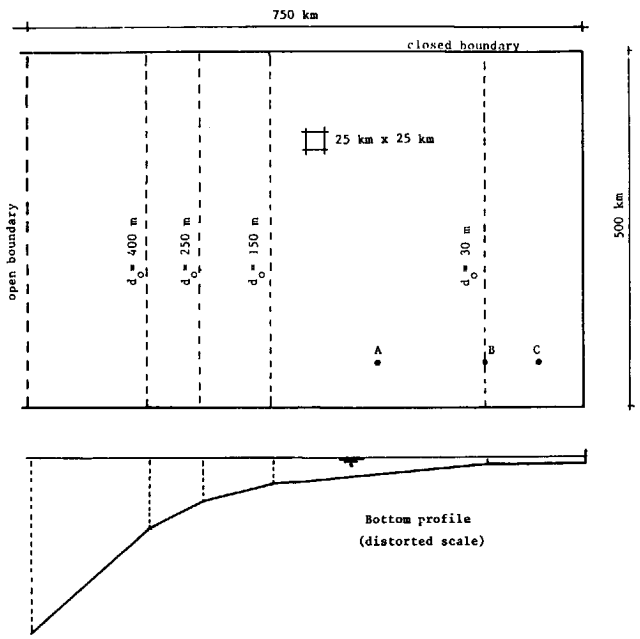

Fig. 9 Layout of the academic shelf sea.

4.3.2 Instationary and inhomogeneous approach

To obtain solutions for variations of wave phase parameters in the situation of the academic shelf sea of figure 9, numerical calculations have been performed using the propagation module of WAVEWATCH ($\Delta\theta$ = 15°, 18 frequencies ranging from 0.05 Hz to 0.29 Hz with ξ =

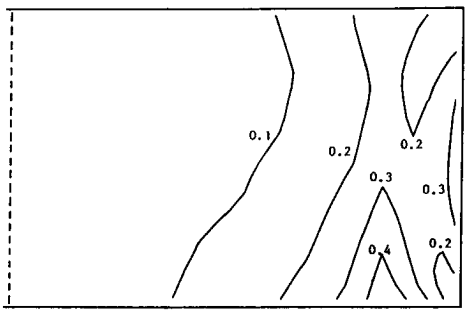

Fig. 10 Maximum current velocities in (m/s) for tide in the academic shelf sea of figure 9.

1.11, $\alpha_{min} = 0.25$). At the open boundary a stationary action density spectrum is imposed, with a mean frequency of 0.1 Hz and a mean direction perpendicular to the open boundary. A Gaussian action distribution over the frequencies is used with a spread of 0.015 Hz, together with a $\cos^2(\theta-\bar{\theta})$ directional distribution. After a few days of simulation the depth, current and wave spectra are periodic (period equal to the tidal period). All results presented here refer to the periodic solution.

From the computed spectra instantaneous average parameters of the variance spectra $F(\omega,\theta)$ are determined cf. equation (2-31) (e.g. $\bar{\omega}$). Tide-induced variations of these parameters are assessed by comparing instantaneous values with their (local) average value over a tidal period (suffix a, e.g. $\bar{\omega}_a$). Results of WAVEWATCH show that the spatial variations of e.g. $\bar{\omega}_a$ are negligible compared to the variations of $\bar{\omega}$ in time. Furthermore the results of WAVEWATCH show that the absolute value of the current-induced variation of the mean wave direction is always smaller than 2°, so that current refraction can be neglected for the situation considered here. Results for this approach (and the following approximations) are presented in figures 11 and 12, and will be discussed in section 4.3.5.

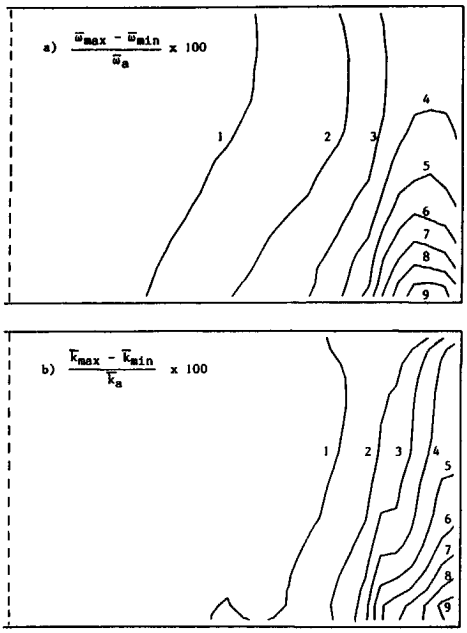

Fig. 11 Ranges of variation of (a) the absolute frequency $\bar{\omega}$ and (b) the wavenumber $\bar{k}$, normalized with the average over the tidal period ($\bar{\omega}_a$ and $\bar{k}_a$ respectively, shelf sea of figure 9).

4.3.3 Quasi-stationary approximation

In a quasi-stationary approximation the absolute frequency $\bar{\omega}$ remains constant in time (cf. the results of section 4.2.2) and approximately equal to $\bar{\omega}_a$ as determined from the results of the calculations for the instationary and inhomogeneous approach. Since the spectrum is narrow banded (i.e. can be described with a single wavenumber and absolute frequency), the wavenumber $\bar{k}$ (= $\bar{k}_s$ in this approximation) can be estimated from the local depth and current using equations (2-6) and (2-1) as :

$$\bar{\omega}_a = \left[g\bar{k}_s \tanh \bar{k}_s d \right]^{\frac{1}{2}} + \bar{k}_s |\underline{U}| \cos(\bar{\theta}_a - \theta_c) \qquad (4\text{-}22)$$

where $\bar{\theta}$ is the mean wave direction and θ_c is the direction of the current velocity. The mean wave direction $\bar{\theta}$ is determined from a

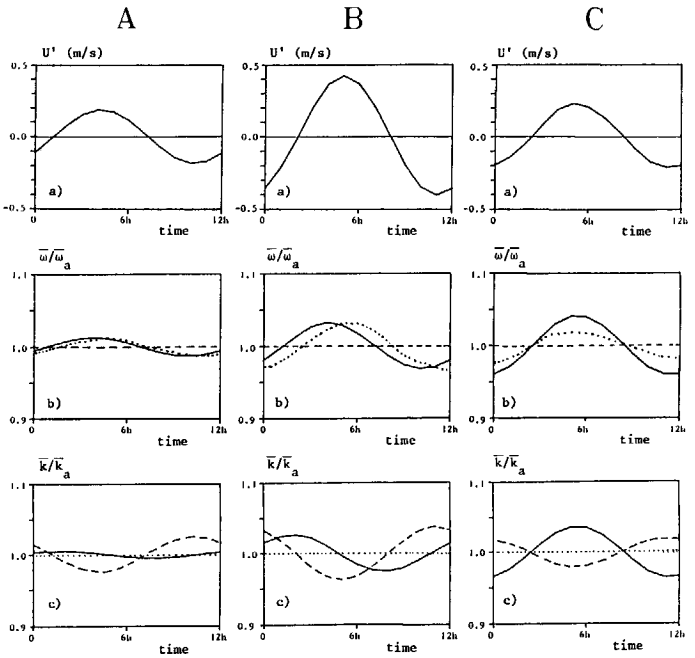

Fig. 12 Parameter values for points A, B and C of figure 9,
—— reference case, – – quasi-stationary approximation,
... quasi-homogeneous approximation

spectrum $F(\omega,\theta)$ as (Kuik et al., 1988) :

$$\bar{\theta} = \arctan(b/a) \qquad (4\text{-}23)$$

with

$$a = \iint \cos\theta \; F(\omega,\theta) \; d\omega \; d\theta$$

$$b = \iint \sin\theta \; F(\omega,\theta) \; d\omega \; d\theta$$

4.3.4 Quasi-homogeneous approximation

In the quasi-homogeneous approximation the wavenumber $\bar{k}$ remains constant in time (cf. the results of section 4.2.3) and approximately equal to $\bar{k}_a$ as determined from the results of the calculations for the instationary and inhomogeneous approach. Assuming that the effects of

the surface level variations are negligible (as in the one-dimensional case) the relative frequency $\bar{\sigma}$ remains constant and approximately equal to $\bar{\sigma}_a$ (= $\bar{\omega}_a$) (equation (2-1) with k = $\bar{k}_a$ and d = d_o). Since the spectrum is narrow banded, the absolute frequency $\bar{\omega}$ (= $\bar{\omega}_h$) can be estimated using equations (2-1) and (2-6) as :

$$\bar{\omega}_h = \bar{\omega}_a + \bar{k}_a |\underline{U}| \cos(\bar{\theta}_a - \theta_c) \qquad (4\text{-}24)$$

4.3.5 Discussion

To obtain insight in the spatial distribution of (the magnitude of) current influences on wave phase parameters, the spatial distribution of the local range of variation of the phase parameters $\bar{\omega}$ and $\bar{k}$ (e.g. $\bar{\omega}_{max} - \bar{\omega}_{min}$), normalized with their local average over a tide cycle (e.g. $\bar{\omega}_a$) are presented in figure 11 (instationary and inhomogeneous approach). Note that the normalized range of variation of the relative frequency $\bar{\sigma}$ is closely related to the normalized range of variation of the wavenumber $\bar{k}$, since linearization of equation (2-3) gives (for narrow banded spectra as considered here) :

$$\frac{\Delta\bar{\sigma}}{\bar{\sigma}_a} \approx \bar{n}_a \frac{\Delta\bar{k}}{\bar{k}_a} \qquad (4\text{-}25)$$

where $\bar{n}_a$ ranges from 0.5 at the deep water boundary to approximately 0.6 in the shallow water area for the depths and waves considered here.

Figure 11 shows that current-induced changes of the absolute frequency and wavenumber are of the same order of magnitude. Consequently neither the change of absolute frequency nor the change of wavenumber can be neglected and both the instationarity and inhomogeneity of depth and current are important with respect to wave-current interactions. The asymmetry of current influences on wave parameters in the direction parallel to the depth contours is a striking feature of figure 11. A comparison with figure 10 shows that this asymmetry roughly corresponds with a similar asymmetry in the current field, but

that the areas with the largest relative variations of wave parameters do not coincide with the areas with the largest current velocities. The latter suggests that the tide-induced changes of wave parameters cannot be calculated from the local (depth and) current velocity only. This is further illustrated in figure 12 with the behaviour in time of several wave and current parameters for selected points in the shallow part of the sea considered (see location map, figure 9). This figure shows that the phase of the tide-induced variations of $\bar{\omega}$ and $\bar{k}$ do not depend on the the local and instantaneous phase of the current velocity (compare e.g. $\bar{k}/\bar{k}_a$ for the locations B and C, note that the quasi-stationary and quasi-homogeneous solutions as also presented in this figure depend on the local current only). Furthermore the local range of variation of $\bar{\omega}$ and $\bar{k}$ clearly does not depend on the local amplitude of the current velocity. This indicates that the wave-current interactions due to tides incorporate cumulative effects.

Since both the instationarity and the inhomogeneity of depth and current are important, quasi-stationary and quasi-homogeneous approximations are bound to induce significant errors in the predicted changes of the wave phase parameters in the case considered here. This is also illustrated in figure 12.

4.4 DISCUSSION

The results as presented in this chapter show that the instationarity of tidal depths and currents has a significant influence on changes in wave phase parameters as induced by variations in depth and current.

The results for the one-dimensional case considered here (section 4.2) indicate that (away from the coast) the effects of current variations are dominant. Changes in both frequencies (ω and σ) are of the same order of magnitude as the Doppler shift $k_o U_p$, however neither $\Delta\omega$ nor $\Delta\sigma$ exactly equals the Doppler shift. Since the change of absolute frequency is generally larger than the change of relative frequency, the instationarity of depth and current seems to have a stronger influence on the changes of wave phase parameters than the inhomogeneity (for the situations considered here). For deep water, the instationarity even becomes dominant and changes of the wave phase

parameters can be estimated using a quasi-homogeneous approximation. In the one-dimensional situation the magnitude of wave-current interactions is related to local parameters only, where both the magnitude of the interactions and the relative importance of instationarity and inhomogeneity are strongly related to the (local) mean relative water depth $k_o d_o$ (or propagation ratio c^*) and θ.

The results for the two-dimensional case considered here confirm the above findings for the one-dimensional case with respect to the importance of the instationarity of depth and current. However, figure 12 clearly shows that for a more realistic tide than that of the one-dimensional cases considered here, tide-induced variations in wave phase parameters cannot be estimated from local depth and current parameters only; cumulative effects must be accounted for.

Particularly interesting are the results for the one-dimensional case for waves in shallow water propagating in approximately the same direction as the tide (e.g. $k_o d_o < 2$, $|\theta| < 20°$). In such conditions tide-induced changes of phase parameters are much larger than local parameters (e.g. the Doppler shift) indicate. Note that these shallow water conditions mainly occur for low frequency waves, e.g. swell, for which the common quasi-stationary approximation in general shows small current influences, because U/c tends to be small. However, for the above large interactions to occur, the waves have to travel with the tide during a period comparable to the tide. In such a period a low frequency wave (e.g. 0.1 Hz) will travel over 500 to 1000 km, over which distances any bottom and/or tide shows large variations. Since such conditions rarely (if at all) occur in natural conditions, it is unlikely (but not impossible) that the above large interactions for shallow water waves occur in natural conditions.

5 WAVE-TIDE INTERACTIONS IN THE NORTH SEA

5.1 INTRODUCTION

Several storms in the North Sea are hindcasted to estimate the nature and magnitude of wave-tide interactions in actual large scale conditions (section 5.3) and to compare numerical results with data (section 5.4). Significant wave-tide interactions are mainly expected to occur in the southern North Sea, since the largest current velocities occur in this area. Therefore the main interest will be focussed on this area. The storm cases were selected using two criteria. First, the cases should be well documented to be able to isolate semi-diurnal tidal modulations in observed data accurately, i.e. wind and wave data should be available at intervals of 1 hour or shorter. Secondly, separate cases should include different meteorological conditions, for which different features of wave-tide interactions are expected to occur.

Wave data in the North Sea are gathered on a routine basis by the the Dutch Ministry of Public Works and Transportation (Rijkswaterstaat). The data are gathered on hourly or half-hourly intervals (i.e. Meetnet Noordzee); data of previous storm seasons, however, are archived in data bases on three hourly intervals. Due to the availability of wave data on (half) hourly intervals, the cases to be considered were limited to the storm season 1987-1988.

The major part of the storm events on the North Sea consist of NW and SW storms. In the southern North Sea both NW and SW storms are interesting for this study since they are expected to illustrate different features of wave-tide interactions for several reasons. First the local Doppler shifts are maximal for SW storms and minimal for NW storms, since the dominant current directions in the southern North Sea are SW and NE. Therefore locally generated wave-tide interactions (related to the local Doppler shift) will be larger for SW winds than for NW winds. Secondly waves are generated locally for SW winds,

whereas waves are generated in the entire North Sea (and possibly the Norwegian Sea) for NW winds. Thus wave-tide interactions will mainly be generated locally for SW winds, whereas cumulative effects of wave-tide interactions might occur for NW winds (in particular when the waves and the tide propagate in the same direction along the British coast for a long period, see section 4.4). Thirdly, fetches are relatively small for SW winds (typically of the order of 100 km) and larger for NW winds (up to 1000 km), resulting in relatively deep water wind waves for nearly all SW wind cases, and in relatively shallow water wind waves and/or swell for (severe) NW storm conditions.

In the storm season 1987-1988 approximately nine isolated SW storm cases and five isolated NW storm cases occurred of which one well documented (moderate) SW storm case, and one well documented (moderate) NW storm case were selected. Furthermore an extreme NW storm with wind force up to Bf 12 occurred in this period, for which, however, insufficient wave data were available. Since this storm is of interest to assess the importance of wave-tide interactions in extreme wind and wave conditions, it is nevertheless also analyzed. The three storm cases are described in section 5.2.

To perform numerical calculations with WAVEWATCH, a bottom grid, wind fields, depth and current fields and wave boundary conditions at upwind model boundaries are required. The bottom schematization (figure 13) was obtained from Rijkswaterstaat. Model wind fields were obtained from the Royal Netherlands Meteorological Institute (KNMI), and consisted of (forecasted) UK6 wind fields of the British Meteorological Office (BMO). Depth and current fields were calculated with the numerical model DUCHESS (e.g. Wang, 1989) and wave boundary conditions were calculated with the model DOLPHIN (Holthuijsen and De Boer, 1988). The above data and models are described in appendix C.

Measured wind and wave data were obtained from Rijkswaterstaat (Meetnet Noordzee) for the locations LEG, Euro-0, K-13-A, and AUK (figure 13, table 2). The wind data consist of wind speeds and directions at 10 m altitude. The wave data consist of measurements with WAVEC buoys (Van der Vlugt, 1984). Wave data obtained with other instruments were

Table 2 Locations

Location	Coordinates	Depth (m)	Wind data	Wave data
LEG	51°55'N 3°40'E	20	yes	no
Euro-0	52° 0'N 3°16'E	26	no	yes
K-13-A	53°13'N 3°13'E	29	yes	yes
AUK	56°24'N 2° 4'E	80	yes	yes

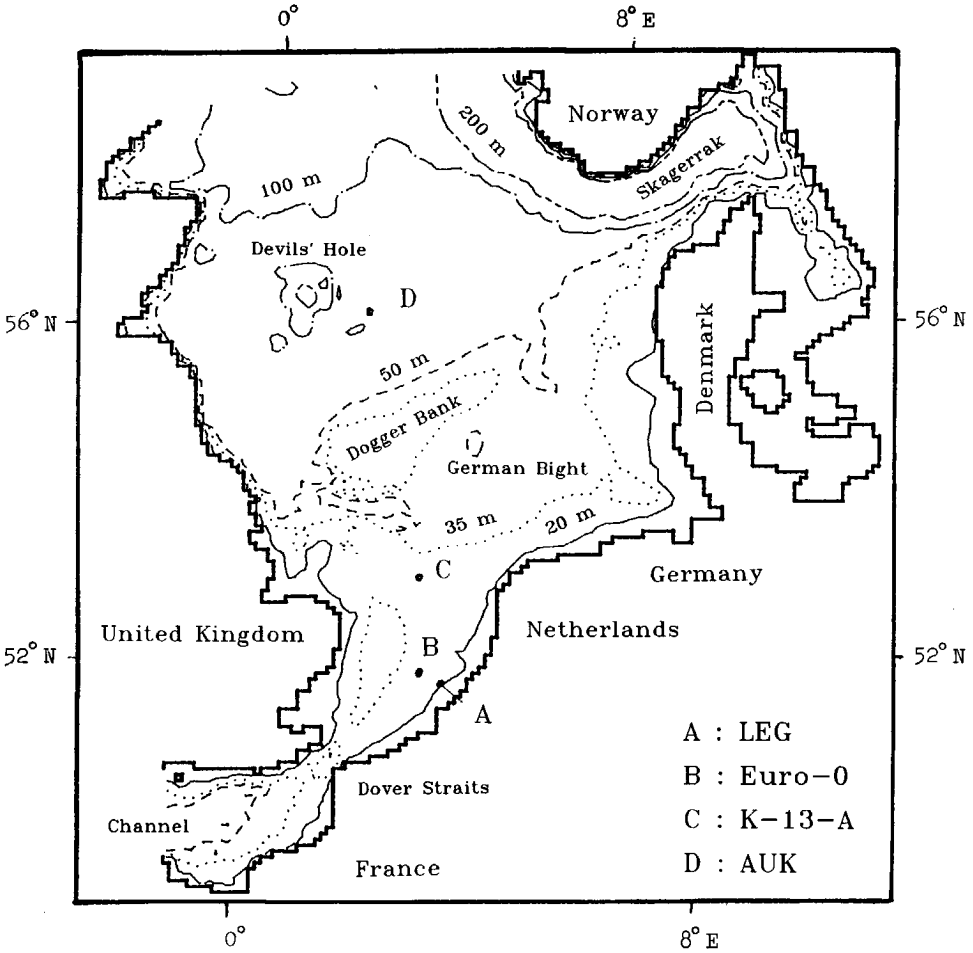

Fig. 13 The North Sea, locations and bottom levels

also available (waverider buoys and wave staffs). However, for all cases only the WAVEC data are used, either since they are the only data still available at hourly intervals (case II), or since the WAVEC data show less gaps than the waverider and wave staff data (which makes the analysis of tidal influences in the data easier). Wind data at location LEG are used in combination with wave data at location Euro-0.

5.2 CASE DESCRIPTION

5.2.1 Introduction

In this section the selected storm cases are described. First, a synoptic description of each period is given. Secondly, wind speeds and directions from measurements and model are given to illustrate the wind conditions and to assess the quality of the model wind fields. Thirdly, (tidal) surface level variations and current velocities are described. Finally, wave conditions as calculated with WAVEWATCH (including all wave-tide interactions) are discussed by considering the spatial distribution of the mean wave direction $\overline{\theta}$ (equation (4-23)) and the significant wave height H_s, defined as

$$H_s = 4 \left[\iint F(\omega,\theta)\ d\omega\ d\theta \right]^{\frac{1}{2}} \qquad (5\text{-}1)$$

Wind and wave conditions, which are distinctly different for the three cases considered, are discussed case by case in separate sections. The current conditions in the southern North Sea are tide dominated for nearly all wind conditions. Therefore the tidal depth and current fields are discussed in the following for all three cases at once, whereas current and water level information relevant for the specific cases is presented in the description of the separate cases.

Typical current velocities and directions for a tidal cycle are shown in figure 14. The maximum current velocities for this period are presented in figure 15. The largest current velocities occur in the southern North sea, with current velocities of 0.5 m/s or more south

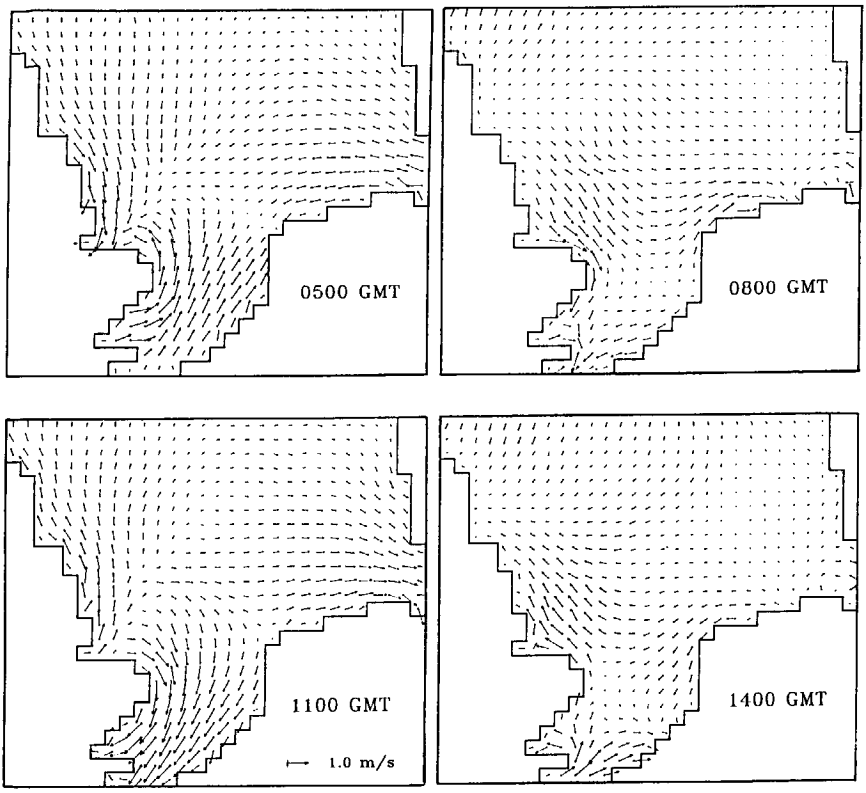

Fig. 14 Current velocities at September 26, 1987.

of K-13-A. Apart from the Dover Straits, where current velocities of over 1.5 m/s occur, the maximum current velocities in the southern North Sea are just over 1 m/s. To assess the dominant current direction, current vectors for the locations Euro-0, K-13-A and AUK are plotted at hourly intervals in figure 16 (the vector points in the direction to which the water flows). The vector plots show that the dominant current directions near Euro-0 are NE and SW. At the location K-13-A no dominant current direction can be distinguished, whereas the dominant current directions at AUK again are NE and SW. At the latter station the current velocities are small and strongly influenced by the wind. The tidal elevations (not presented here) have a range of approximately 1 m in the central and northern North Sea, 1~3 m in the southern North Sea and up to 5 m in the Dover Straits.

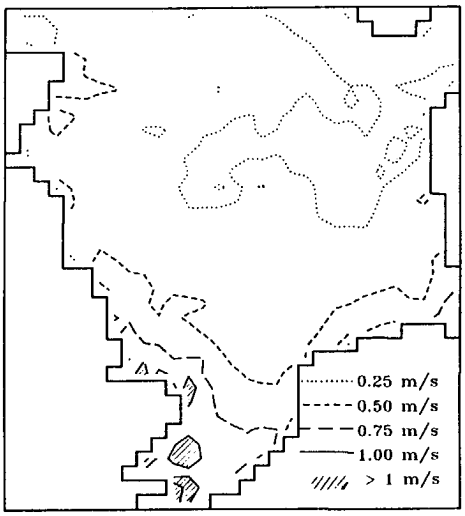

Fig. 15 Maximum current velocities at September 26, 1987.

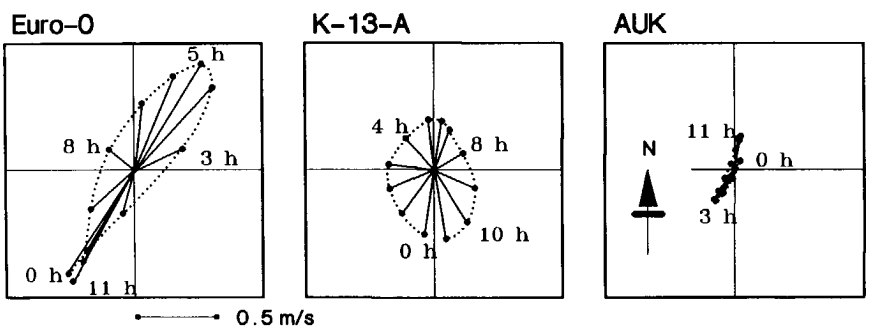

Fig. 16 Current vectors for locations Euro-0, K-13-A and AUK at September 26, 1987 (time in hours GMT).

5.2.2 **Case I : Moderate SW storm**

Case I consists of a series of southwesterly storms in the southern North Sea in the period of January 1 through January 4 1988. In the preceding days several depressions pass over the northern North Sea, resulting in SW winds over the North Sea for several days. From January 1 through January 4 three depressions travel over Scotland or the Shetland Islands in NE directions towards Scandinavia, where they

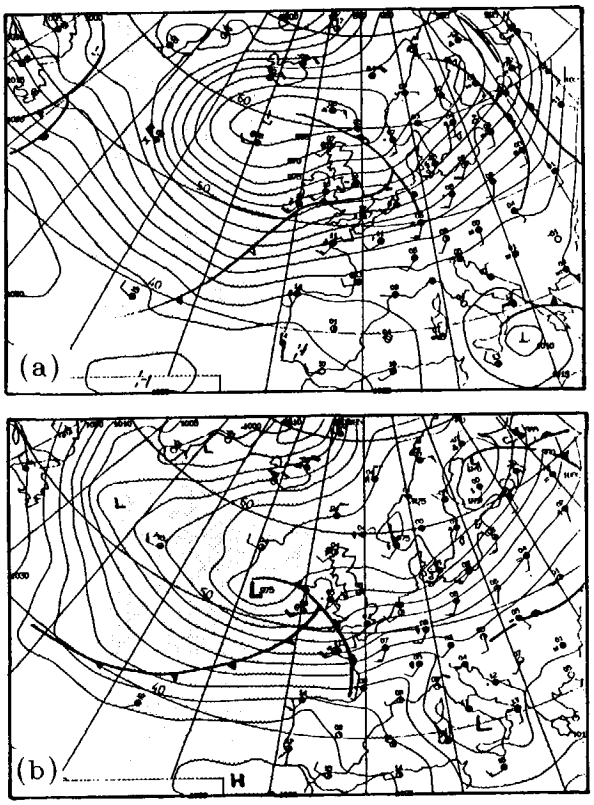

Fig. 17 Weather maps for January 2 1988, 0000 GMT (a) and January 3 1988, 1200 GMT (b) (source : dagelijkse weerberichten KNMI, ISSN 0168-9371)

become stationary and fill in (see figure 17). These depressions result in SW winds of up to Bf 7 for four days, first over the entire North Sea (January 1), later mainly near the Dutch coast and in the German Bight.

Wind speeds and directions for locations LEG, K-13-A and AUK from the UK6 model (i.e. input for WAVEWATCH) and measurements are presented in figure 18. This figure shows differences between the model wind direction and the data at all three locations of typically 20°~30°. The wind speeds of the model show a poor agreement with the data. At January 1 and 2 the wind speeds at location Euro-0 (and AUK) are underestimated by up to 6 m/s, whereas at January 3 wind speeds at K-13-A are overestimated by up to 4 m/s.

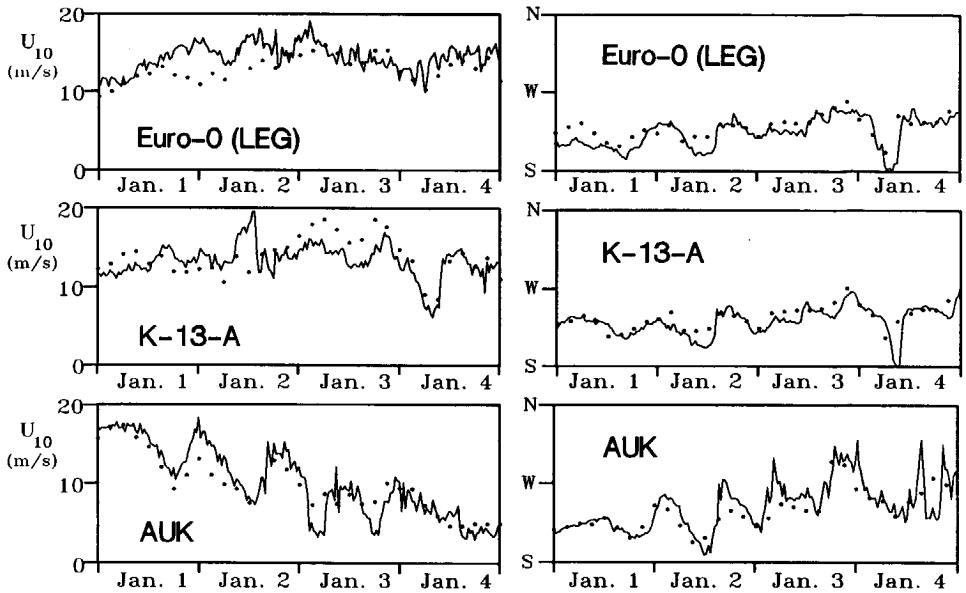

Fig. 18 Wind speeds and directions for case I at the locations Euro-0, K-13-A and AUK. • model , —— data

Such errors in the wind speed for the southern North Sea are understandable considering the relatively coarse wind grid of the UK6 model. Due to interpolations needed to obtain wind speeds at arbitrary grids, data for grid points on land is mixed with data for grid points at sea. Since wind speeds (U_{10}) on land are usually much smaller than wind speeds on sea, the large underestimations at particular at Euro-0 are explained. Such errors in particular occur for SW winds (E. Bouws, personal communication).

Considering local effects of wave-tide interactions such as the local Doppler shift, the current velocity in the propagation direction of the waves U_p ($= |\underline{U}|\cos(\bar{\theta}-\theta_c)$) is a more interesting parameter than the velocity vector $\underline{U}$. The spatial distribution of maximum and minimum current velocities U_p for case I is shown in figure 19. This figure shows that the largest current velocities U_p (positive and negative) occur in the southern North Sea southwest of the locations Euro-0 and LEG. The largest following currents ($U_p > 0$) are concentrated to a

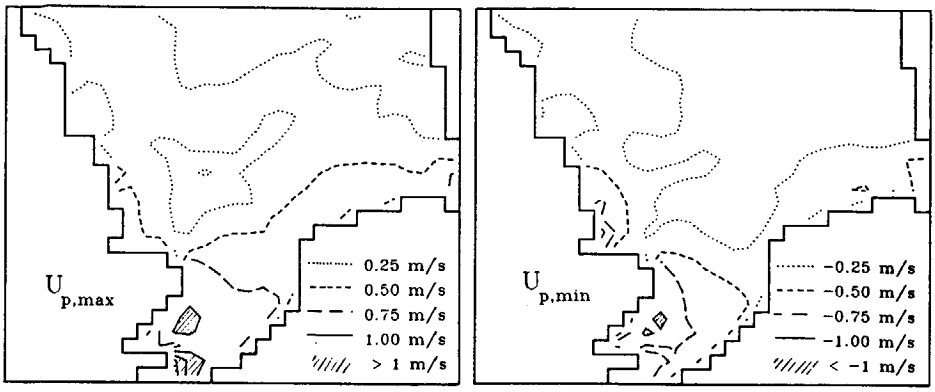

Fig. 19 Minimum and maximum current velocities in the propagation direction of the waves for case I (January 1-2 1988).

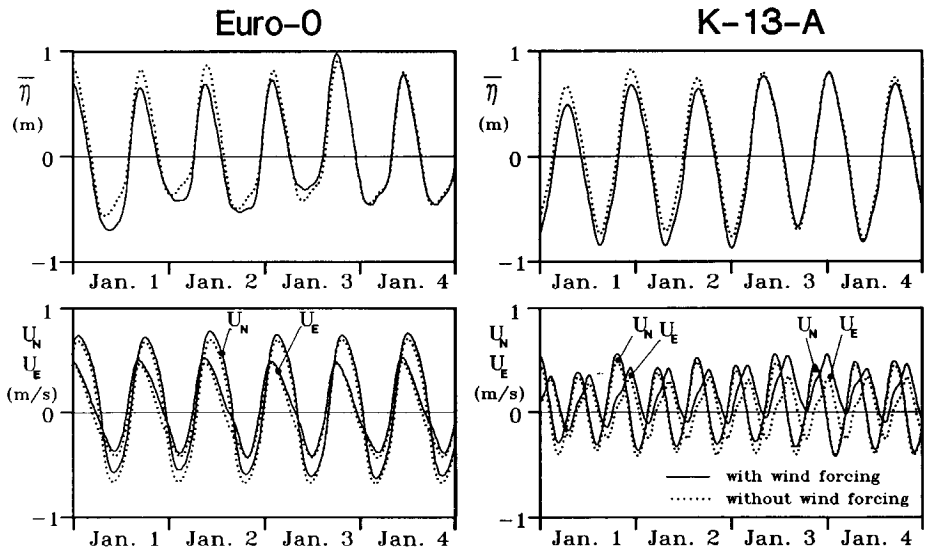

Fig. 20 Water levels $\bar{\eta}$ and velocity components U_N and U_E for case I at locations Euro-0 and K-13-A (1988).

somewhat lesser extent along the Dutch coast and in the German Bight. The differences between absolute values of the maximum and minimum current velocities U_p are largely attributed to wind forcing, as is illustrated in figure 20. This figure shows water levels $\bar{\eta}$ and

velocity components U_N and U_E (northward and eastward directions respectively) at the locations Euro-0 and K-13-A, as calculated with or without wind forcing. In particular the eastward current component at K-13-A shows a significant wind influence on January 3 and 4. Figure 20 furthermore shows a small wind-induced set-down for the first two days (approximately 0.2 m at both locations).

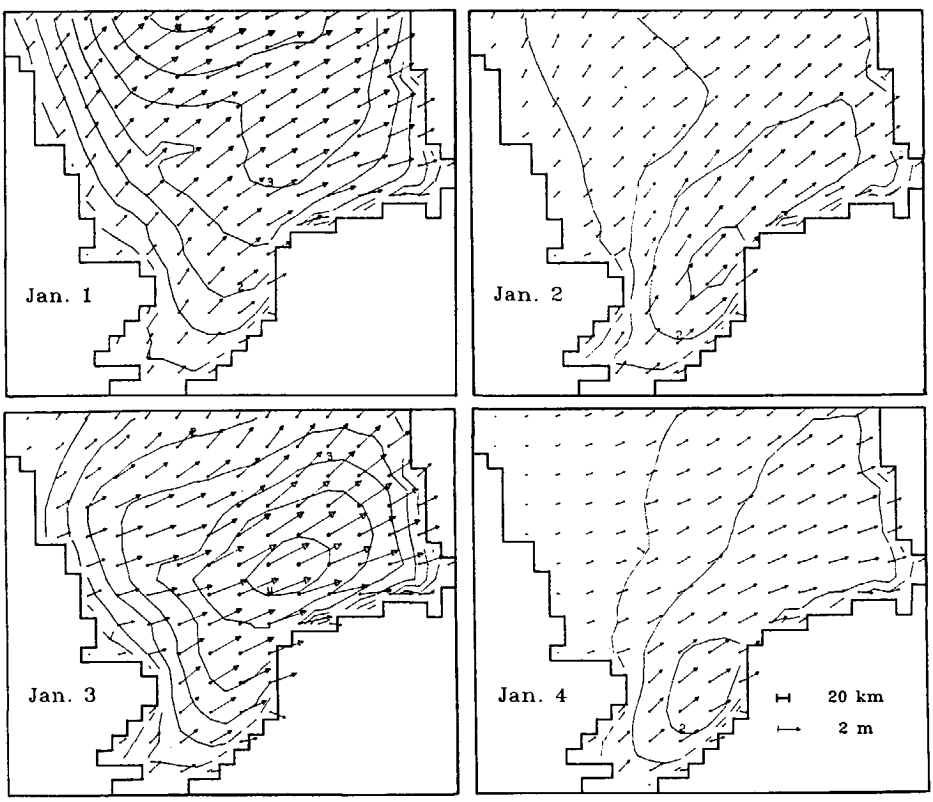

Fig. 21 Significant wave height for January 1, 2, 3 and 4 1988, 1200 GMT (contours every 0.5 m, starting with H_s = 1 m).

Significant wave heights H_s (equation (5-1)) and mean wave directions $\bar{\theta}$ (equation (4-23)) at 1200 GMT for all four days of case I are presented in figure 21 (vectors pointing in the direction to which the waves propagate). This figure shows wave heights of up to 4 m for the

central North Sea and wave heights of up to 2 m south of Euro-0 and LEG. For January 1 the largest wave heights occur over the entire North Sea, whereas for the following three days the largest wave heights are concentrated near the Dutch coast and in the German Bight. Mean wave periods (not presented here) south of Euro-0 are typically 5 s, whereas the maximum mean period in case I is approximately 7.5 s.

5.2.3 **Case II : Moderate NW storm**

Case II consists of a single northwesterly storm over the entire North Sea in the period of September 26 through September 28, 1987. In the preceding days a weak depression passes over the northern North Sea and the Norwegian Sea, resulting in weak SW winds over the entire North Sea. At September 26 a high pressure area became stationary over Ireland and a depression became stationary over the northern Baltic Sea (see figure 22). Both systems remain more or less unchanged until September 28, resulting in moderate NW winds over the entire North Sea and Norwegian Sea. The wind force is up to Bf 7 for the northern North Sea and Bf 6 in the southern North Sea.

Wind speeds and directions for locations LEG, K-13-A and AUK from the UK6 model and from measurements are presented in figure 23. This figure shows a reasonable agreement between measured and calculated

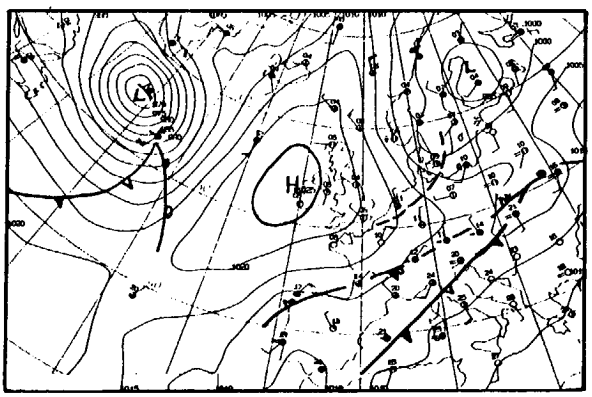

Fig. 22 Weather map for September 27 1987, 0000 GMT

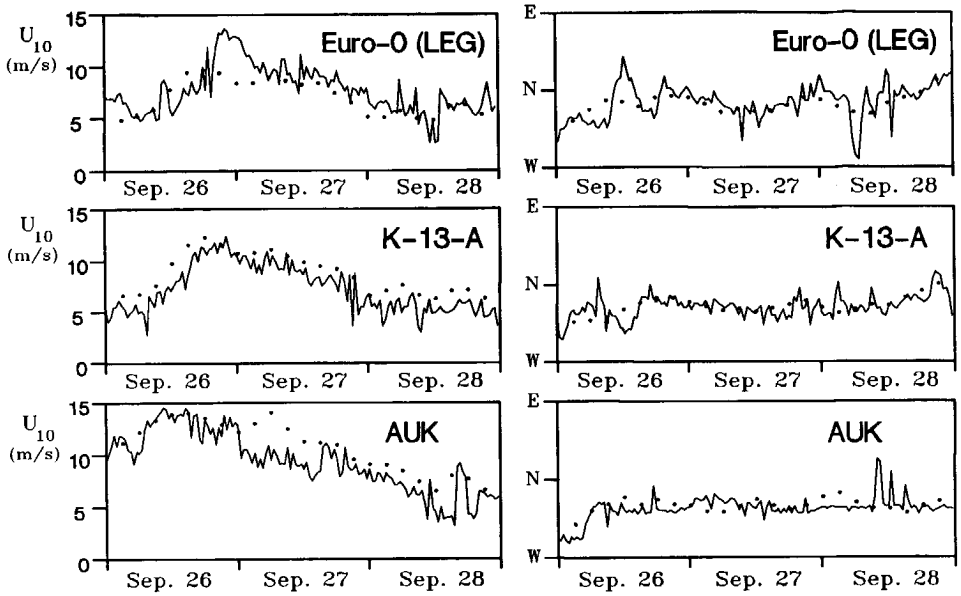

Fig. 23 Wind speeds and directions for case II at the locations Euro-0, K-13-A and AUK. • model , —— data

wind directions, except for changes in wind direction at locations Euro-0 and K-13-A on September 26. The wind speeds of the model again show a poor agreement with the data. For locations AUK and K-13-A the largest wind speeds occur, which in general are overestimated by the model. At location Euro-0 wind speeds are smaller and in general underestimated, in particular around midnight September 26.

The spatial distribution of maximum and minimum current velocity U_p for September 27 and 28 are presented in figure 24. This figure shows that the largest current velocities U_p (both following and opposing) occur in the southern part of the North Sea near the British coast. Wind influences on the currents are small, whereas the wind induces a small increase in the mean water level $\bar{\eta}$ at the first half of the period considered. This is illustrated in figure 25 for the locations Euro-0 and K-13-A.

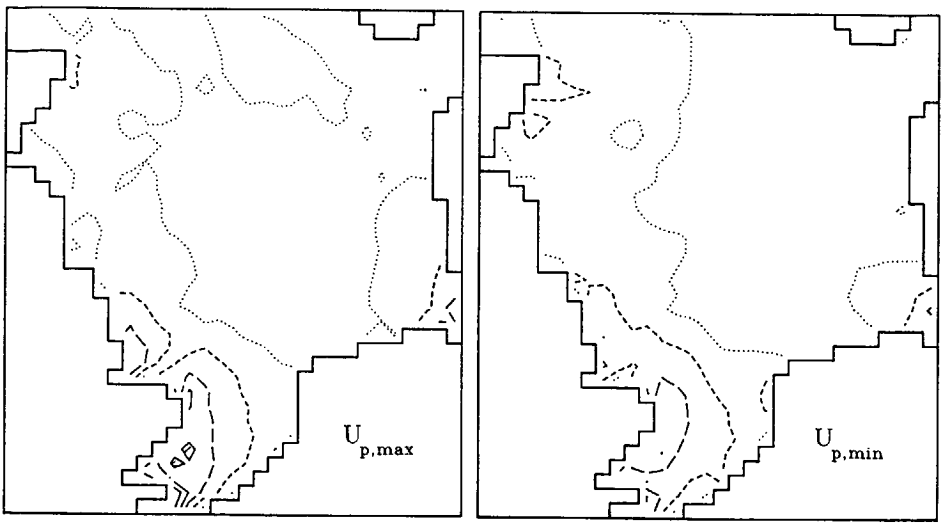

Fig. 24 Maximum and minimum current velocities in the propagation direction of the waves for case II (September 27-28 1987). Legend as in figure 19.

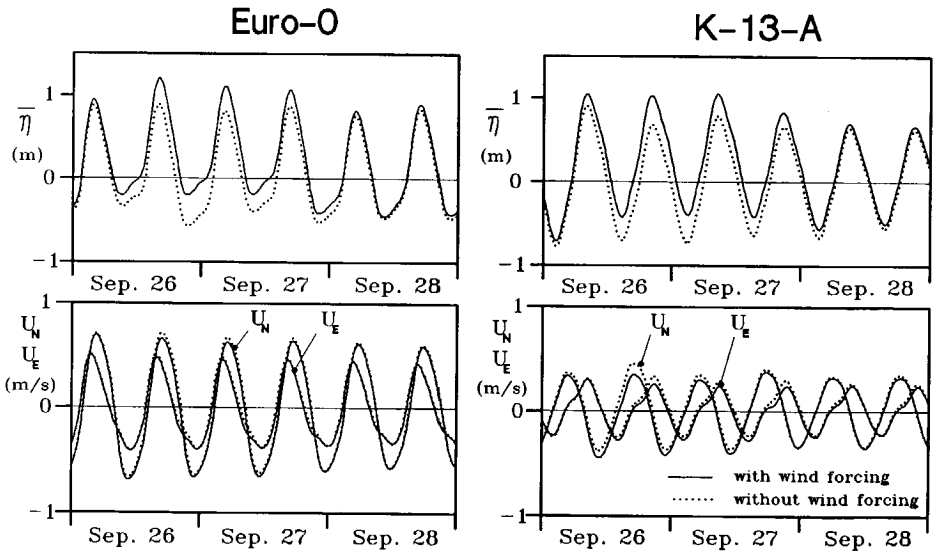

Fig. 25 Water levels $\overline{\eta}$ and velocity components U_N and U_E for case II at locations Euro-0 and K-13-A (1987).

Wave heights and directions for September 27 and 28, 0000 GMT are presented in figure 26. This figure shows that the largest wave heights are concentrated in the northern and eastern parts of the North Sea (up to 4 m). The wave heights in the southern North Sea are smaller (1~2 m). Wave periods (not presented here) in the central North Sea are as large as 9 s, whereas the wave periods in the southern North Sea are typically 6~7 s. The relatively large wave periods compared to the wave heights in the southern North Sea and near the British coast suggest that a significant part of the wave energy in these areas is generated in the central and northern North Sea (i.e. swell) and possibly even in the Norwegian Sea.

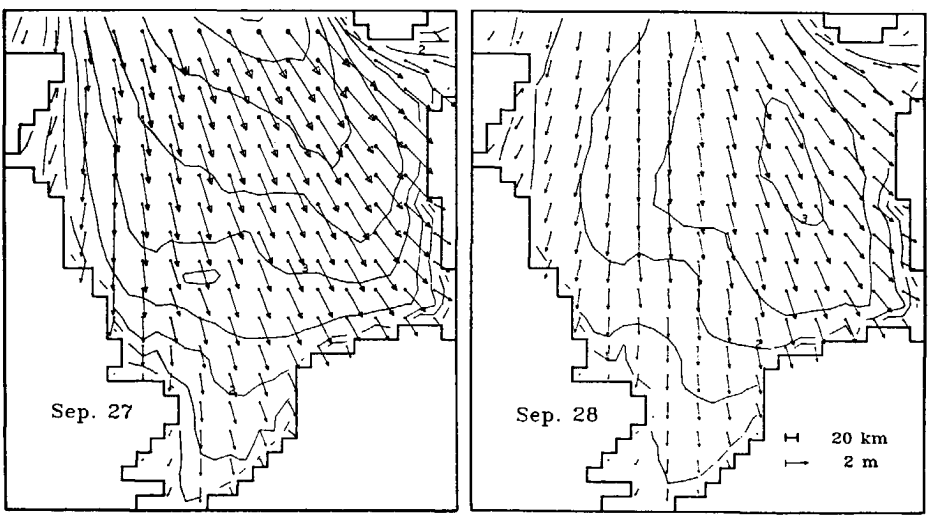

Fig. 26 Significant wave heights for September 27 and 28 1987, 0000 GMT (contours every 0.5 m, starting with H_s = 1 m).

5.2.4 **Case III : Severe NW storm**

Case III consists of a single northwesterly storm on the entire North Sea in the period of February 28 and 29, 1988. This storm is caused by a high pressure area on the Atlantic and a low pressure area over Norway (see figure 27) and causes a wind force of Bf 12 in the Northern North Sea. In the preceding days the above system slowly

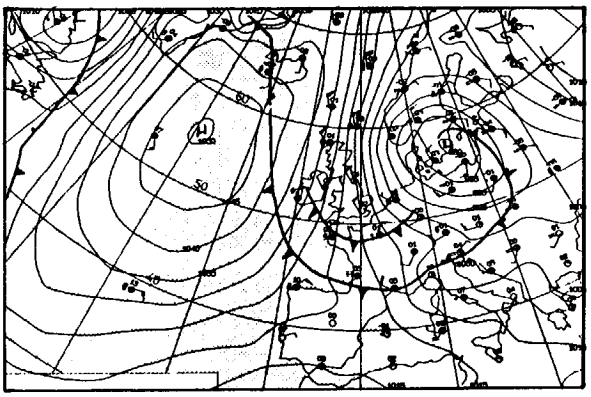

Fig. 27 Weather map for February 29 1988, 0000 GMT

builds up, resulting in moderate NW winds over the North Sea and the Norwegian Sea. Since no (continuous) wave data are available for this period, the quality of the wind field need not be assessed.

The spatial distribution of maximum and minimum current velocity U_p is shown in figure 28. This figure shows that the largest following currents ($U_p > 0$) occur in the southern North Sea near the British coast and over the Dogger Bank. The largest opposing currents are concentrated near the British coast, both in the southern North Sea and near Scotland. The current velocities are strongly influenced by the wind, as is illustrated in figure 29 for the location Euro-0 and K-13-A. This figure also shows a significant wind-induced increase in the mean water level of up to 1.5 m at Euro-0.

Wave heights (H_s) and directions ($\bar{\theta}$) for February 28 and 29 1200 GMT are presented in figure 30. This figure shows extreme wave heights of over 11 m for the central North sea and over 5 m for the southern North Sea. The largest mean periods (not presented here) are over 12 s for the central North Sea and 8-10 s for the southern North Sea.

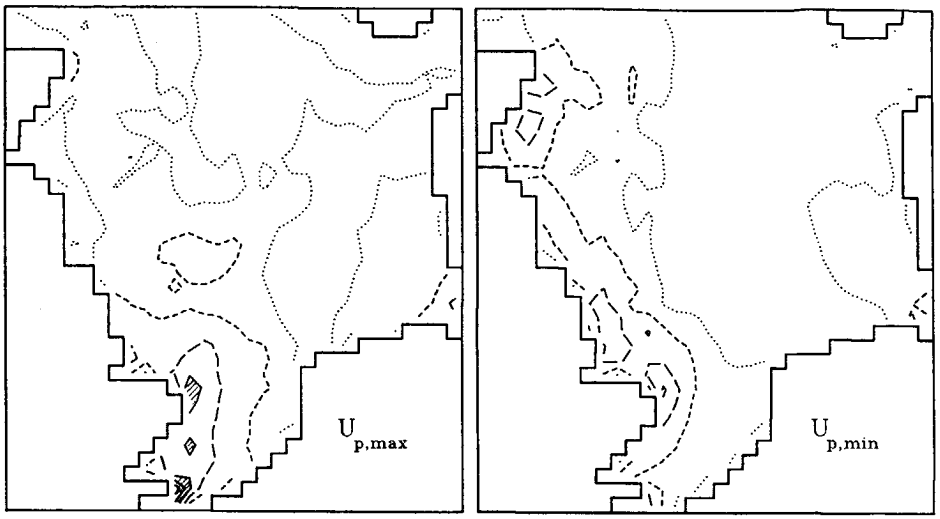

Fig. 28 Maximum and minimum current velocities in the propagation direction of the waves for case III (February 28-29 1988). Legend as in figure 19.

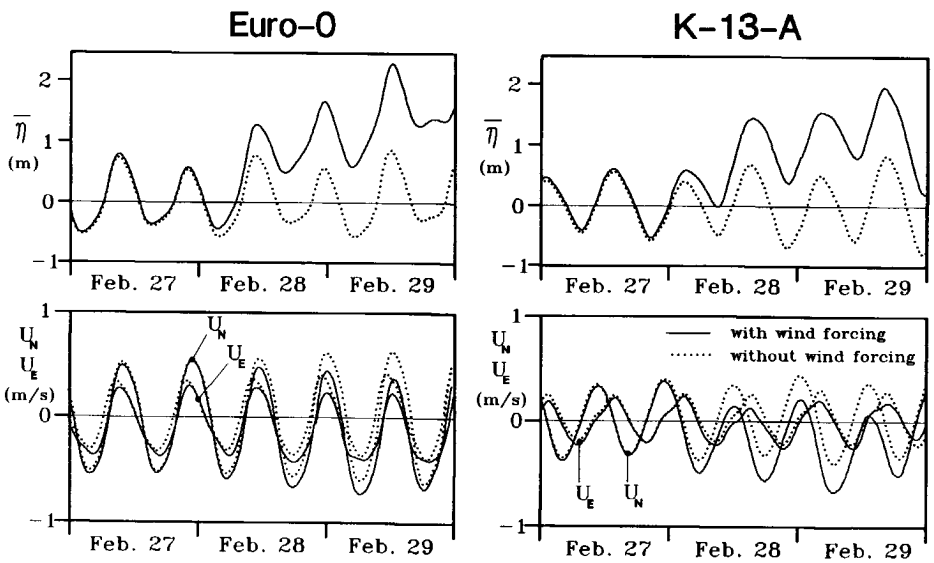

Fig. 29 Water levels $\bar{\eta}$ and velocity components U_N and U_E for case III at locations Euro-0 and K-13-A.

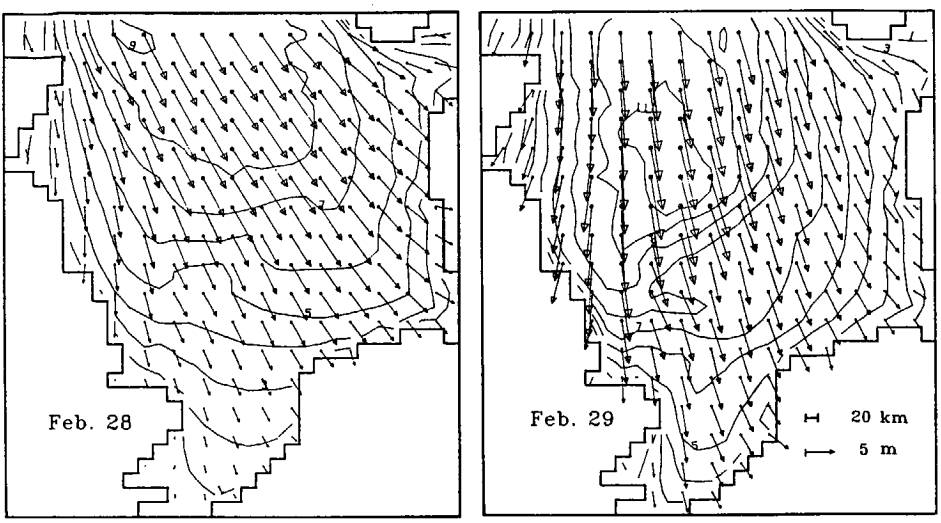

Fig. 30 Significant wave heights for February 28 and 29 1988, 1200 GMT (contours every 1.0 m).

5.3 CALCULATED WAVE-TIDE INTERACTIONS

5.3.1 Introduction

To estimate the influence of several wave-tide interaction mechanisms, numerical calculations have been performed with WAVEWATCH. By considering the six versions of WAVEWATCH as presented in table 3, the effects of (a) the total wave-tide interactions, (b) changes in absolute frequency (i.e. depth and current instationarity), (c) depth and current refraction, (d) currents in general and (e) (tidal) surface level variations in general, can be isolated. Version A of WAVEWATCH (see table 3) is used as the reference version. The total influence of tides and storm surges on waves is assessed by comparing the results of WAVEWATCH version C (without tides and storm surges) with the results of the reference version A. The influence of a single mechanism is isolated by comparing the results of one of the B versions of WAVEWATCH, in which the mechanism to be considered is neglected, with the results of the reference version A.

Table 3 Definition of different versions of WAVEWATCH

version	description
A	WAVEWATCH including all wave-tide interactions
B_1	WAVEWATCH without frequency shifts due to the instationarity of depth and current
B_2	WAVEWATCH without depth and current refraction
B_3	WAVEWATCH without (tidal) currents, i.e.(tidal) surface level variations only.
B_4	WAVEWATCH without (tidal) surface level variations, i.e. currents only.
C	WAVEWATCH including depth refraction due to the bathymetry, but without currents and surface level variations (i.e. the previous state-of-the-art).

The analysis and discussion of the model results consist of three parts. First, time series of wave parameters at selected locations are presented and discussed (section 5.3.2); secondly, the relation between tide and surge induced modulations of wave parameters and local parameters of the tides and surges is investigated (section 5.3.3) and finally the spatial distribution of tide and surge induced modulations of wave parameters is assessed (section 5.3.4). In all three sections the results are discussed case by case, since the cases have been selected to represent different aspects of wave-tide interactions.

To limit the number of data to be presented, wave-tide interactions are analyzed in detail for the locations Euro-0 and K-13-A only. These two locations were selected since they are located in areas with significant current velocities and since routine measurements of wave data are performed at these locations. An analysis of wave-tide interactions at these locations can be used in interpreting the routine measurements at these sites.

To limit the number of results to be presented, the analysis of wave-tide interactions is here limited to integral parameters of the

spectrum, i.e. the significant wave height H_s (equation (5-1)), the mean direction $\bar{\theta}$ (equation (4-23)), the mean absolute period T_a, the mean relative period T_r and the mean wave length L :

$$T_a = \overline{2\pi/\omega} \tag{5-2}$$

$$T_r = \overline{2\pi/\sigma} \tag{5-3}$$

$$L = \overline{2\pi/k} \tag{5-4}$$

where the overbar denotes the average over the variance density spectrum $F(\omega,\theta)$ as in equation (2-31). Note that T_r and L are closely related since σ and k satisfy equation (2-1) locally, so that either T_r or L could be omitted (see e.g. section 4.3.2). For convenience of discussion however, both are considered here.

Since effects of wave-tide interactions within the spectrum can be much more distinct than effects of wave-tide interactions on average spectral parameters (as will be shown below), the total variance in four spectral bands (F_1 through F_4) is also assessed for some of the cases:

$$F_n = \int_{f_{a_1}}^{f_{a_2}} \int_0^{2\pi} F(f_a,\theta)\, d\theta\, df_a \tag{5-5}$$

F_1 : $f_{a_1} = 0.04$ Hz , $f_{a_2} = 0.1$ Hz

F_2 : $f_{a_1} = 0.1$ Hz , $f_{a_2} = 0.2$ Hz

F_3 : $f_{a_1} = 0.2$ Hz , $f_{a_2} = 0.3$ Hz

F_4 : $f_{a_1} = 0.3$ Hz , $f_{a_2} = 0.5$ Hz

At locations K-13-A and Euro-0 the 4^{th} band (F_4) is in the high frequency saturation range of the spectrum for all cases considered here. The first band (F_1) is always at the low frequency flank of the spectrum (frequencies lower than the spectral peak frequency). Note that the variance in the latter frequency band equals the parameter E_{10} as used in ship admittance policy for the port of Rotterdam. The middle two frequency bands include the spectral peak.

5.3.2 Model results for Euro-0 and K-13-A

Case I : (moderate SW storm)

For the moderate SW winds of case I, waves at the southern North Sea are essentially deep water waves. Therefore tidal surface level variations do not influence wave propagation or generation, and wave-tide interactions are essentially caused by currents only. At the locations Euro-0 and K-13-A the results of WAVEWATCH versions A and B_4 (or C and B_3) indeed are identical, so that the results of calculations with surface level variations only or currents only (WAVEWATCH versions B_3 and B_4) need not be discussed separately. Furthermore refraction shows no influences at the locations considered here (i.e. results of WAVEWATCH versions A and B_2 are practically identical, tide-induced modulations of $\overline{\theta}$ of the order of 1°). For depth refraction this was expected, since the waves are essentially in deep water. For current refraction this is less obvious, but still expected, since the tidal currents in the southern North Sea are relatively uniform with small gradients (see e.g. figure 14). Consequently the results of WAVEWATCH version B_2 (no refraction) or the behaviour of the mean direction $\overline{\theta}$ need not be discussed.

In figure 31 the significant wave height H_s, the mean absolute and relative periods T_a and T_r and the mean wave length L are presented as a function of time (January 1 and 2 only, since the calculations with the B versions of WAVEWATCH have been performed for this period only). The effects of the total wave-tide interaction is assessed by comparing the solid and dotted lines in this figure (WAVEWATCH versions A and C respectively). Figure 31 shows that the effects of the total wave-tide interactions are distinct in all parameters considered here (i.e. of the order of 10% for Euro-0). At location Euro-0 the effects of wave-tide interactions are significantly larger than at location K-13-A, which corresponds to the stronger current velocities at Euro-0 (see figures 19 and 20). Apparently the wave-tide interactions are mainly dominated by the local currents. The effects of the tides are most pronounced in the absolute period and least pronounced in the relative period.

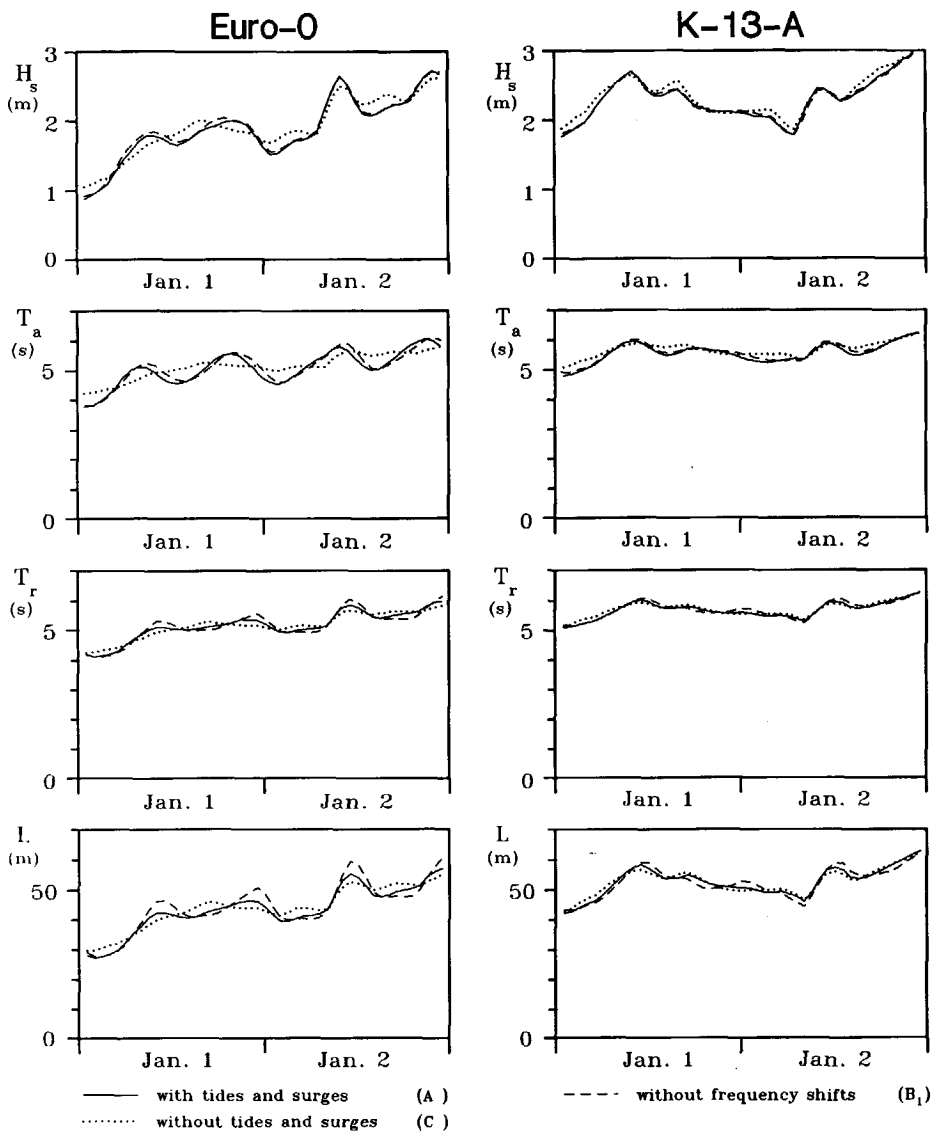

Fig. 31 Significant wave height, mean absolute and relative periods and mean wave length at locations Euro-0 and K-13-A for case I (1988).

The distinct tide-induced modulations of the absolute period suggests that the instationarity of depth and current is important. If, however, the instationarity is neglected (B_1, dashed lines in figure 31), a tide-induced modulation of the absolute period with approximately the same amplitude, but with a delay of 1 to 2 hours is observed. The latter modulation of the absolute period can only be caused in the generation process, due to either the correction to the wind speed (U_{10_r} versus U_{10}), or due to indirect effects of modulations of wavenumber and intrinsic frequency. Ignoring the instationarity of

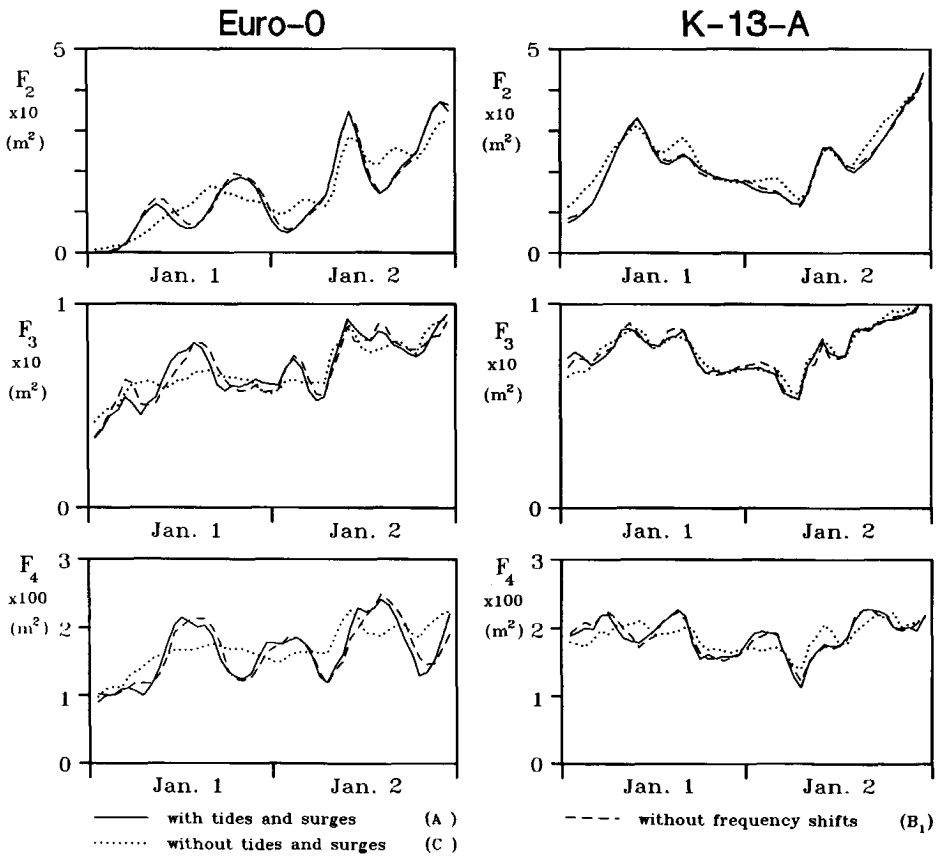

Fig. 32 Total variance in several frequency bands at locations Euro-0 and K-13-A for case I (1988).

depth and current has little effect on the predicted wave heights, but introduces significant errors in the predicted wave lengths at the two locations considered here.

In figure 32 the total variance in several frequency bands is shown (F_2 through F_4, F_1 is negligible for this case). The total variance in separate frequency bands is obviously much more sensitive to tidal influences than integral parameters of the spectrum. The behaviour of the variance in the separate frequency bands will be discussed in more detail in the following section.

Case II : (moderate NW storm)

As in case I, the waves in case II are essentially in deep water so that all wave-tide interactions are caused by currents. Only the variance in the lowest frequency band considered (F_1, figure 34) shows a small influence of the surface level variations (and of depth refraction). The discussion of the effects of wave-tide interactions on mean wave parameters is therefore again limited to the results of WAVEWATCH versions A, C and B_1 (with tides and surges, without tides and surges and without instationarity respectively). As in case I, tidal influences on the mean direction $\overline{\theta}$ are negligible.

In figure 33 mean wave parameters are presented. The effects of tides and surges are somewhat smaller than in case I, which is understandable since the components of the current velocity in the mean propagation direction of the waves are smaller due to the different mean wave directions (compare e.g. figures 16, 21 and 26). The effects of the tides are most pronounced in the wave length and practically negligible in the wave height (in particular at Euro-0).

At Euro-0 the tidal modulations of the absolute and relative period are of the same order of magnitude. This suggests that the effects of the instationarity of depth and current cannot be ignored compared to the effects of the inhomogeneity. In this case such a conclusion is supported by the results of WAVEWATCH version B_1 (without instationarity, dashed lines in figure 33), in which such a modulation of the absolute period is not observed. At K-13-A modulations of the absolute

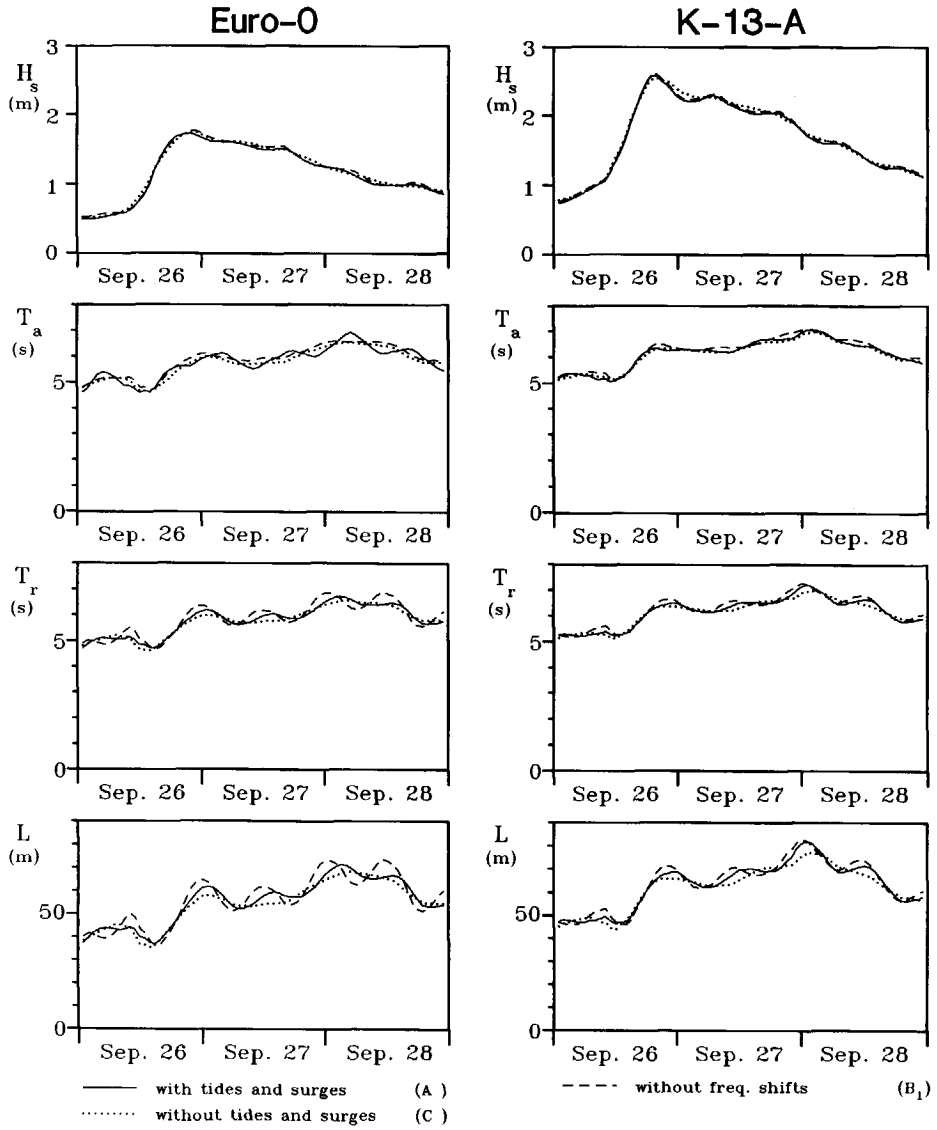

Fig. 33 Like figure 31, case II (1987).

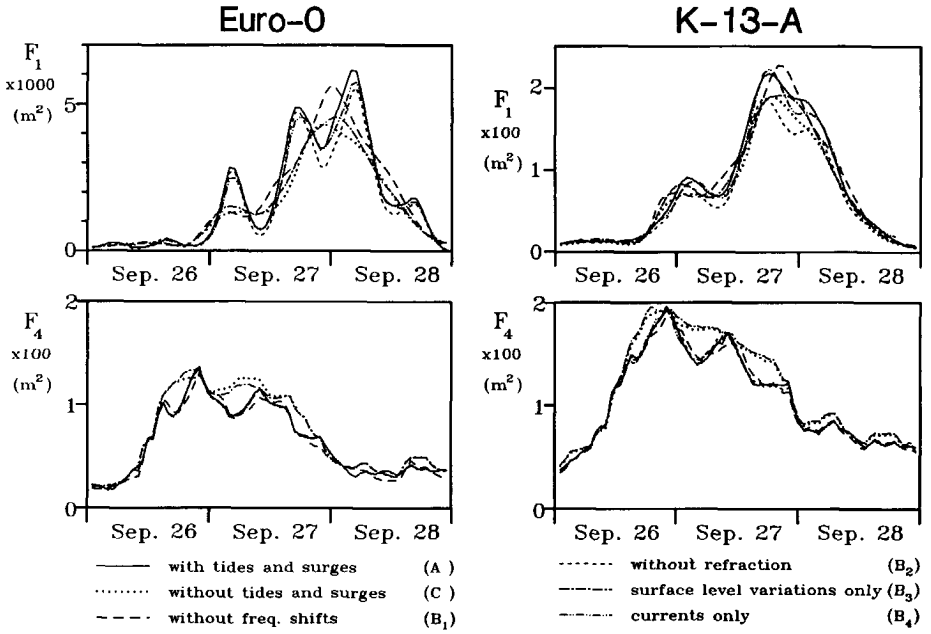

Fig. 34 Like figure 32, case II (1987).

and relative period are too small to discuss the effects of the instationarity using the data of figure 33 only.

In figure 34 the total variance in the highest and lowest frequency bands (F_1 and F_4) are presented. The first half of this period shows distinct effects of the local winds on the high frequency variance F_4 (high variance levels at times of high wind velocities, see figure 23), which decrease in the second half of this period. The low frequency variance in the second half of the period is consequently generated elsewhere, i.e. it corresponds to swell. The low frequency variance F_1 shows large influences of wave-tide interactions, in particular at Euro-0. All mechanisms considered (instationarity, refraction, surface level variations and currents) have a distinct influence on the predicted low frequency variance.

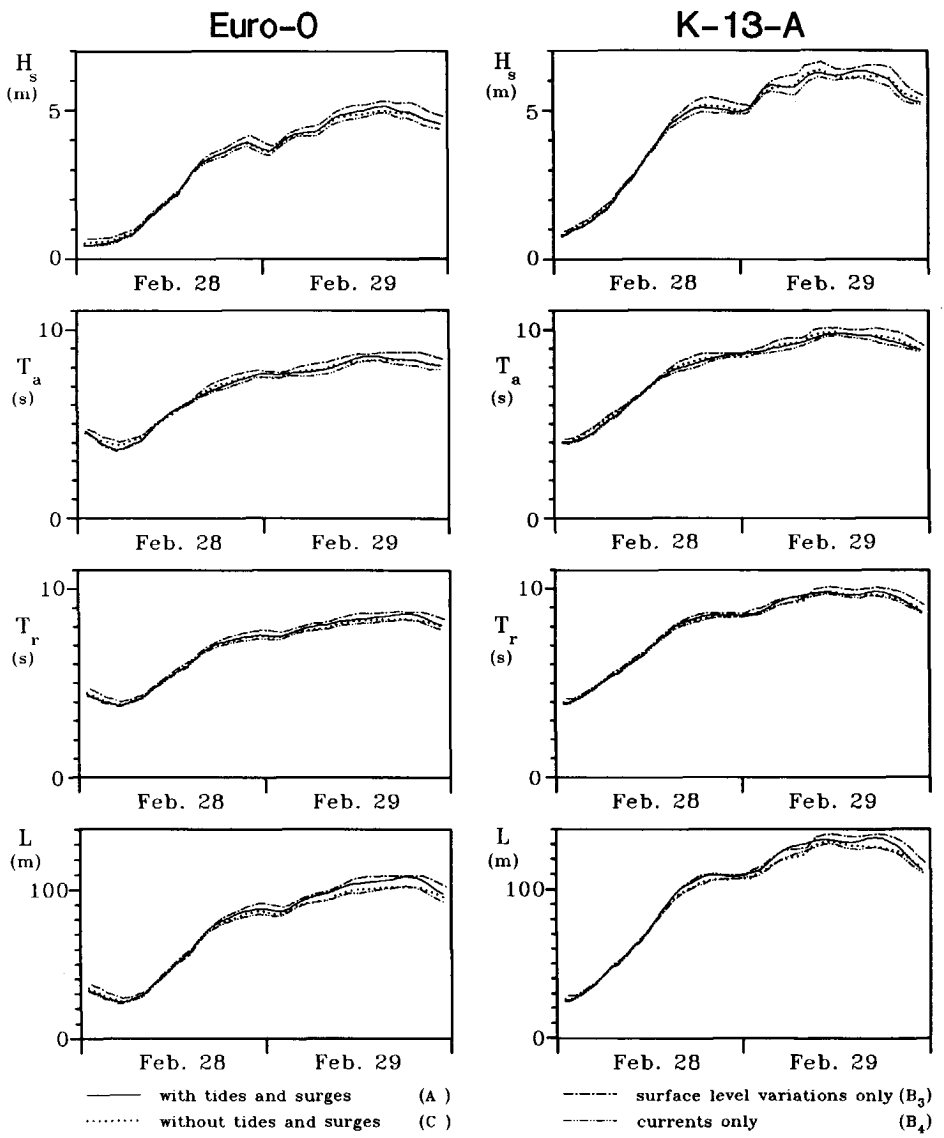

Fig. 35 Like figure 31, case III (1988).

Case III : (severe NW storm)

In figure 35, integral wave parameters for case III are presented. For convenience of presentation, the results of WAVEWATCH versions B_1 and B_2 (no instationarity or refraction) are not presented in this figure. The effects of depth and current instationarity are roughly identical to those of case II, and will be discussed in more detail in the following section. Effects of (depth) refraction can be distinguished in all mean wave parameters. For all mean wave parameters considered here, except for the mean direction $\overline{\theta}$ (change at Euro-0 up to 5°), the effects of refraction are smaller than those of surface level variations or currents (for the locations considered here).

The effects of the total wave-tide interactions as presented in figure 35 (WAVEWATCH version A versus C, solid and dotted lines) are smaller than in the other two cases, and are practically negligible. The separate contributions of surface level variations and currents to the total wave-tide interactions are significantly larger (compare results of WAVEWATCH versions B_3 and B with A and C respectively), but still small. For the case and locations considered here the effects of surface level variations and currents largely cancel out.

As shown in figure 35, the effects of surface level variations and currents occur on a time scale which is much larger than the period of the tide. A comparison with the time scales of modulations of e.g. the mean water level $\overline{\eta}$ (see figure 29), suggests that the interactions are dominated by influences of the storm surge rather than the tide. For this particular case some influence of surface level variations might be expected since the waves at the southern North Sea are in shallow water and since the surface level is significantly increased by wind forcing. The surface level variations result in a increase of wave heights, periods and lengths. This can be explained since the waves at the southern North Sea are severely depth limited. The increase in water depth due to the storm surge (figure 29) reduces the energy dissipation at the bottom boundary layer and consequently results in larger and longer waves. The currents on the other hand result in reduced wave heights, periods and lengths. This can be explained from the wind-induced currents, which in the southern North sea are systematically in the propagation direction of the waves (figures 28 and

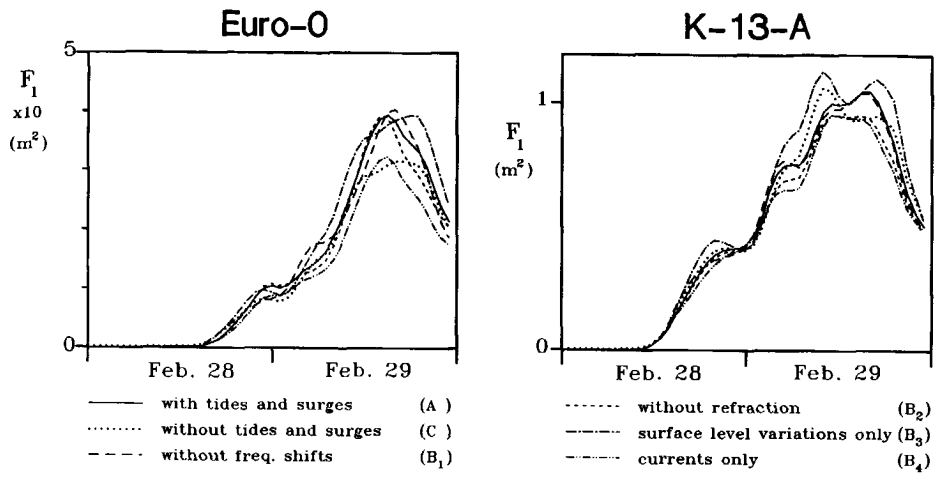

Fig. 36 Like figure 32, case III (1988).

29). Such residual currents reduce the effective (i.e. relative) wind speed and the effective fetch, resulting in smaller wave heights and lengths than would be obtained if the currents are neglected.

To illustrate the influence of the tides and surges on details of the spectrum, figure 36 shows the total variance in the lowest frequency band considered (F_1). Without discussing details of the results of the different versions of WAVEWATCH, it can nevertheless be concluded that this figure shows distinct influences of all mechanisms considered.

5.3.3 Wave-tide interactions in relation with the local depth and current

The relation between tidal variations of wave parameters and local parameters of the tides (and surges) is of interest, since such a relation can show to which extent wave-tide interactions can be estimated from local parameters of the tide only. In the numerical calculations the effects of wave-tide interactions are isolated simply by considering the differences in the results of calculations with WAVEWATCH versions A and C. For the significant wave height H_s for

instance, the tide-induced modulation ΔH_s for a given time and place is calculated as :

$$\Delta H_s = H_{s,A} - H_{s,C} \qquad (5\text{-}6)$$

where the suffices A and C indicate results of WAVEWATCH version A and C respectively. Considering the results as presented in the previous section, wave-tide interactions are dominated by currents (except for the extreme conditions of case III). As follows from the Doppler-type equation (2-6), the current velocity which governs wave-tide interactions is the current velocity in the propagation direction of the waves U_p. For any time and location U_p is estimated from the results of the reference version A of WAVEWATCH as :

$$U_p(t) = |\underline{U}| \cos(\theta_c - \overline{\theta}) \qquad (5\text{-}7)$$

where θ_c is the current direction and $\overline{\theta}$ the mean wave direction (equation (4-23)). As in the previous section, the mean direction $\overline{\theta}$ will not be assessed since current influences on the mean direction in general are small (of the order of magnitude of 1°). Furthermore the mean wave length will not be assessed, since it is related directly to the relative period through in equation (2-1).

Case I : (moderate SW storm)

In figure 37 tide-induced modulations of several mean wave parameters at Euro-0 and K-13-A are presented as a function of the current velocity U_p. For both locations the tide-induced modulations of the mean wave parameters show a clear hysteretic dependence on the (local) current velocity U_p. Both the modulation of the wave height ΔH_s and of the absolute period ΔT_a show a systematic decrease with increasing current velocity U_p, with a phase shift relative to the current velocity. This phase shift practically disappears when ΔH_s and ΔT_a are shifted backwards in time by approximately 1.5 h and 1 h respectively, resulting in a one-to-one dependence of ΔH_s and ΔT_a on U_p (decreasing ΔH_s and ΔT_a for increasing U_p). Consequently the phase shift corresponds to time lags of approximately 1.5 h for the wave height and 1 h for the absolute period. The time lags could be caused by effects

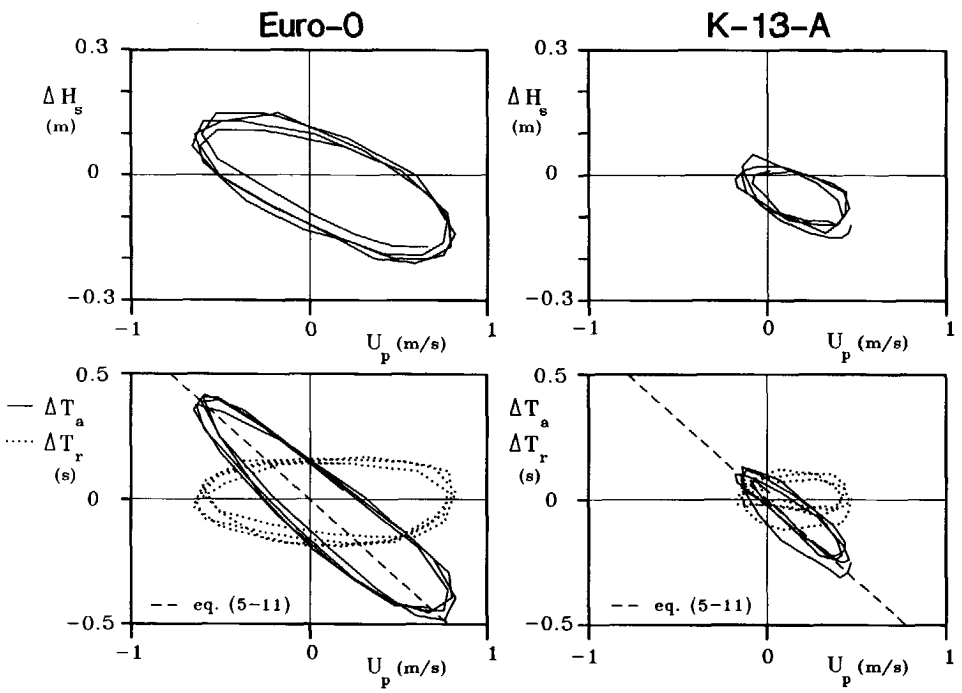

Fig. 37 Current-induced modulations of the wave height, absolute and relative period as a function of the current velocity in the propagation direction of the waves U_p (Case I, January 1-2 1988).

of propagation or generation; however, the actual origin of the effects is not easily isolated. Note that such time lags cannot be related to numerical errors, since they are much larger than the numerical time step (i.e. 15 min.).

The tide-induced modulations of the relative period are strongly related to those of the absolute period, the difference corresponding to the Doppler shift. For narrow-banded spectra, the difference between the absolute and relative period can be calculated directly as a function of U_p and the mean relative depth $\bar{k}d$. For narrow banded spectra, using equation (2-1), equations (2-6) becomes :

$$\bar{\omega} = \bar{\sigma} + \bar{\sigma}^2 \left[g \tanh(\bar{k}d) \right]^{-1} U_p \qquad (5\text{-}8)$$

which, using equations (5-2) and (5-3), can be written as :

$$T_a = T_r \left[1 + 2\pi \left[g \tanh(\bar{k}d)\, T_r \right]^{-1} U_p \right]^{-1} \qquad (5\text{-}9)$$

The second term in the brackets at the right hand side of this equation is much smaller than 1 for relatively small differences between the absolute and relative periods. Using a first order Taylor series expansion for the term on the right hand side, the difference between the absolute and relative period becomes :

$$T_a - T_r = -2\pi \left[g \tanh(\bar{k}d) \right]^{-1} U_p \qquad (5\text{-}10)$$

Figure 37 shows that tide-induced modulations of the absolute period are much larger than the corresponding modulations of the relative period. This suggests that the change in absolute period (except for the phase lag) can be estimated using a quasi-homogeneous approximation, in which the change of absolute period corresponds to the Doppler shift, so that :

$$\Delta T_a = -2\pi \left[g \tanh(\bar{k}d) \right]^{-1} U_p \qquad (5\text{-}11)$$

As is illustrated in figure 37, this equation indeed describes the change of absolute period, except for the phase lag. Consequently the instationarity of depth and current is dominant. If the instationarity is neglected (WAVEWATCH version B_1), the time lag of the modulations of the absolute period ($\Delta T_a = T_{a,B_1} - T_{a,C}$ in such an approach) becomes even larger, as follows from figure 31 (i.e. the modulations dashed line for T_a show a small time lag compared to the modulation of solid line). Similarly the modulation of the relative frequency becomes approximately twice as large, if the instationarity is neglected (see figure 31).

In figure 38 the tide-induced modulations of the total variance in several frequency bands are presented. The tide-induced modulations at both locations show similar behaviour. At the lowest frequency band shown (F_2), the total variance decreases with increasing current velocity U_p, with a time lag of approximately 2 hours. At the middle

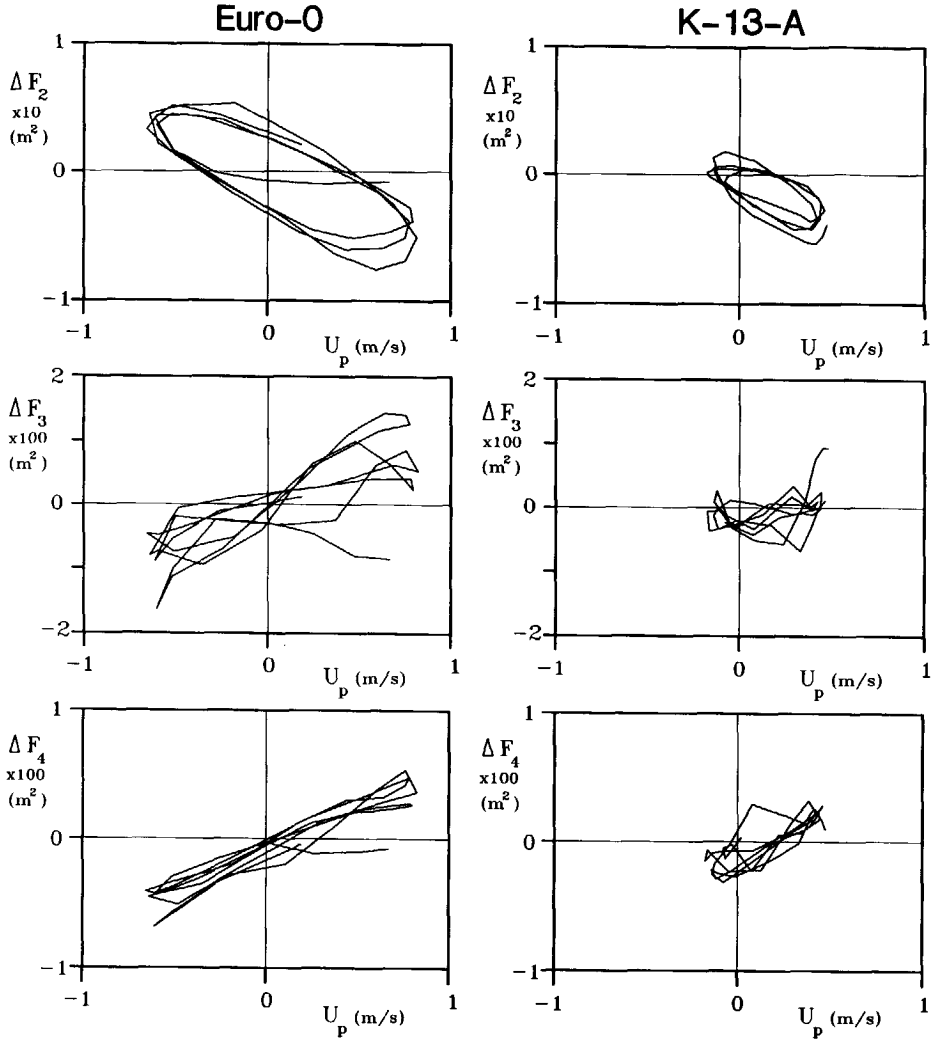

Fig. 38 Current-induced modulations of the total variance in several (absolute) frequency bands as a function of the current velocity in the propagation direction of the waves U_p (case I, January 1-2 1988).

frequencies (F_3) the tide-induced modulations of the total variance does not show a clear correlation with U_p. At the high frequency tail, the total variance (F_4) shows an increase with increasing current velocity U_p, without time lags.

The behaviour of the total variance in the lowest frequency band is similar to the tide-induced changes of the significant wave height and the absolute period as shown in figure 37. Considering the different scales for the different panels in figure 38, the major part of the tide-induced modulations of the wave height are concentrated in this frequency band. Consequently the current-induced modulations of the variance in the lowest frequency bands should show the same behaviour as the current-induced modulations of the significant wave height. Considering the behaviour of the mean absolute period, the spectral peak shifts to higher (absolute) frequencies for increasing values of U_p, so that the low frequency tail of the spectrum is also expected to shift to higher frequencies. Consequently the spectral density at fixed frequencies in the low frequency tail of the spectrum decreases with increasing current velocity, which explains the behaviour of the total variance in these low frequency bands.

The behaviour of the current-induced modulations of the total variance in the high frequency tail of the spectrum (F_4) can be explained by assuming that at these high frequencies the spectrum is saturated, which makes the high frequency tail of the k-spectrum (and the relative frequency spectrum) invariant with respect to currents. The high frequency tail is generally parameterized as :

$$F(f_r) = C\, f_r^{-m} \qquad (5\text{-}12)$$

C is a constant with dimension L^2T^{1-m} and m is a non-dimensional constant, equal to 4 or 5. Applying a Jacobean transformation to this spectral shape, an expression for the shape of the high frequency tail of the absolute frequency spectrum is obtained :

$$F(f_a) = C\, f_a^{-m} \left[1 - kU_p/\omega \right]^{1-m} \left[1 + kU_p/\omega \right]^{-1} \qquad (5\text{-}13)$$

This equation shows an increase of the saturation level of the absolute frequency spectrum for increasing current velocities U_p; for $kU_p/\omega \ll 1$, this increase is proportional to U_p, which is in qualitative agreement with the results as presented in figure 38. Figure 38 furthermore shows no time lag between the current-induced modulation in F_4 and U_p, which suggests that the current-induced modulations of

the high frequency flank of the spectrum are locally determined. This could be expected since the variance density at the high frequency tail of the spectrum is locally determined.

The middle frequency band describes the transition between the two extreme frequency bands. Since this frequency band can contain both the spectral peak and parts of the high and low frequency flanks, the low correlation is explained.

Since the variance in the different frequency bands show similar behaviour in the other two cases, they will not be discussed in the following.

Case II : (moderate NW storm)

In figure 39, tide-induced modulations of several mean wave parameters are presented as a function of the current velocity U_p. As in case I, these modulations are strongly related to the current velocity U_p. However, the behaviour for both cases shows large differences. In case II the tide-induced modulation of the wave height shows a time lag of approximately 3 hours compared to the current velocity U_p. Although the current velocities U_p at Euro-0 are clearly larger than at K-13-A, the modulations of the wave height ΔH_s are smaller, unlike in case I. This behaviour has not been explained satisfactorily. Furthermore current-induced modulations of the wave periods at K-13-A in case II show a different behaviour than in case I, which is discussed below.

Figure 39 shows that at location K-13-A the modulations of the relative period are more distinct than the modulations of the absolute period. This suggests that the effects of inhomogeneity of depth and current dominate over effects of instationarity for this location. Considering figure 14, location K-13-A is just south of a region with strong variations of the current direction. This results in relatively large spatial gradients of the current velocity U_p, in particular in NE-SW and N-S direction (see figure 24). Since the waves in this case approach K-13-A from northerly directions (see figure 26), they encounter significant gradients of U_p just before reaching K-13-A.

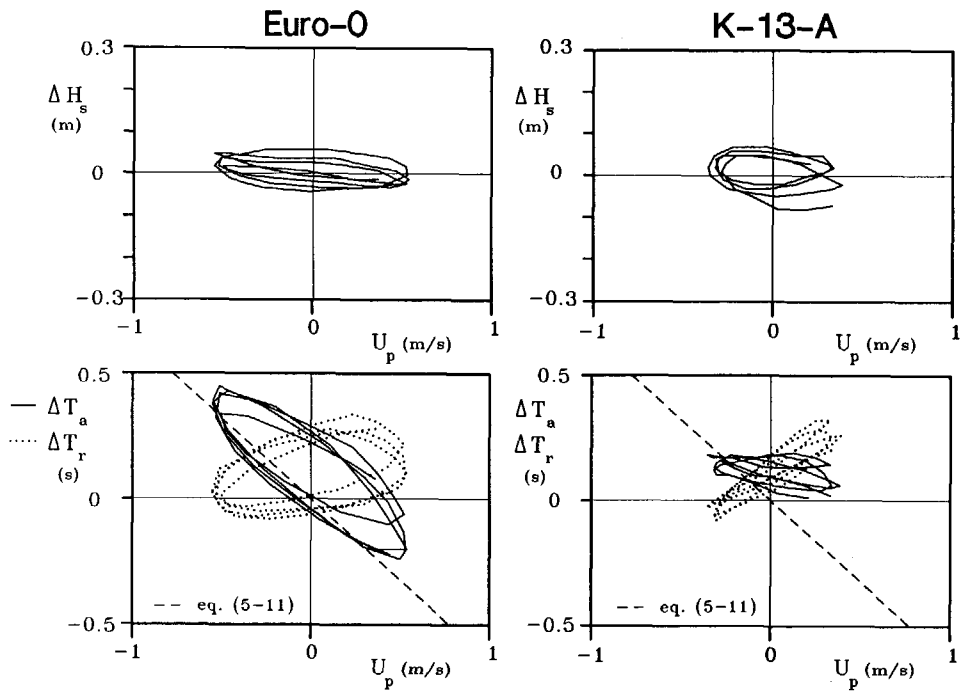

Fig. 39 Like figure 37, case II, September 27-28 1987.

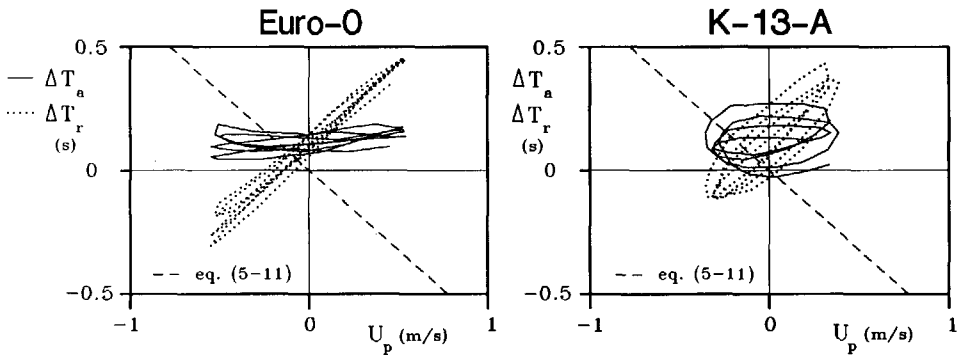

Fig. 40 Current-induced modulations of the absolute and relative period as a function of the current velocity in the propagation direction of the waves U_p. Case II, September 27-28 1987, instationarity of depth and current neglected.

This explains the apparent dominance of depth and current inhomogeneity at K-13-A.

At Euro-0 the tidal modulations of the absolute period are more distinct than those of the relative period(figure 39). Apparently the instationarity is dominant at Euro-0 as in case I.

The effects of the instationarity at both locations is further illustrated with the results of WAVEWATCH version B_1 (no instationarity) in figure 40, where tide-induced modulations of the absolute and relative period for this version of WAVEWATCH (i.e. $T_{a,B_1} - T_{a,C}$ and $T_{r,B_1} - T_{r,C}$) are presented in figure 40. A comparison of figures 39 and 40 shows that the instationarity causes practically the entire current-induced modulation of the absolute period at Euro-0, including the phase lag. At K-13-A the instationarity has a much smaller influence on the modulations of the periods (i.e. the inhomogeneity is dominant).

Case III : (severe NW storm)

In figure 41 tide-induced modulations of the significant wave height and the mean absolute and relative period are presented for case III as a function of the current velocity U_p.

The tide-induced modulations of the wave heights at Euro-0 and K-13-A show large differences. At K-13-A the modulation of wave height is strongly related to the tidal current velocity, displaying a similar oscillating character. At Euro-0, however, the modulation of wave height is shows both a trend and an oscillation, where the trend dominates, suggesting a dominant influence of the wind-induced increase of the mean water level, as discussed in section 5.3.2.

The tide-induced modulations of the absolute and relative periods at locations K-13-A and Euro-0 differ as in case II. At K-13-A both the relative and absolute period show distinct tide-induced modulations. Compared to case II, the modulation of the relative period is less dominant. This might be explained as the waves in case III come from more westerly directions (figure 30) than in case II, resulting in smaller spatial gradients of U_p (figure 28) and consequently in a

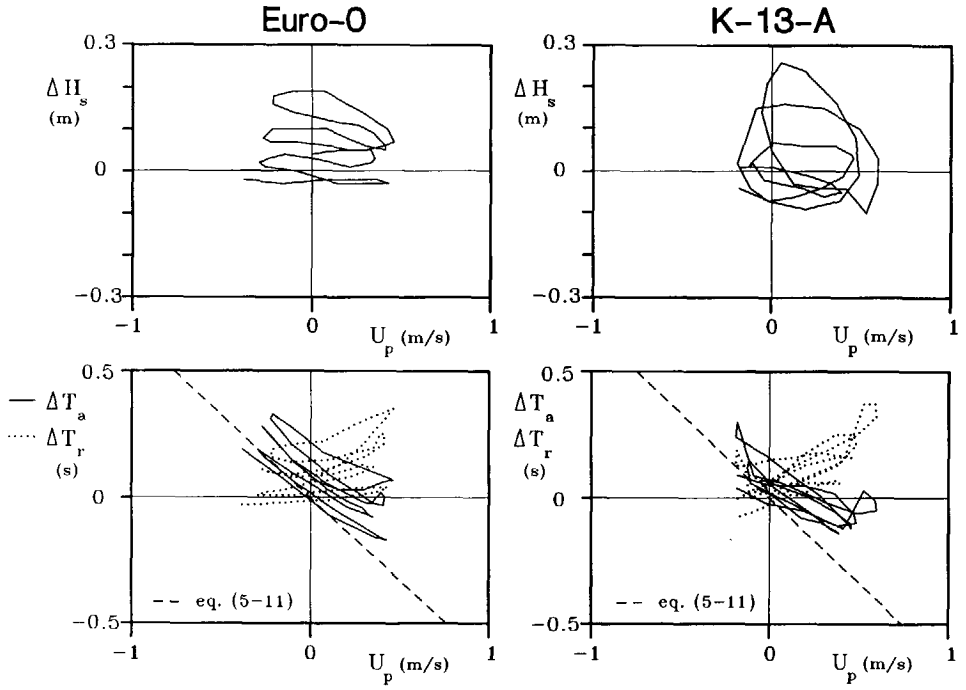

Fig. 41 Like figure 37, case III, February 28-29 1988

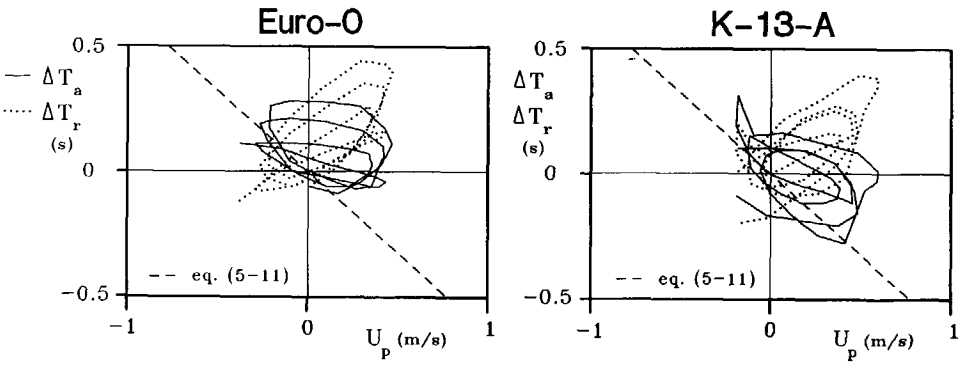

Fig. 42 Like figure 40, case III, February 28-29 1988, instationarity of depth and current neglected.

smaller effect of the inhomogeneity than in case II. At Euro-0 the change of absolute period is slightly dominant, as in case II, again indicating the importance of depth and current instationarity for this case. The importance of the instationarity at both locations is illustrated in figure 42, where modulations of the absolute and relative periods as calculated with WAVEWATCH version B_1 (without instationarity) are presented. A comparison of figures 41 and 42 clearly shows the significance of the instationarity for both locations.

5.3.4 Spatial distribution of wave-tide interactions

The spatial distribution of the effects of wave-tide interactions is assessed by considering the spatial distribution of the normalized local rms differences between the results of different versions of WAVEWATCH (i.e. the coefficient of variation CV). For e.g. the significant wave height the coefficient of variation $CV(H_s)$ is defined as :

$$CV(H_s) = \frac{\left[\frac{1}{T} \int \left[H_s - H_{s,A} \right]^2 dt \right]^{\frac{1}{2}}}{\frac{1}{T} \int H_{s,A} \, dt} \qquad (5\text{-}14)$$

where the suffix A denotes the results of the reference version A of WAVEWATCH and where T is the duration of the averaging period (typically several tidal periods). The coefficient of variation is determined for the mean wave parameters H_s, T_a, T_r and L (of the latter two one again is more or less redundant). For the mean direction $\overline{\theta}$ the normalization of the rms deviation is meaningless and it is therefore omitted.

For the cases II and III, the total variance in the lowest frequency band (F_1, 0.04 Hz - 0.1 Hz) is also assessed for several reasons. First the effects of tides and surges on details of the spectrum are much larger than the effect on mean wave parameters, as is shown in section 5.3.2. Secondly the variance in this frequency band is of interest since all aspects of wave tide interactions considered here

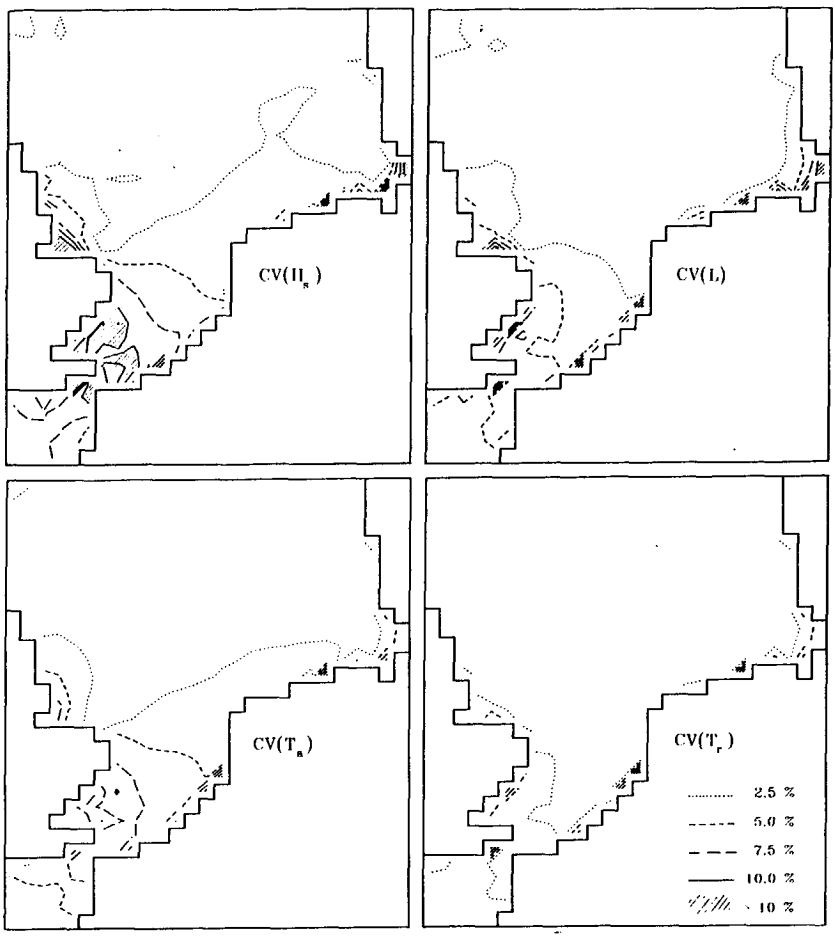

Fig. 43 Coefficients of variation of mean wave parameters for the total wave-tide interaction (WAVEWATCH version C versus A), case I.

have a distinct influence on the tide-induced modulations of F_1. Finally the low frequency variance is interesting since it is used in the policy of ship admittance to the port of Rotterdam ("E_{10}").

Case I : (moderate SW storm)

Coefficients of variation for case I have been determined for the 48 h period of January 1-2 1988. Coefficients of variation of mean wave

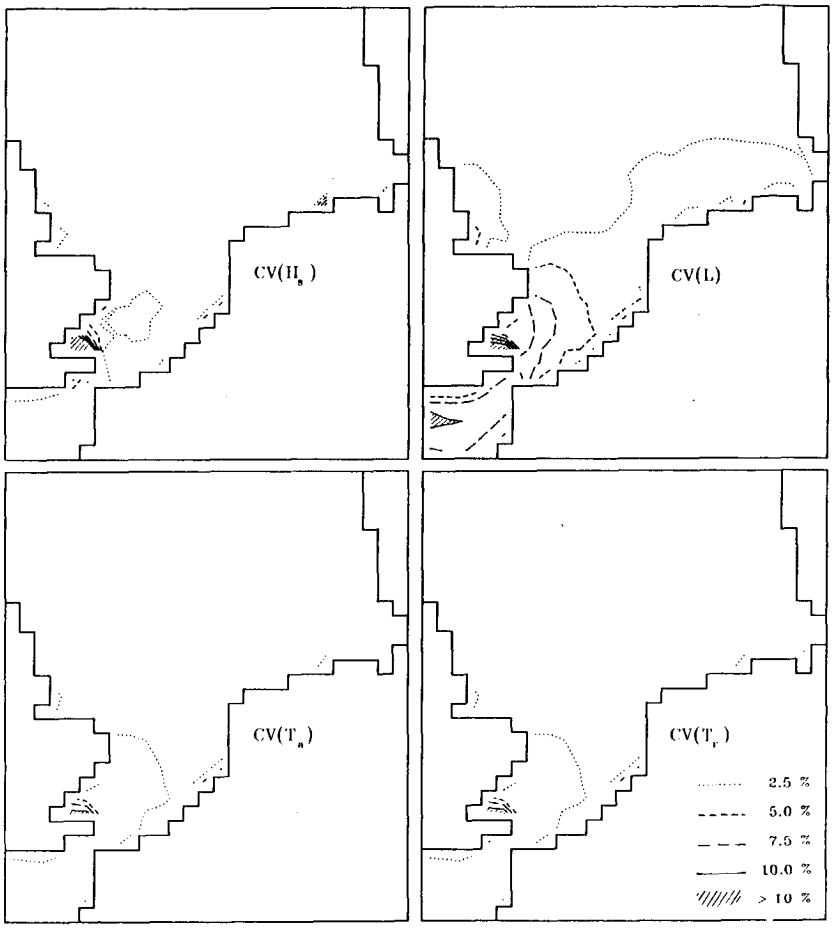

Fig. 44 Coefficients of variation of mean wave parameters for the effect of depth and current instationarity (WAVEWATCH version B_1 versus A), case I.

parameters for the total effect of wave-tide interactions (i.e. WAVEWATCH version C versus A) are presented in figure 43. The wave-tide interactions are manifested most strongly in the significant wave height and the mean absolute period with coefficients of variation of up to 15% and 10% respectively. The magnitude of the tidal influences on the wave height and the absolute period strongly correspond to the local magnitude of extreme current velocities in the mean propagation direction of the waves U_p (figure 19). Since waves are essentially in

deep water, all refraction is caused by currents. The tide-induced rms difference in mean propagation direction $\Delta\bar{\theta}_{rms}$ (not presented here) is smaller than 2.5° for all grid point except for extremely shallow water grid points adjacent to the coast (depths of 2 m and less). Since this study considers tides away from the coast only, such grid points are not relevant for this study and they will not be considered in the discussion of the results. The results for these points, however, have not been eliminated from the figures.

Coefficients of variation of mean wave parameters for the effect of instationarity of depth and current on wave-tide interactions (i.e. WAVEWATCH version B_1 versus A) are presented in figure 44. This figure shows that the instationarity has a distinct influence on the mean wave length (coefficients of variation just below 10%), but much smaller influences on the wave height and periods. Note that the coefficients of variation $CV(T_a)$ and $CV(T_r)$ are identical, which was expected since ignoring the instationarity does not change the mean value of T_a and T_r over one tidal period, and since the difference between T_a and T_r has to correspond to the local Doppler shift both if the instationarity is neglected or accounted for. Since the coefficients of variation for the instationarity show similar behaviour in the other two cases, with, however, a significantly smaller magnitude, they will not be discussed for the other two cases.

Case II : (moderate NW storm)

Coefficients of variation for case II have been determined for the 48 h period of September 27-28 1987. Coefficients of variation of mean wave parameters for the total effect of wave-tide interactions (i.e. WAVEWATCH version C versus A) are presented in figure 45. As in case I, the effects of wave-tide interactions are most strongly manifested in the significant wave height and in the mean wave length (coefficients of variation of up to 5% and 10% respectively). Furthermore the magnitude of these coefficients of variation again is strongly related to the local extreme current velocities U_p (see figure 24). As in case I, the tides show a negligible influence on the mean direction ($\Delta\bar{\theta}_{rms} < 2.5°$).

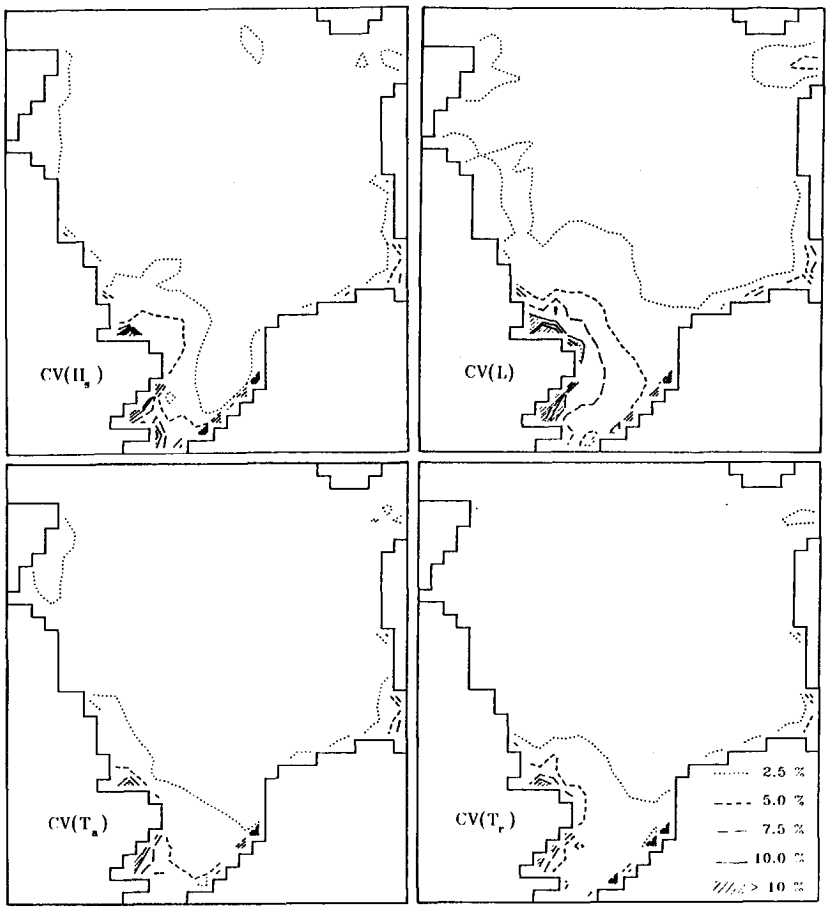

Fig. 45 Coefficients of variation of mean wave parameters for the total wave-tide interaction (WAVEWATCH version C versus A), case II.

Unlike in case I, refraction has a distinct effect on mean wave parameters in case II. Since $\Delta\bar{\theta}_{rms}$ is negligible when calculations with and without the tide are intercompared, the effects of refraction are caused by bottom refraction and consequently have a systematic nature (instead of the oscillating nature of purely tidal interactions). Coefficients of variation for refraction (i.e. WAVEWATCH version C versus B_2) are presented in figure 46. The effects of refraction are manifested mainly in the mean direction ($\Delta\bar{\theta}_{rms}$ up to 7.5°), the

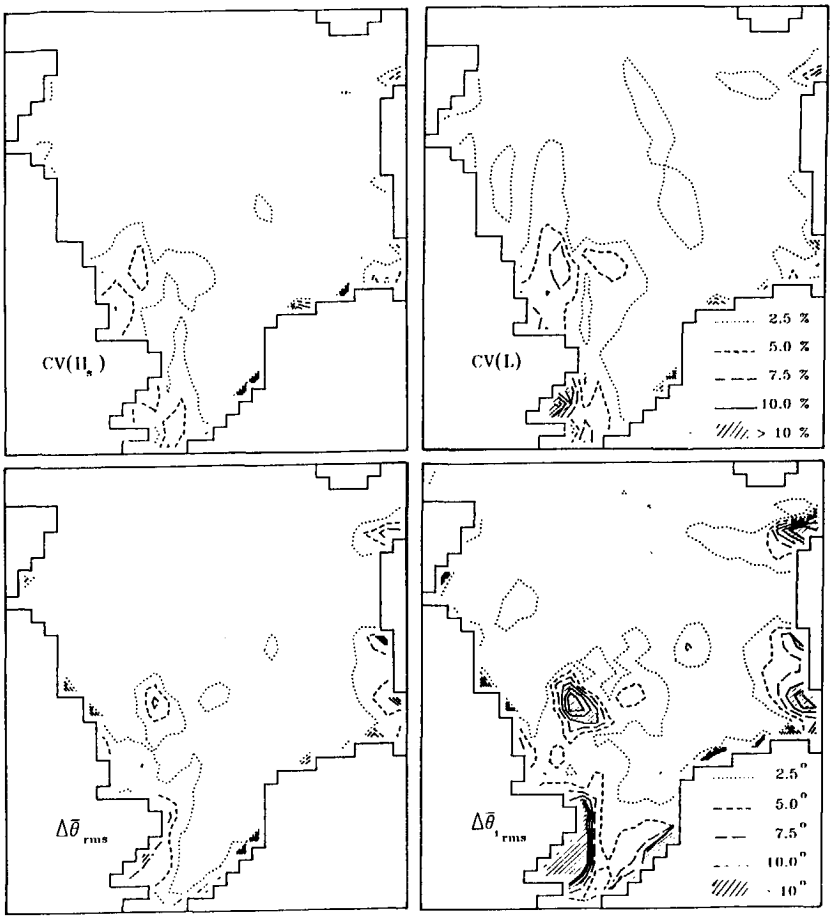

Fig. 46 Coefficients of variation for H_s and L and rms differences of the overall mean direction $\bar{\theta}$ and mean direction in the low frequency band 1 due to refraction (WAVEWATCH version B_2 versus A) case II.

significant wave height and the mean wave length (coefficients of variation of up to 5% and 7.5% respectively). Effects of refraction on the mean wave parameters at the central North Sea are mainly related to bottom slopes in particular at the west end of the Dogger bank. The mean direction $\bar{\theta}_1$ in the low frequency interval of 0.04 Hz to 0.10 Hz shows a similar pattern, with much larger changes of direction ($\Delta\bar{\theta}_{1\,rms}$ up to 15°) than for the mean overall direction $\bar{\theta}$, as would be expected in cases of bottom refraction.

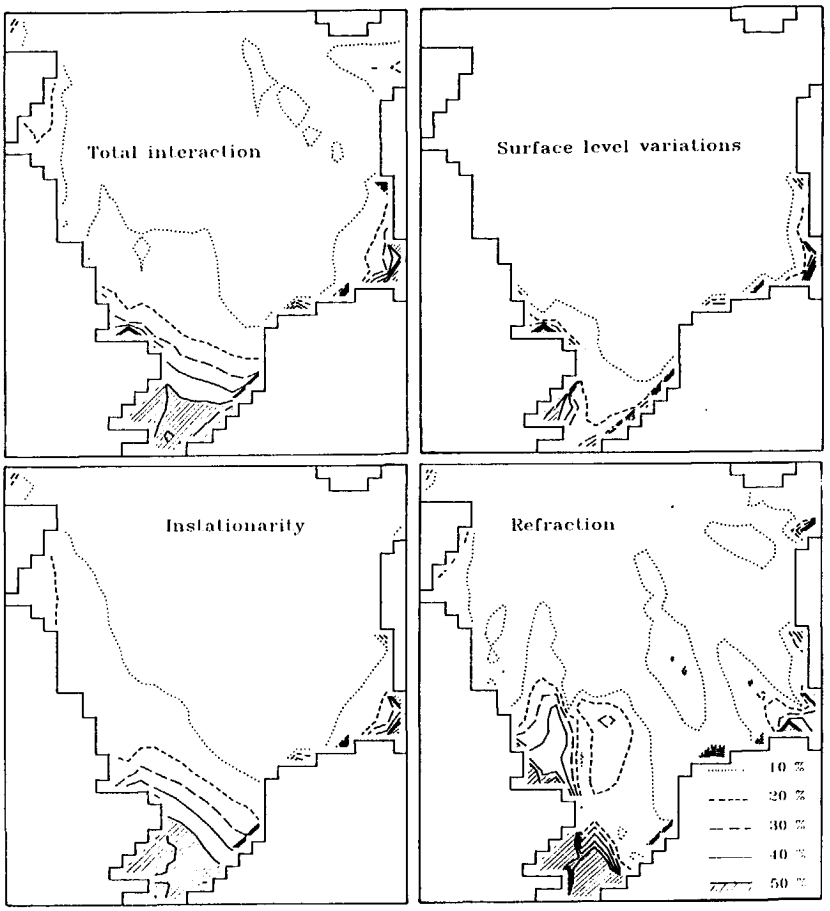

Fig. 47 Coefficients of variation of the low frequency variance $CV(F_1)$ for the total wave-tide interactions, surface level variations, instationarity and refraction, case II.

Tide-induced modulations of details of the spectrum are much stronger than those of mean wave parameters, as is shown in section 5.3.2. This is further illustrated in figure 47 by considering coefficients of variation for the low frequency variance F_1, which in the southern North Sea has values of over 50% for the total influence of the tides. This figure clearly shows that instationarity, refraction, surface level variations and currents all have a large influence on the predicted variance at low frequencies.

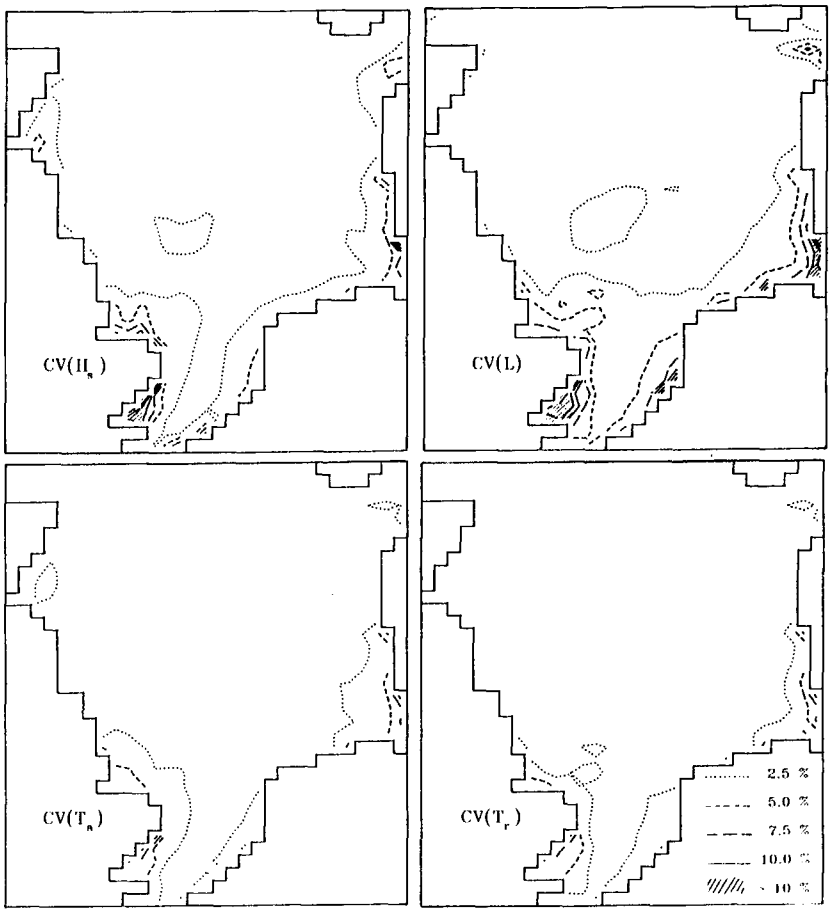

Fig. 48 Coefficients of variation of mean wave parameters for the total wave tide interaction (WAVEWATCH version C versus A), case III.

Case III : (severe NW storm)

Coefficients of variation for case III have been determined for a 25 h period starting at 2200 GMT February 28 1988 (i.e. the peak of the storm only). They are shown in figure 48 for the total effect of wave-tide interactions. As in cases I and II, the effects of wave-tide interactions are strongest in the significant wave height and in the mean wave length. Like in cases I and II, the magnitude of the tidal

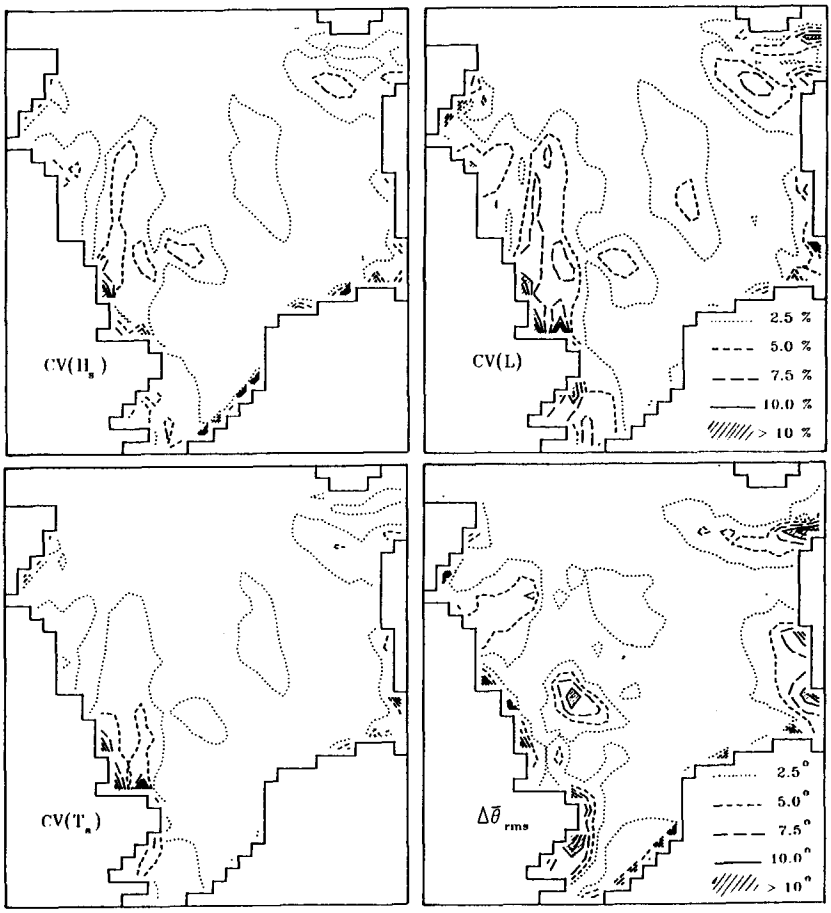

Fig. 49 Coefficients of variation of mean wave parameters and rms differences of the mean direction due to refraction (WAVEWATCH version B_2 versus A), case III.

influences is strongly related to the local extreme current velocities U_p (figure 28) and the tidal effects of the mean direction are negligible.

Bottom-induced refraction has a distinct influence on mean wave parameters for this case, as is illustrated in figure 49. Refraction causes rms variations of the mean wave direction of up to 12.5° and coefficients of variation of the wave height and the wave length of up to 5%

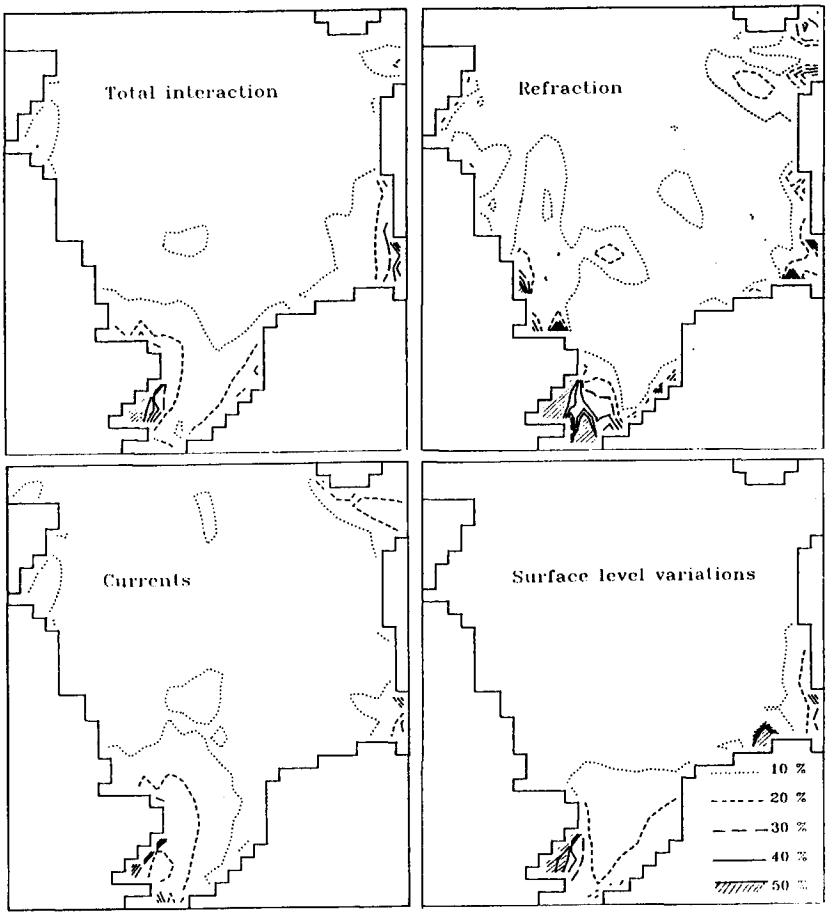

Fig. 50 Coefficients of variation for low frequency variance $CV(F_1)$ for the total wave-tide interaction, refraction, surface level variations and currents, case III.

and 7.5% respectively. The effects of refraction on the wave periods are somewhat smaller ($CV(T_a) \approx CV(T_r)$). In figure 49 several features of the bottom topography can be distinguished, such as the Dogger bank, the slopes at the south side of the Skagerrak and the Devils' Hole. A comparison of figures 48 and 49 shows that (bottom-induced) refraction in general has a larger impact on the waves than the tides in this specific case.

Finally coefficients of variation of the low frequency variance $CV(F_1)$ are presented in 50. This figure again shows large influences of all mechanisms considered (coefficients of variation of the order of 20%). The coefficients of variation are smaller than in case II, which is explained from the much higher low frequency variance level in case III (i.e. the coefficients of variation are smaller since the rms difference in equation (5-14) increased less than the mean value).

5.3.5 Discussion

The results of WAVEWATCH as presented in this section illustrate the relevance of wave-tide interactions at the (southern) North Sea. All separate wave-tide interaction mechanisms considered in this study play a distinct role in one or more of the cases considered here, except for current refraction. Whereas the magnitude of the wave-tide interactions is strongly related to the local magnitude of the current velocity in the propagation direction of the waves U_p (section 5.3.4), details of wave-tide interactions cannot be estimated using local parameters of the tide only (section 5.3.3).

Only for the wave height, the magnitude of the tide-induced modulations is not clearly related to the magnitude of the velocity U_p.

In case II the wave height modulations at K-13-A are larger than at Euro-0, in spite of the larger current velocities at the latter location (see e.g. figure 39). Such differences have not been explained satisfactory. Note that similar effects occur in case III for the tidal modulation of the wave height (see figure 41, note that the wave height modulation at Euro-0 is mainly surge-induced).

Furthermore, the wave height shows significant tide-induced modulations in case I, but only small modulations in cases II and III. Apart from the wind direction and speed, there are two significant differences between the conditions of case I on the one hand and cases II and III on the other hand. First, in case I the waves in the southern North Sea are locally generated, whereas for cases II and III such waves are for a significant part generated in the central North Sea. Secondly the waves in case I are essentially in deep water, whereas the waves in particular in case III are no longer in deep water. Both the local generation and the relative depth (through e.g. variations

in the energy dissipation due to bottom friction) might have a significant effect on tide-induced modulations of the wave height. With the present study, however, this cannot be investigated so that the above differences between the results of case I and the results for H_s of cases II and II cannot be explained satisfactorily.

The instationarity of depth and current, which is typical for tides in shelf seas, has a distinct role in wave-tide interactions. The analysis of results for Euro-0 and K-13-A shows the complicated nature of the effects of instationarity. In general, the instationarity causes modulations of the absolute period, which however, can also be caused by the wind (dashed lines in figure 31). For given wind conditions, the relative importance of the instationarity varies in space (compare e.g. the changes of absolute and relative period at Euro-0 and K-13-A in case II, figure 39). Furthermore the relative importance of the instationarity at a fixed location can vary with varying wind conditions (compare e.g. the changes of absolute and relative period at K-13-A in cases I and II, figures 37 and 39). Finally the instationarity has a distinct influence on the time lags between the variations of the local current velocity U_p and the tide-induced modulations of the periods. In case II, the time lag at Euro-0 seems to be caused by the instationarity (compare figures 39 and 40), but in case III a time lag occurs at Euro-0 only if the instationarity is neglected (compare figures 41 and 42).

Note that large modulations of the absolute period (i.e. large compared to equation (5-11)), as found in the one-dimensional academic case of section 4.2 for shallow water and waves travelling in the same direction as the tide, do not occur here. This was already anticipated in the corresponding discussion (section 4.4).

Depth refraction due to bottom level variations has a distinct influence in both NW storm cases considered here. The effects of refraction are limited to areas with large gradients of the bottom level and show a small spreading over downwind areas. This is explained by the broad directional distribution of wind seas and possibly by effects of generation and dissipation. For swell with a narrow directional distribution effects of refraction might spread over larger areas. Note that the regions with the largest effects of

depth refraction in general do not coincide with regions with the largest effects of wave-tide interactions and that (for the cases considered here) Euro-0 and K-13-A are not in areas with the largest effects of refraction.

For the moderate storm conditions considered here (cases I and II), the effects of wave-tide interactions on mean wave parameters are caused by currents only. For increasing severity of storm conditions, the effects of surface level variations due to tides and storm surges become increasingly important (see e.g. case III), which was expected considering the corresponding decrease of relative depth the increase of (wind-induced) surface level variations.

Two remarks have to be made on the results for case III. First, the current velocities and water level variations due to the astronomical tide (i.e. without wind forcing) are relatively small, since the period of case III practically coincides with neap-tide (compare e.g. figure 20, 25 and 29 or figures 37, 39 and 41). In severe storm conditions during spring-tide, semi-diurnal effects of wave-tide interactions are expected to be significantly larger. Secondly, the effects of currents and the mean surface level variations more or less cancel out in case III. This does not necessarily occur in all severe storm conditions. Consequently, the relative magnitude of effects of tides and storm surges on waves in severe storm conditions can become larger than in case III. However, considering the small differences between parameter values as calculated with the different versions of WAVEWATCH (see figure 35), the total effects of tides and storm surges on waves in extreme conditions is expected to be small in any extreme case.

Tidal influences within the spectrum are much larger than tidal influences on mean wave parameters. In particular the effects of tides on low frequency variance (or energy) is striking. Whereas wave-current interactions for monochromatic waves suggest a decreasing effect of currents with decreasing frequency due to decreasing Doppler shifts and relative current velocities U/c_g, the results of this study show extreme tidal influences on the low frequency variance F_1 (see e.g. figure 34). This large impact of tides on low frequency wave energy is explained from the steep gradients in the low frequency

flank of frequency spectra, where small shifts of the spectral peak frequency can cause large modulations of the variance in fixed frequency bands. Such modulations of peak frequency are not simply determined from the local current velocity only (as discussed above for the mean absolute and relative periods).

5.4 COMPARISON OF MODEL RESULTS WITH DATA

5.4.1 Introduction

In this section only the total wave-tide and wave-surge interactions will be considered, since it is virtually impossible to isolate effects of separate mechanisms in data. For cases I and II wave data were available for the locations Euro-0, K-13-A and AUK. Since no relevant effects of wave-tide interactions were found at location AUK, the comparison of the model results with data is limited to the other two locations. In the comparison only the significant wave height and the mean absolute period are considered, since these parameters can be obtained directly from the data, i.e. without any assumptions on directional distribution of the measured spectrum. The mean direction, which is also obtained from the data without assumptions, is not assessed since it did not show significant tidal influences. In the following, tidal effects in model and data are intercompared first by comparing overall measured wave heights and periods with similar parameters calculated with or without inclusion of tidal effects (WAVEWATCH versions A and C, section 5.4.2). However, such a comparison appears to be strongly hampered by errors in the hindcasts. For this reason an attempt is made in section 5.4.3 to isolate tidal influences in model and data.

5.4.2 Direct comparison

Measured and hindcasted significant wave heights and mean absolute periods for cases I and II are presented in figure 51. For both cases the hindcasts show poor results, due to which a direct evaluation of tidal influences on the wave parameters becomes practically impossible. Only the predicted oscillation of the absolute period at Euro-0 is more or less recognizable in the data. Before the tidal influences

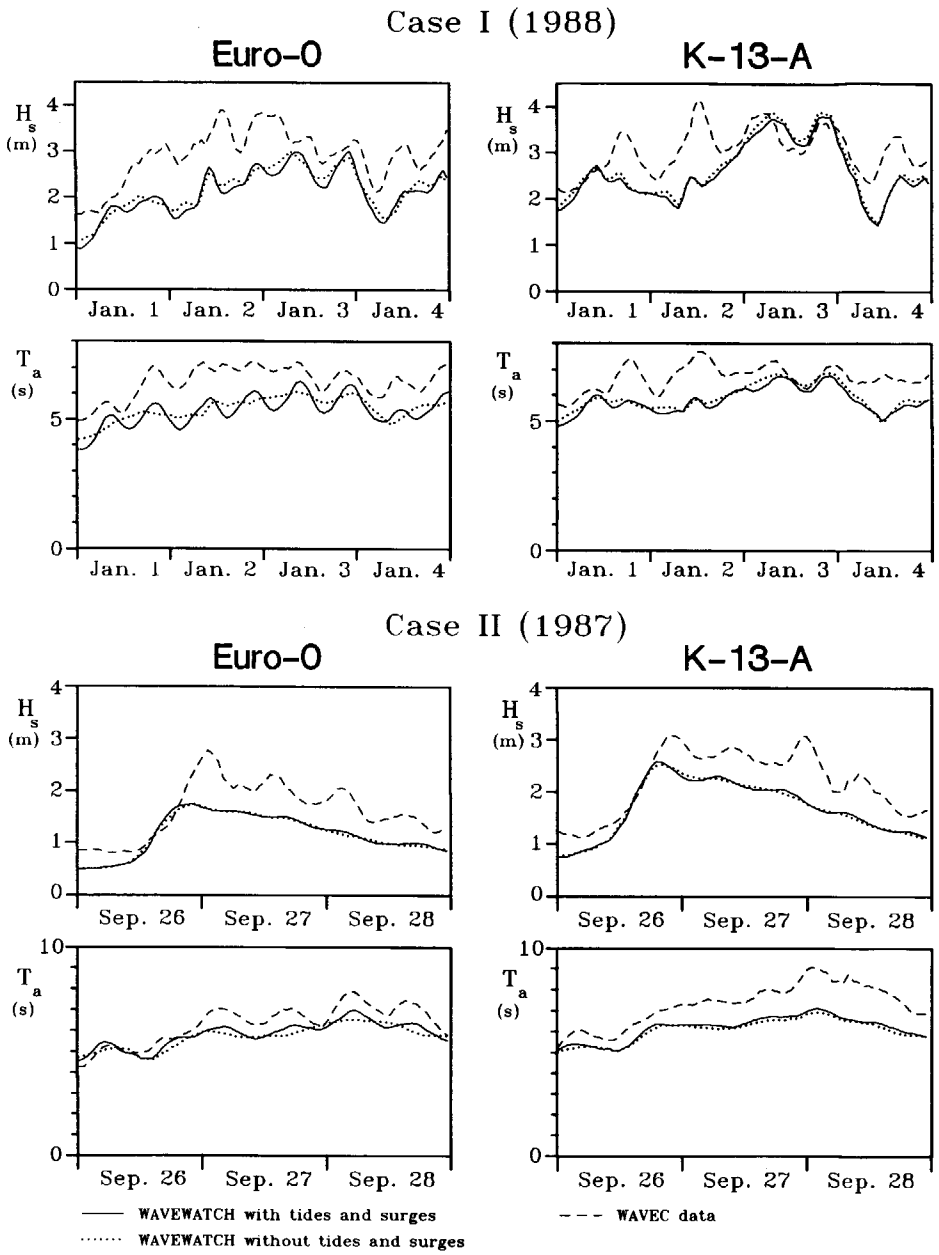

Fig. 51 Measured and predicted significant wave height and absolute period at locations Euro-0 and K-13-A for cases I and II.

in the model results and the data are assessed further, the large errors in the hindcasts will be discussed.

A comparison of figure 51 with the measured and calculated wind speeds, in particular those in figure 18, suggests that errors in the wave parameters are related to errors in the input wind field. Therefore the correlation between errors in wind speed and those in wave parameters is assessed. In particular at Euro-0 in case I (SW winds) the local wind speed is expected to be representative for the entire area of wave generation, since the waves at Euro-0 then are generated in a relatively small part of the southern North Sea. Hence local errors in the wind field are expected to be representative for the entire area of wave generation and the relation between errors in the hindcast and errors in the wind field can be assessed by comparing local errors only. Local errors in the wind speed at K-13-A in case I are less representative for the average error of the wind speed in the area of wave generation (i.e. the southern North Sea south and southwest of K-13-A), as follows directly from a comparison of errors in the wind speeds at Euro-0 and K-13-A (figure 18). Similarly (local) errors in the wind speed for case II are not expected to be representative for the areas of wave generation in case II. Consequently the comparison of errors in wave parameters with local errors of the wind speed should concentrate on Euro-0 in case I.

Since figures 18, 23 and 51 suggest that the dominating time scales of errors in both wind and wave models are larger than the tidal period, both the wind speed and the wave parameters of model and measurements are smoothed before errors are determined. The smoothing was performed using a straightforward (i.e. block type) 12 h running average. From these smoothed wind and wave parameters relative errors of e.g. the significant wave height are determined as :

$$\epsilon_{H_s} = \frac{H_{s,measured} - H_{s,calculated}}{H_{s,calculated}} \qquad (5\text{-}15)$$

To obtain the best possible (linear) correlation between wind and wave errors at Euro-0, a time lag of 3 h was applied to the errors of the wave parameters. The errors of the significant wave height and the

absolute period as a function of the local errors in the wind speed are presented in figure 52. At Euro-0 in case I the errors in wave parameters are strongly correlated to local errors in wind speed, so that errors in the hindcast are strongly related to errors in the wind field. As expected, the correlation between errors in wave parameters and errors in the local wind speed is less pronounced or even absent at K-13-A or in case II.

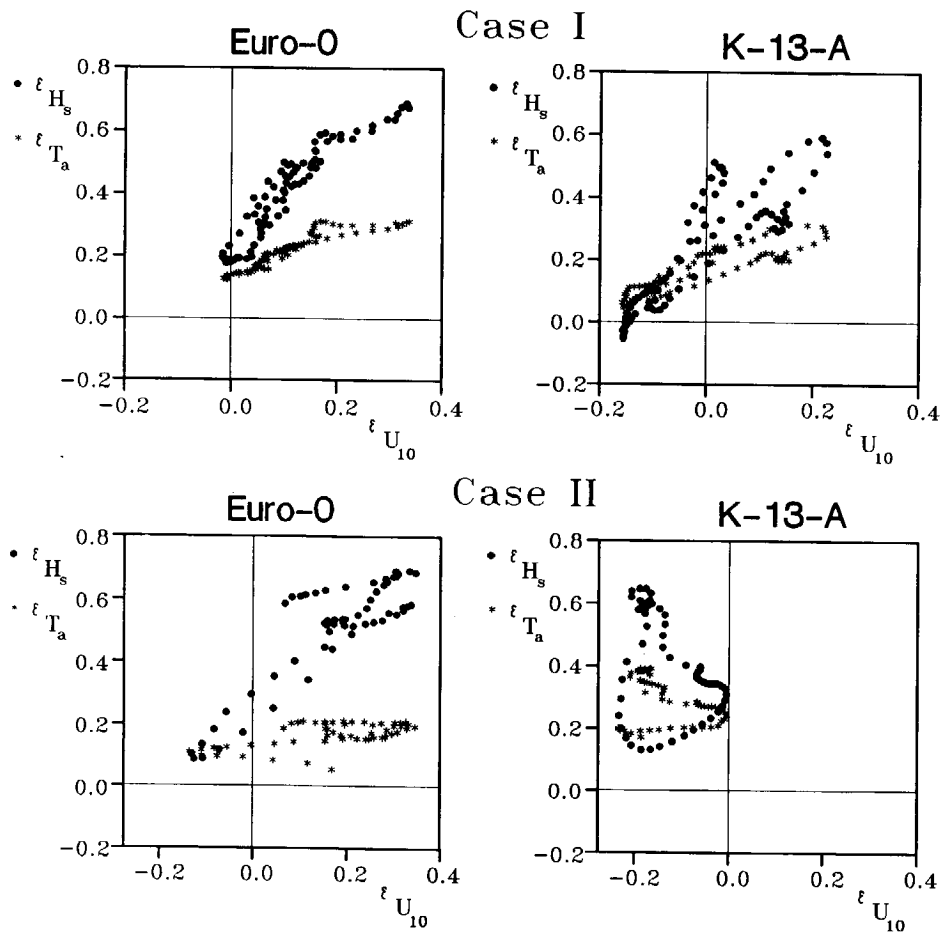

Fig. 52 Errors in significant wave height and absolute period as a function of errors in the wind speed (variations with periods longer than 12 h only).

5.4.3 Isolated tidal effects

Since the quality of the predicted tidal influences on wave parameters cannot be assessed using a straightforward intercomparison of overall model results and data, tidal influences in model and data have to be isolated. Depth and current variations in cases I and II show small contributions of storm surges (section 5.2), so that only pure tidal modulations of wave parameters have to be considered here.

In the numerical results the tidal influences have been isolated as in section 5.3.3 by considering the differences between the results of WAVEWATCH versions A and C (with and without tides and surges respectively), as in equation (5-6). Such isolated effects in the model results will be denoted as the calculated modulations and are marked with the suffix c (e.g. $\Delta H_{s,c}$).

Tidal influences in the observed data cannot be isolated directly. Although modulations within a selected frequency band can be isolated using filtering techniques, this does not identify the origin of such modulations. Apart from tides and surges, the wind is obviously a possible source of modulations of wave parameters. Therefore variations of the wind speed in the same frequency band as the isolated modulations of wave parameters will also be assessed.

Tides in the North Sea are dominated by the M_2 tide, which has a period of 12 h 25 min. Therefore observed data have been filtered to obtain modulations with periods between approximately 15 h and 9 h, by using straightforward running averages. Such modulations will be denoted as the observed modulations and are marked with the suffix o (e.g. $\Delta H_{s,o}$).

Before results of isolated modulations of wave data are presented and discussed, observed variations of the wind speed with periods between approximately 15 h and 9 h will be assessed (ΔU_{10}, denoted as the "fast" variations of the wind speed). Such variations are presented in figure 53. A comparison of figures 18, 23 and 53 shows that observed fast variations of the wind speed ΔU_{10} can be as large as 20% of the average wind speed for the cases considered here. These fast

variations of the wind speed (ΔU_{10}) appear to contribute significantly to observed modulations of wave parameters (e.g. $\Delta H_{s,o}$, see below).

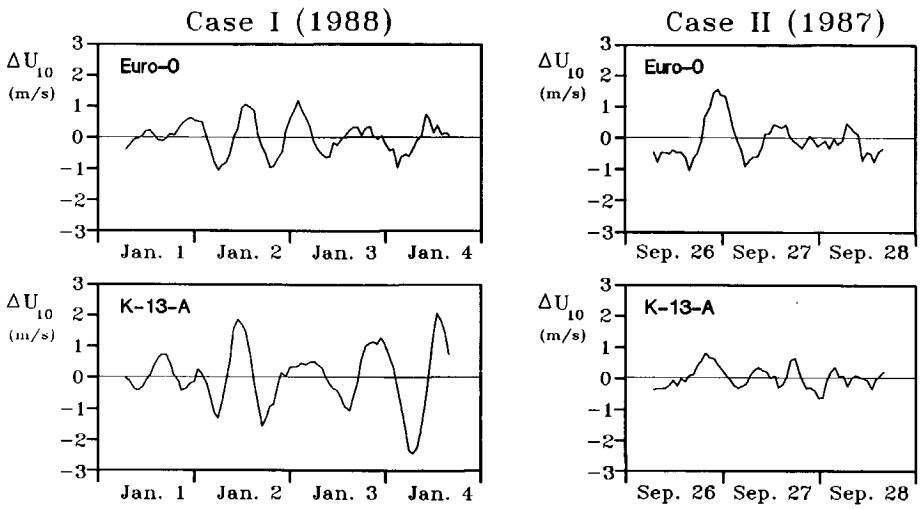

Fig. 53 Observed variations of the wind speeds ΔU_{10} at locations Euro-0 and K-13-A.

Therefore the observed and calculated modulations will be compared in two ways. First, observed modulations of mean wave parameters (e.g. $\Delta H_{s,o}$) are compared with calculated modulations (e.g. $\Delta H_{s,c}$), to investigate to which extent the tides are responsible for the observed modulations. Secondly, the correlation between the observed fast variations of the wind speed and observed modulations of mean wave parameters is investigated.

In figure 54 calculated and observed modulations of the wave height and absolute period are intercompared. This figure shows that observed modulations of the wave height ($\Delta H_{s,o}$, dashed lines) in general are much larger than the calculated modulations ($\Delta H_{s,c}$, solid lines). Since the calculated modulations incorporate effects of tides only, and since the observed modulations contain effects of both tides and

fast variations of the wind speed, this suggests that wave height modulations are dominated by fast variations of the wind speed.

Figure 54 furthermore shows that at K-13-A observed modulations of the absolute period ($\Delta T_{a,o}$, solid lines) are much larger than the calculated modulations ($\Delta T_{a,c}$, dashed lines), suggesting that fast variations of the wind speed also dominate here. At Euro-0, however, observed and calculated modulations of the absolute period are of similar magnitude. This suggests that tidal effects dominate the observed modulations of the absolute period at Euro-0.

To investigate the apparent dominance of the fast variations of the wind speed (ΔU_{10}) further, such variations are intercompared with their assumed effects on wave parameters. The wind-induced modulations of the wave parameters are estimated as the difference between the observed modulation of the wave parameter (due to wind and tides) and the calculated modulation (due to tides only). For instance for the significant wave height H_s, the apparently wind-induced modulation $\Delta H_{s,w}$ is calculated as :

$$\Delta H_{s,w} = \Delta H_{s,o} - \Delta H_{s,c} \qquad (5\text{-}16)$$

To allow for a direct comparison of the above wind and wave data, they are normalized with their rms value for the period considered. For instance the normalized wave height modulation $\Delta\tilde{H}_{s,w}$ is calculated as :

$$\Delta\tilde{H}_{s,w} = \Delta H_{s,w} \,/\, \left[\Delta H_{s,w}\right]_{rms} \qquad (5\text{-}17)$$

Since $\Delta\tilde{U}_{10}$ describes the local variations of the wind speed only, good correlations between $\Delta\tilde{U}_{10}$ and $\Delta\tilde{H}_{s,w}$ of $\Delta\tilde{T}_{a,w}$ are expected in conditions of active wave generation only. For the second half of the period of case II, where waves at Euro-0 and K-13-A consist for a major part of swell (see section 5.3.2, page 81), a good correlation cannot be expected, even if e.g. $\Delta\tilde{H}_{s,w}$ is indeed caused by wind speed variations.

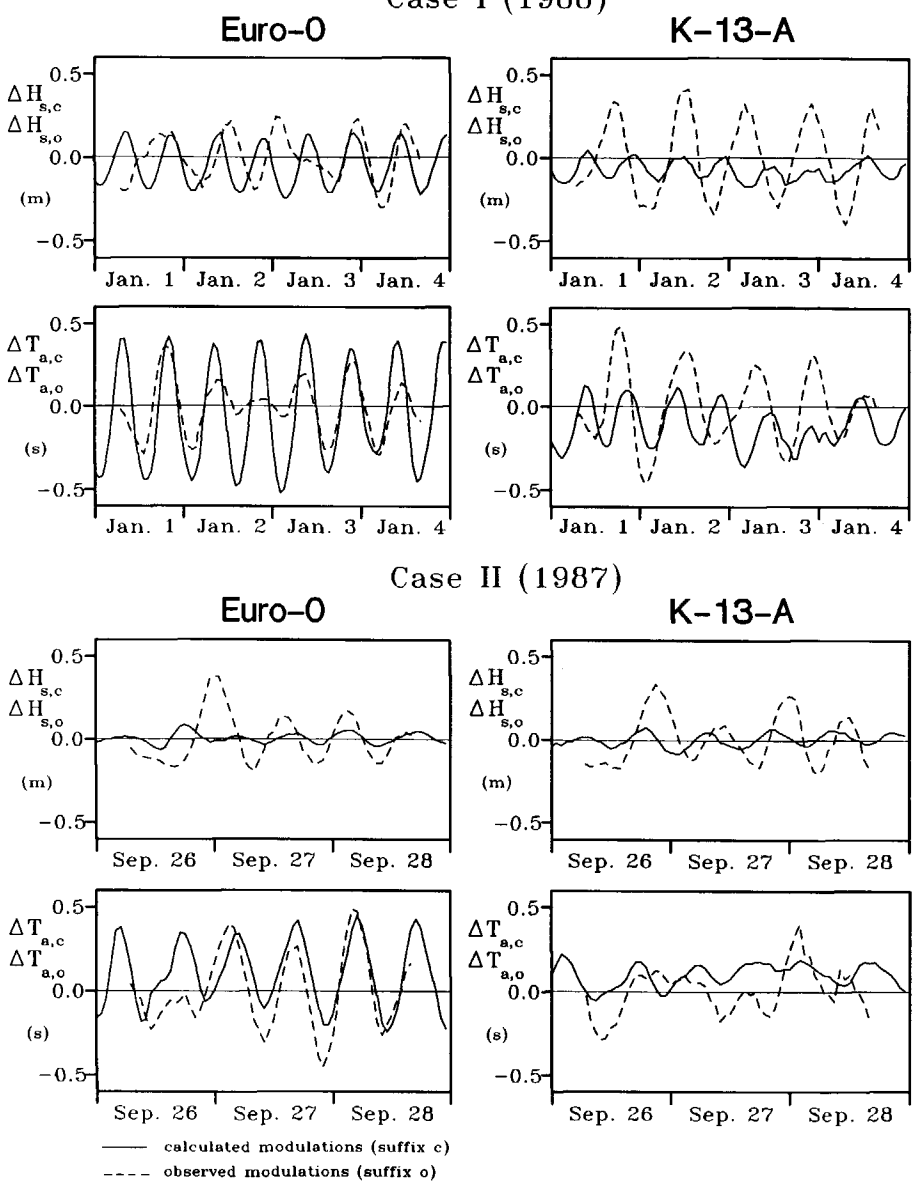

Fig. 54 Observed and calculated modulations of the significant wave height and the mean absolute period at Euro-0 and K-13-A for cases I and II. —— : calculated modulations; --- : observed modulations.

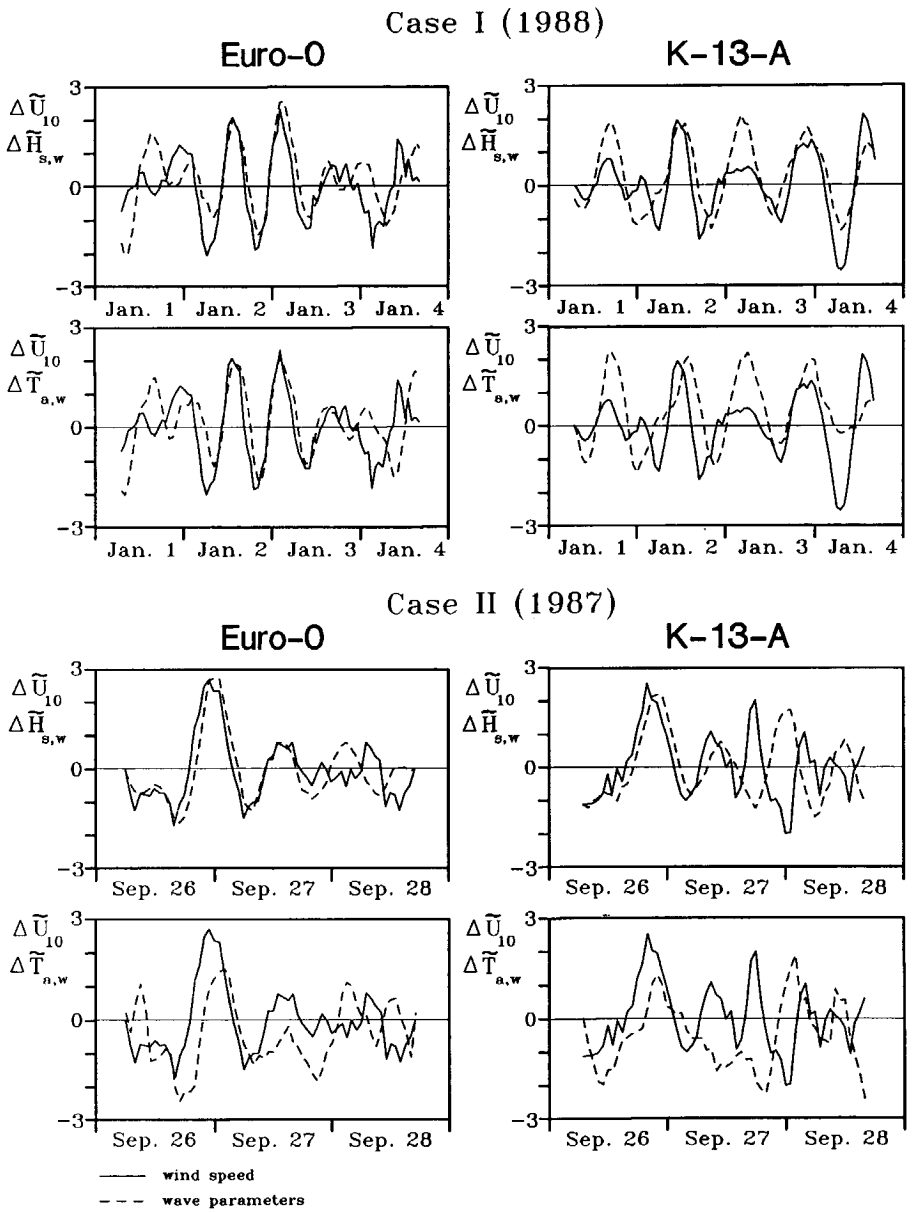

Fig. 55 Normalized fast variations of the wind speed (solid lines) and apparently wind-induced modulations of mean wave parameters (dashed lines) at Euro-0 and K-13-A for cases I and II.

In figure 55 $\Delta\tilde{H}_{s,w}$ and $\Delta\tilde{T}_{a,w}$ are compared to $\Delta\tilde{U}_{10}$. This figure shows a fair degree of correlation between $\Delta\tilde{H}_{s,w}$ and $\Delta\tilde{U}_{10}$, except for the swell in the second half of case II. The correlation between $\Delta\tilde{T}_{a,w}$ and $\Delta\tilde{U}_{10}$ is less
pronounced but still clear (except for the second half of case II). It therefore appears that $\Delta\tilde{H}_{s,w}$ and $\Delta\tilde{T}_{a,w}$ indeed are wind-induced as suggested above.

Finally an intercomparison of the observed modulations of wave parameters in figures 54 and 55 illustrates the significance of both the tides and the fast variations of the wind speed.

First, for a given locations and time observed modulations of the significant wave height show low correlations with the observed modulations of the absolute period ($\Delta H_{s,o}$ and $\Delta T_{a,o}$, dashed lines in figure 54), whereas the the modulations due to the variations of the wind speed ($\Delta\tilde{H}_{s,w}$ and $\Delta\tilde{T}_{a,w}$, dashed lines in figure 55) show much higher correlations. The latter high correlations are expected when modulations are caused by wave generation, since both $\Delta H_{s,w}$ and $\Delta T_{a,w}$ then should be highly correlated with the variations of the wind speed ΔU_{10}.

Secondly, the differences between calculated and observed modulations of the absolute period ($\Delta T_{a,c}$ and $\Delta T_{a,o}$, solid and dashed lines in figure 54) at Euro-0 for case I nicely illustrate the effects of the fast variations of the wind speed of figure 53. The modulation of the absolute period seems to be tide-dominated except for January 2 (figure 54). At the latter day, however, significant wind speed variations ΔU_{10} occur with similar periods as the tide (figure 53), which show a high correlations with $\Delta H_{s,w}$ (figure 55). Since $\Delta H_{s,w}$ is defined as the difference between the calculated and observed modulations, the differences between $\Delta T_{a,c}$ and $\Delta T_{a,o}$ at Euro-0 on January 2 1988 is obviously caused by wind speed variations.

5.4.4 Discussion

For the cases considered in this study, computed tide-induced modulations of the significant wave height and the mean absolute period are much smaller than errors in the hindcasts. Such errors are predominantly related to the slowly varying errors in the wind field (i.e.

errors which vary with time scales larger than the period of the tide). These errors make a direct comparison of tidal influences in model and data virtually impossible.

For the cases considered here fast modulations of the wave height are related to fast modulations of the wind speed rather than to tides. Wind speed variations are less dominant with respect to modulations of the absolute period but still significant.

Figure 53 shows that the above fast variations of the wind speed have the character of noise rather than that of a variation with a dominant frequency or period. Considering figures 18 and 23 the fast variations of the wind speed furthermore do not dominate the wind field. Although little is known about variations of the wind in this frequency range, the variations observed here do not seem extraordinary and probably occur frequently in wind fields. Unfortunately, wind speed variations on these time scales are usually not investigated by meteorologists or wave modellers. Considering the results presented here, such investigations would appear to be very worthwhile.

6 DISCUSSION

6.1 RESULTS

6.1.1 Introduction

In this section the results of this study with respect to wave-tide interactions are summarized and discussed. First, the significance of wave-tide interaction mechanisms (including surges) will be assessed qualitatively. Then the modulations of mean wave parameters and the spectrum due to wave-tide interactions will be discussed in more detail. Finally, the magnitude of effects of tides and surges on mean wave parameters and on the absolute frequency spectrum will be discussed and compared with wind-induced modulations as observed in this study.

6.1.2 Wave-tide interaction mechanisms

Both the academic cases and the North Sea hindcasts considered in this study clearly show the significant influence of the instationarity of depth and current on effects of tides and surges on wind waves in shelf seas. These effects occur mainly in the tide-induced modulations of the (absolute and relative) wave frequency and the wavenumber.

The one-dimensional academic cases with monochromatic unidirectional waves on a one-dimensional tide (section 4.1) indicate that wave-tide interactions (away from the coast) are mainly caused by currents and that the effects of tidal surface level variations are negligible. The results of the North Sea hindcasts confirm the above dominance of currents for the moderate conditions of cases I and II. For the extreme wind and wave conditions of case III, however, the North Sea hindcasts show that the relative contributions of surface level variations and currents are of comparable importance (see section 5.3.5). In the latter case modulations of wave parameters seem to be

related to the storm surge rather than the tide (as discussed in section 5.3.2, page 83).

The effects of current refraction have been assessed in the two-dimensional academic cases and in the North Sea hindcasts. In all these cases the effects of current refraction appeared to be negligible. Note that depth refraction due to the bottom topography (but not due to surface level variations of tides and surges) as assessed in the North Sea hindcasts has distinct influences on mean wave parameters, even for the relatively moderate wind and wave conditions (and thus, relatively short waves) of case II.

6.1.3 Modulations of mean wave parameters and spectra

Tide-induced modulations of the wave frequencies and the wavenumber have been studied extensively in both the academic cases and in the North Sea hindcasts. The academic one-dimensional case clearly shows that the instationarity of tidal depths and currents is dominant over the inhomogeneity with respect to wave-tide interactions. In such one-dimensional cases, however, inhomogeneity of depth and current is related to the wave character of the tide only. In more realistic situations, inhomogeneity of depth and current is also related to the bathymetry and the two-dimensional structure of the tide. Calculations for the two-dimensional academic shelf sea considered in this study (section 4.2) show that in more realistic conditions the effects of instationarity nevertheless remain significant (i.e. relative modulations of the absolute frequency are larger than those of the wavenumber). This is confirmed by the results of the North Sea hindcasts. The North Sea hindcasts (and to a lesser extent the two-dimensional academic cases) furthermore show that the relative importance of instationarity and inhomogeneity varies in space and time and that the effects of wave-tide interactions cannot be estimated from local depth and current parameters only.

Tide-induced modulations of the wave height have been studied for the North Sea hindcasts only. Whereas modulations of the wave height are distinct in case I (SW storm), such modulations are much smaller in cases II and III (NW storms), both in absolute magnitude and when

compared to the relative magnitude of the modulation of wave periods and the wave length in the corresponding cases. Furthermore the cases with NW winds show a larger modulation of the wave height at K-13-A than at Euro-0, in spite of the stronger currents at Euro-0. As discussed in section 5.3.5, such behaviour might be explained from effects of relative depth, or by the degree of wave generation in the area where the strongest currents occur; however, this behaviour is not yet understood. Effects of tides on wave heights could well be investigated further using a numerical model in academic cases.

Tide-induced modulations within the (absolute frequency) spectrum have been considered in the North Sea hindcasts only. These tide-induced modulations can be much more pronounced than those of the mean wave parameters. As discussed in section 5.3.5, the large modulations of the low frequency flank of the spectrum in particular are mainly contributed to relatively small frequency shifts in combination with steep gradients in the spectrum. At higher frequencies, the relative current velocity U/c_g becomes larger, which explains strong tide-induced modulations in this part of the spectrum. Since a major part of the modulations within the spectrum is related to changes of frequency, it is strongly influenced by the instationarity of depth and current and cannot be estimated from local depth and current parameters only. Only modulations of the high frequency saturation range are predominantly caused by the local current only.

The above remarks concern the absolute frequency spectrum. Tide-induced modulations of the relative frequency spectrum will be different. For the latter spectrum the high frequency saturation range is expected to remain unchanged by currents, since the k-spectrum in this range is expected to remain unchanged and since components of this range are essentially in deep water. At lower frequencies, however, the spectrum will show significant tidal influences, since the peak frequency (or the mean relative frequency) shows tidal influences.

6.1.4 Magnitude of effects

The North Sea hindcasts show tidal modulations of mean wave parameters (T_a, T_r, L and H_s) of typically 5% to 10%, where the relative importance decreases with increasing severity of the storm conditions.

Modulations of the spectral density due to tides and surges can be of the same order of magnitude as the average spectral density over a tidal cycle for any frequency range. At Euro-0 for instance, the total variance of part of the saturation range F_4 shows modulations with an amplitude of approximately 40% of the mean total variance F_4 for the SW winds of case I, whereas the low frequency variance F_1 shows even larger modulations in case II (figures 32 and 34 respectively).

The analysis of data for the North Sea hindcasts shows that wind-induced modulations of mean wave parameters with periods between approximately 12.5 h and 3 h are of the same order of magnitude as tide-induced modulations, or larger. In particular the wave height modulations seem to be wind-dominated for the cases considered here. As discussed in section 5.4.4 wind speed variations responsible for the above modulations of mean wave parameters seem to be poorly investigated, and both these wind speed variations and their impact on wind waves deserve further attention.

6.2 IMPLICATIONS

6.2.1 General implications

The necessity of incorporating wave-tide interactions in an analysis of wave parameters depends on the magnitude of the interactions and the nature and scope of the study for which the wave parameters are needed. Obviously the implications for studies considering details of the spectrum are much larger than for studies considering mean wave parameters.

The relatively small influence of wave-tide interactions on mean wave parameters limits the impact of such interactions when assessing mean wave parameters. This is illustrated by the potential errors in wave observations. These are of the same order of magnitude ($\approx$ 10%, e.g. WAMDI group, 1988) as the effects of wave-tide interactions for the southern North Sea. This makes it difficult to decide whether or not to assess wave-tide interactions. However, the results as presented in section 5.4.3, which indicate that modulations of wave heights show a

much higher correlation with modulations of the wave periods if the tides are accounted for, illustrate that the assessment of wave-tide interactions for mean wave parameters for the southern North Sea can nevertheless be useful. Note that it is difficult to isolate tidal effects in wave observations, since effects of tides cannot be calculated from local parameters of the tide only, nor can they be isolated using straightforward filtering techniques.

The relatively large effect of wave-tide interactions on details of the spectrum has impacts in several fields of investigation, in particular where the dynamic behaviour of ships and structures is considered.

For relatively high frequencies, this is illustrated here with a study of Peters and Boonstra (1988), who considered fatigue loading of the Euro-0 platform. Observed amplitudes of acceleration of the platform (their figure 4), with a dominant frequency of 0.38 Hz (i.e. the natural frequency of the platform), show for SW winds modulations comparable to those of F_4 as described above.

The tide induced modulations of low frequency variance has impacts on e.g. the policy for ship admittance at the port of Rotterdam, or for e.g. offshore workability.

6.2.2 Implications for wave modelling

Before considering the necessity of incorporating wave-tide interactions in wave models, it is noted (again) that neither a quasi-stationary nor a quasi-homogeneous approximation should be used if wave-tide interactions are accounted for. Since (furthermore) wave-tide interactions cannot be estimated from the local depth and current only, parameterizations of effects of wave-tide interactions will be complicated if feasible at all. Therefore wave-tide interactions have to be fully accounted for if considered in wave models.

The usefulness of incorporating wave-tide interactions in wave models depends both on the purpose of the model and on the (potential) accuracy of such models. In the discussion below a distinction is made between research models and operational forecast models. It seems clear that wave-tide interactions should be accounted for when

assessing the spectrum. It is not so clear when considering mean wave parameters. Therefore, mean wave parameters are considered next.

Since research models in a hindcast mode can use analyzed wind fields (instead of forecast wind fields), which can be of high quality, the accuracy of such models is limited mainly by the physics and numerics of the model. Third generation wave models then are potentially much more accurate than is suggested by e.g. the overall hindcast results in this study. For instance the wave heights for Euro-0 and K-13(-A) as hindcasted with the WAM model using good quality analyzed wind fields show rms errors of 15% only (e.g. WAMDI group 1988, figures 13 and 14 and table 3). Such errors are of the same order of magnitude as the effects of wave-tide interactions on mean wave parameters found in this study, and may well be caused by these (neglected) interactions to a substantial degree. If improvements of wave models are considered to bring down the above errors even further, it therefore seems necessary to incorporate wave-tide interactions in the models.

For the question whether to incorporate the effects of tides and surges in operational (forecast) wave models, their contribution to the accuracy of forecast results have to be assessed. In other words, for wave forecast models only the magnitude of the effects of wave tide interactions compared to the potential accuracy of the model is of interest. The accuracy of forecast models is determined by the quality of the wind field rather than the above potential accuracy of wave models, as is illustrated here in section 5.4.2. The case studies presented here illustrate that it is not yet useful to incorporate wave-tide interactions in operational models in view of the large overall errors.

The large impact of the errors of operational wind models on operational wave models is generally recognized and improvement is sought using several approaches. Since errors in the wind prediction might partially be caused by unaccounted effects of wind waves on the surface roughness of oceans (e.g. Janssen, 1982, 1989; Maat et al., 1989), an improvement might be found in the direct coupling of wind and wave models. Another approach to improve results would be the real-time incorporation of measured wave data in operational models

(data assimilation). Several methods for data assimilation have been investigated recently or are presently being investigated. In one method, the available wave data are simply imposed on the initial wave fields using some empirical spatial spreading function (e.g. Janssen et al. 1989). Using such an approach, the effects of the data assimilation are limited to relatively small scale areas around the observation locations and the additional data are lost from the model rather rapidly. A more sophisticated method of data assimilation is presently investigated by members of the WAM group. In this approach measured wave data and a numerical wave model are used to improve the quality of wind fields using inverse modelling techniques. The wind fields thus improved are used in the actual forecast run of the wave model. The first experiments with such an approach (De Valk and Calkoen, 1989) show promising results. If such an approach is used, it would be recommendable to incorporate effects of tides and surges in the wave model, since tidal effects on waves are otherwise contributed to errors in the wind field. The potential effects of tides in such data assimilation schemes is illustrated here with the results of section 5.4.3, which show a significantly improved correlation between variations of wind and wave parameters with periods of 12.5 h and less, if the observed modulations of wave parameters are corrected for tidal influences.

7 CONCLUSIONS AND RECOMMENDATIONS

This study on effects of tides and storm surges on wind waves in shelf seas has given rise to the following conclusions. Tides and storm surges have to be treated as instationary media for wind wave propagation in shelf seas. Both the instationarity and the inhomogeneity of depth and current play a significant role in wave-tide interaction so that neither a quasi-stationary nor a quasi-homogeneous approximation to wave-current interactions can be used. Futhermore the above interactions are predominantly caused by currents, rather than surface level variations, in particular for relatively moderate wind and wave conditions.

For the North Sea the tide and surge induced modulations of mean wave parameters are typically 5% ~ 10% and decrease with increasing severity of wind and wave conditions. Tide induced variations of spectral densities can be of the same order of magnitude as the average spectral density over a tidal period.

In the three North Sea cases analyzed, the tide-induced modulations of mean wave parameters (in particular the wave height) were found to be smaller than wind-induced modulations of mean wave parameters.

It is recommended that the effects of wave-tide interactions on wave heights are investigated further, in particular with respect to the effects of relative depth and active wave generation. Furthermore the wind input in wave forecast models needs to be improved; the occurrence of wind speed variations with periods of approximately 12.5 h and smaller and their effects on wind waves should also be investigated in detail.

Acknowledgements

I want to express my gratitude to the Dutch Ministry of Public Works and Transportation (Rijkswaterstaat), in particular R. van Dijk, J. de Ronde, A.J. van der Kerk, and H. Ligtvoet, for supplying the bottom schematization of the North Sea, the tidal boundary conditions for the computation of depth and current fields for the North Sea, and observed wind and wave data.

For supplying the wind fields used in the North Sea hindcasts, I want to express my gratitude to the Royal Netherlands Meteorological Institute (KNMI), in particular H.W. Riepma and E. Bouws.

An operational version of the numerical model DOLPHIN was made available by Digital Hydraulics Holland B.V. The use of this model was greatly appreciated.

I would like to thank my colleagues at the Delft University of Technology, KNMI, Delft Hydraulics and Rijkswaterstaat, and members of the WAM group for their support, suggestions and comments.

In particular I would like to thank all members of the Fluid Mechanics Group of the Faculty of Civil Engineering of the Delft University of Technology for their continuous interest and help, in particular my supervisor Jurjen Battjes for his suggestions and comment and Nico Booij for helping me with the numerics.

Most of all I would like to thank Leo Holthuijsen for his continuous advice, help and good spirits.

REFERENCES

Abbott, M.B., 1979: *Computational Hydraulics*, Pitman, London

Bagnold, R.A., 1946: Motion of waves in shallow water. Interaction between waves and sand bottoms. *Proc. Roy. Soc. London*, A, **187**, 1-15

Barber, N.F., 1949: Behaviour of waves on tidal streams. *Proc. Roy. Soc. London, A*, **198**, 81-93

Battjes, J.A. and J.P.F.M. Janssen, 1978: Energy loss and set-up due to breaking of random waves. Proc. 16th Int. Conf. Coastal Engineering, Hamburg, 569-587

Bouws, E. and G.J. Komen, 1983: On the balance between growth and dissipation in an extreme depth-limited wind-sea in the southern North Sea. *J. Phys. Oceanogr.*, 13 no 9, 1653-1658

Bretherthon, F.P. and C.J.R. Garrett, 1968: Wave trains in inhomogeneous moving media. *Proc. Roy. Soc. London*, A, **302**, 529-554

Bretschneider, C.L., 1973: in *Shore Protection Manual*, U.S. Army CERC, Corps of Engineers, Techn. Rep. no. 4

Brevik, I., 1980: Flume experiment on waves and currents. II. Smooth bed, *Coastal Engineering*, **4**, 89-110

Brevik, I. and B. Aas, 1980: Flume experiment on waves and currents. I. Rippled bed, *Coastal Engineering*, **3**, 149-177

Carlsen, N.A., 1967: Measurements in the turbulent wave boundary layer. Coastal Engng. Lab. and Hydraulic Lab., Techn. Univ. Denmark, Basic Res. - Prog. Rep. no. 14, 2-3. (from: Jonsson, 1978)

Cavaleri, L., L. Bertotti and P. Lionello, 1989: Shallow water application of the third-generation WAM wave model. *J. Geophys. Res.*, **94**, C6, 8111-8124

Charnock, H., 1955: Wind stress on a water surface. *Quart. J. Roy. Meteor. Soc.*, **81**, 639-640

Chen, Y.H. and H. Wang, 1983: Numerical model for nonstationary shallow water wave spectral transformations, *J. Geophys. Res.*, **88 C14**, 9851-9863

Christoffersen, J.B., 1982: *Current depth refraction of dissipative water waves*. Institute of Hydrodynamics and Hydraulic Engineering, Techn. Univ. Denmark, Series paper no. 30

Christoffersen, J.B. and I.G. Jonsson, 1985: Bed friction and dissipation in a combined current and wave motion. *Ocean Engineering*, 12, 5, 387,423

Collins, J.I., 1972: Prediction of shallow water spectra. *J. Geophys. Res.*, **77**, 15, 2693-2707

Dingemans, M.W., M.J.F. Stive, J. Bosma, H.J. de Vriend and J.A. Vogel, 1986: Directional near-shore wave propagation and induced currents. Proc. 20th Int. Conf. Coastal Engineering, Taipei, 1092-1106

Fredsøe, J., 1984: Turbulent boundary layers in wave-current motion. *J. Hydraulic Eng.*, ASCE, **110** (HY8), 1103-1120

Gelci, R., H. Cazalé and J. Vassal, 1956: Utilization des diagrammes de propagation à la prévision énergétique de la houle. *Bulletin d'information du commité central d'océanographie et d'études des côtes*, **8**, 169-197

Gelci, R., H. Cazalé and J. Vassal, 1957: Prévision de la haule. La méthode des densités spectroangulaires. *Bulletin d'information du commité central d'océanographie et d'études des côtes*, **9**, 416-435

Graber, H.C., 1984: *A parametric wind-wave model for arbitrary water depths*. Ph.D. thesis Massachusetts Institute of Technology.
Graber, H.C. and O.S. Madsen, 1988: A finite-depth wind-wave model. Part I: Model description. *J. Geophys. Res.*, **87**, C1, 469-481
Grant, W.D. and O.S. Madsen, 1979: Combined wave and current interaction with a rough bottom, *J. Geophys. Res.*, **84**, C4, 1797-1808
Grant, W.D. and O.S. Madsen, 1982: Movable bed roughness in unsteady oscillatory flow. *J. Geophys. Res.*, **87**, C1, 469-481
Groen, P. and R. Dorrestein, 1976: *Zeegolven*, third edition (in Dutch). Staatsuitgeverij, The Hague
Hasselmann, K., 1960: Grundgleichungen der Seegangsvoraussage. *Schiffstechnik*, **7** heft 39, 191-195
Hasselmann, K., 1961: On the non-linear energy transfer in a wave spectrum. In: *Ocean Wave Spectra*. Prentice-Hall, 191-197
Hasselmann, K., 1962: On the non-linear energy transfer in a gravity wave spectrum. Part 1. General theory. *J. Fluid Mech.* **12** no. 4, 481-500
Hasselmann, K., 1963a: On the non-linear energy transfer in a gravity wave spectrum. Part 2. Conservation theorems, wave-particle correspondence, irreversibility. *J. Fluid Mech.* **15** no. 2, 273-281
Hasselmann, K., 1963b: On the non-linear energy transfer in a gravity wave spectrum. Part 3. Evaluation of the energy flux and swell-sea interaction for a Neuman spectrum. *J. Fluid Mech.* **15** no. 3, 385-398
Hasselmann, K., 1968: Weak-interaction theory of ocean waves. In: *Basic developments in fluid mechanics*, Vol 2, M. Holt (ed.), Academic Press, New York, 117-182
Hasselmann, K., 1974: On the spectral dissipation of ocean waves due to whitecapping. *Bound.-Layer Meteor.*, **6** no 1-2, 107-127
Hasselmann, K., T.P. Barnett, E. Bouws, H. Carlson, D.E. Cartwright K. Enke, J.A. Ewing, H. Gienapp, D.E. Hasselmann, P. Kruseman, A. Meerburg, P. Müller, D.J. Olbers, K. Richter, W. Sell and H. Walden, 1973: Measurements of wind-wave growth and swell decay during the Joint North Sea Wave Project (JONSWAP). *Ergänzungsheft zur Deutschen Hydrographischen Zeitschrift*, **12**
Hasselmann, K. and J.I. Collins, 1968: Spectral dissipation of finite-depth gravity waves due to turbulent bottom friction. *J. Mar. Res.*, **26**, 1, 1-12
Hasselmann, K. and S. Hasselmann, 1985a: Computations and parameterizations of the nonlinear energy transfer in a gravity-wave spectrum. Part I: A new method for efficient computations of the exact nonlinear transfer integral. *J. Phys. Oceanogr.*, **15**, 1369-1377
Hasselmann, K. and S. Hasselmann, 1985b: The wave model EXACT-NL. In: *Ocean wave modelling*, the SWAMP group, Plenum Press, New York and London
Holthuijsen, L.H., 1980: Methoden voor golfvoorspelling part I and II (in Dutch), Technische Adviescommissie voor de Waterkeringen.
Holthuijsen, L.H. and S. de Boer, 1988: Wave forecasting for moving and stationary targets. in *Computer modelling in ocean engineering*, Eds. B.Y. Schrefler and O.C. Zienkiewicz, Balkema, Rotterdam, 231-234
Holthuijsen, L.H., N. Booij and T.H.C Herbers, 1989: A prediction model for stationary, short crested waves in shallow water with ambient currents, *Coastal Engineering*, **13**, 23-54
Janssen, P.A.E.M., 1982: Quasi-linear approximation for the spectrum of wind -generated water waves. *J. Fluid Mech.*, **117**, 493-506

Janssen, P.A.E.M., 1989: Wave-induced stress and the drag of air flow over sea waves, *J. Phys. Oceanogr.*, **19**, 745-754
Janssen, P.A.E.M., P. Lionello, M. Reistad and A. Hollingsworth: Hindcast and data assimlitation studies with the WAM model during the seasat period. *J. Geophys. Res.*, **94**, 973-993
Jeffreys, H., 1925: On the formation of water waves by wind. *Proc. Roy. Soc. London*, A, **107**, 189-206
Jonsson, I.G., 1963: Wave boundary layers. Proc. 10th Congr. IAHR, London, I, 85-92
Jonsson, I.G., 1966a: Wave boundary layers and friction factors. Proc. 10th Int. Conference on Coastal Engineering, Tokyo, Japan, 127-148
Jonsson, I.G., 1966b: The friction factor for a current superimposed on waves. Coastal Engng. Lab. and Hydraulic Lab., Techn. Univ. Denmark, Basic Res. - Prog. Rep. no. 11, 2-12 (from: Brevik, 1980)
Jonsson, I.G., 1978: *A new approach to rough turbulent boundary layers*. Techn. Univ.Denmark, ISVA series paper no. 17
Jonsson, I.G., 1980: A new approach to oscillatory rough turbulent boundary layers. *Ocean Engineering*, **7**, 109-152
Jonsson, I.G. and N.A. Carlsen, 1976: Experimental and theoretical investigations in an oscillatory turbulent boundary layer, *J. Hydraulic Research*. **14**, 45-60
Justesen, P., 1988: Prediction of turbulent oscillatory flow over rough beds. *Coastal Engineering*, **12**, 257-284
Kajiura, K., 1968: A model of the bottom boundary layer in water waves. *Bulletin of the earthquake research institute*, **46**, 75-123
Kamphuis, J.W., 1975: Friction factor under oscillatory waves. *Journal of the Waterways, Ports, Harbours and Coastal Engineering division*, ASCE, **101** WW2, 135-144
Kamphuis, J.W., 1978: Attenuation of gravity waves by bottom friction. *Coastal Engineering*, **2**, 111-118
Kemp P.H. and R.R. Simons, 1982: The interaction of waves and a turbulent current: waves propagating with the current. *J. Fluid Mech.*, **116**, 227-250
Kemp P.H. and R.R. Simons, 1983: The interaction of waves and a turbulent current: waves propagating against the current, *J. Fluid Mech.*, **130**, 73-89
Komen, G.J., S. Hasselmann and K. Hasselmann, 1984: On the existence of a fully developed wind-sea spectrum. *J. Phys. Oceanogr.*, **14**, 1271-1285
Krylov, Yu.M., S.S. Strekalov and V.F. Tsyplukhin, 1976: Wind waves and their influence on structures (in Russian). *Hydrometoizdat*, Leningrad (from: Holthuijsen, 1980)
Kuik, A.J., G.Ph. van Vledder and L.H. Holthuijsen, 1988: A method for the routine analysis of pitch-and-roll buoy wave data. *J. Phys. Oceanogr*, **18**, 1020-1034
LeBlond, P.H. and L.A. Mysak, 1978: *Waves in the Ocean*. Elsevier, Amsterdam
Longuet-Higgins, M.S. and R.W. Stewart, 1960: Changes in the form of short gravity waves on long waves and tidal currents. *J. Fluid Mech.*, **8**, 565-583
Longuet-Higgins, M.S. and R.W. Stewart, 1961: The changes in amplitude of short gravity waves on steady non-uniform currents. *J. Fluid Mech.*, **10**, 529-549
Longuet-Higgins, M.S. and R.W. Stewart, 1962: Radiation stress and mass transport in gravity waves, with application to 'surf-beats'. *J. Fluid Mech.*, **10**, 529-549

Maat N., C. Kraan and W.A. Oost, 1989: The roughness of wind waves, accepted for publication in *Bound.-Layer Meteor.*

Madsen, O.S., Y.-K. Poon and H.C. Graber, 1988a: Spectral wave attenuation by bottom friction: theory. Abstracts book 21st Int. Conf. Coastal Eng., Malaga, 185-186

Madsen, O.S., Y.-K. Poon and H.C. Graber, 1988b: Spectral wave attenuation by bottom friction: theory. Proc. 21st Int. Conf. Coastal Eng., Malaga, 492-504

Madsen, O.S. and M.M. Rosengaus, 1988: Spectral wave attenuation by bottom friction: experiments. Proc. 21st Int. Conf. Coastal Eng., Malaga, 849-857

Mathiesen, M., 1984: Current depth refraction of directional wave spectra. *Proc. Symp. Description and Modelling of Directional Seas,* Denmark, Dan. Hydraul. Inst. and Dan. Maritime Inst., Paper C6

Mei, C.C., 1983: *The applied dynamics of ocean surface waves,* Wiley, New York

Miles, J.W., 1957: On the generation of surface waves by shear flows. *J. Fluid Mech.*, 3 no. 2, 185-204

Miles, J.W., 1959a: On the generation of surface waves by shear flows. Part 2. *J. Fluid Mech.*, **6** no. 4, 568-582

Miles, J.W., 1959b: On the generation of surface waves by shear flows. Part 3. *J. Fluid Mech.*, **6** no. 4, 583-598

Miles, J.W., 1960: On the generation of surface waves by turbulent shear flows. *J. Fluid Mech.*, **7** no. 3, 469-478

Miles, J.W., 1962: On the generation of surface waves by shear flows. Part 4. *J. Fluid Mech.*, **13** no. 3, 443-448

Peregrine, D.H., 1976: Interaction of water waves and currents. *Advances in applied mechanics,* **16**, 9-117

Peregrine, D.H. and I.G. Jonsson, 1983: *Interaction of waves and currents,* Miscellaneous report no. 83-6, CERC, U.S. Army Corps of Engineers

Peters, H.C. and H. Boonstra, 1988: Fatigue loading on a single pile platform due to combined action of waves and currents. Proc. 5th Int. Conf. on the Behaviour of Offshore Structures, 1015-1034

Phillips, O.M., 1957: On the generation of waves by turbulent wind. *J. Fluid Mech.*, **2** no. 5, 417-445

Phillips, O.M., 1960: On the dynamics of unsteady gravity waves of finite amplitude. Part I. *J. Fluid Mech.*, **9**, 193-217

Phillips, O.M., 1966: *The dynamics of the upper ocean,* 1st edition. Cambridge University Press

Phillips, O.M., 1977: *The dynamics of the upper ocean,* 2nd edition. Cambridge University Press

Phillips, O.M., 1985: Spectral and statistical properties of the equilibrium range in wind-generated gravity waves. *J. Fluid Mech.*, **156**, 505-531

Putman, J.A. and J.W. Johnson, 1949: The dissipation of wave energy by bottom friction, EOS Trans. AGU, **30**(1), 67-74

Radder, A.C., 1979: On the parabolic equation method for water-wave propagation. *J. Fluid Mech.*, **95**, 159-176

Sakai, T., M. Koseki and Y. Iwagaki, 1983: Irregular wave refraction due to current, *J. Hydraulic Eng.*, **109**, 1203-1215

Sell, W. and K. Hasselmann, 1974: Computation of non-linear energy transfer for JONSWAP and empirical wind wave spectra. Rep. Inst. Geophys., Univ. Hamburg (from: Hasselmann et al. 1973)

Shemdin, O., K. Hasselmann, S.V. Hsiao and K. Heterich, 1978: Nonlinear and linear bottom interaction effects in shallow water, in : Turbulent fluxes through the sea surface, wave dynamics and prediction. NATO Conf. Ser. V, Vol 1, 347-365

Simons, R.R., A.J. Grass and A. Kyriacou, 1988: The influence of currents on wave attenuation. Proc. 21st Int. Conf. Coastal Engineering, Malaga, 363-376

Skovgaard, O. and I.G. Jonsson, 1976: Current depth refraction using finite elements. Proc. 15th Int. Conf. Coastal Engineering, 721-737

Snyder, R.L., F.W. Dobson , J.A. Elliott and R.B. Long, 1981: Array measurements of atmospheric pressure fluctuations above surface gravity waves. *J. Fluid Mech.*, **102**, 1-59

Sobey, R.J., 1986: Wind-wave prediction. *Annual review fluid mech.*, 18, 149-172

Stijn, Th.L. van, J.C.H. van Eijkeren and N. Praagman, 1987: A comparison of numerical methods for air quality models. KNMI scientific reports WR-87-6

SWAMP group, 1985: *Ocean wave modelling*, Plenum Press, New York and London

SWIM group, 1985: A shallow water intercomparison of three numerical wave prediction models (SWIM). *Quart. J. Roy. Meteor. Soc.*, 111, 1087-1112

Tayfun, M.A., R.A. Dalrymple and C.Y. Yang, 1976: Random wave-current interaction in water of varying depth. *Ocean Engineering*, 3, 403-420

Tolman, H.L., 1988: Propagation of wind waves on tides. Proc. 21st Int. Conf. Coastal Engineering, Malaga, 512-523

Tolman, H.L., 1989: The numerical model WAVEWATCH: a third generation model for the hindcasting of wind waves on tides in shelf seas. *Communications on Hydraulic and Geotechnical Engineering*, Delft Univ. of Techn., ISSN 0169-6548, Rep. no. 89-2

Unna, P.J., 1941: White horses. *Nature*, **148**, 226-227

Unna, P.J., 1942: Waves on tidal streams. *Nature*, **149**, 219-220

Unna, P.J., 1947: Sea waves. *Nature*, **159**, 239-242

Valk, C.F. de and C.J. Calkoen, 1989: Wave data assimilation in a third generation wave prediction model for the North Sea. An optimal control approach. Delft Hydraulics Report H676

Vlugt, A.J.M. van der, 1984: Experiences with the WAVEC-buoy. *Proc. Symp. Description and Modelling of Directional Seas*, Denmark, Dan. Hydraul. Inst. and Dan. Maritime Inst., Paper A3

Voogt, L., 1985: Een getijmodel van de Noordzee gebaseerd op de JONSDAP-1976 meting (in Dutch). Rijkswaterstaat note WWKZ-84G.006

WAMDI group, 1988: The WAM model - a third generation ocean wave prediction model. *J. Phys. Oceanogr.*, 18, 1775-1810

Wang, Z.B., 1989: Mathematical modelling of morphological processes in estuaries, *Communications on Hydraulic and Geotechnical Engineering*, Delft Univ. of Techn., ISSN 0169-6548, Rep. no. 89-1

Weber, S.L., E. Bouws and L.G. de Bruin, 1988: A comparison of bottom dissipation source functions for a severe depth limited storm. KNMI memo OO-88-07

Weber, S.L. 1989: *Surface gravity waves and turbulent bottom friction*. Thesis, Univ. of Utrecht, the Netherlands

Whitham, G.B., 1965: A general approach to linear and non-linear dispersive waves using a Lagrangian. *J. Fluid Mech.*, 22, 273-283

Whitham, G.B., 1974: *Linear and nonlinear waves*, Wiley, New York

Yanenko, N.N., 1971: *The method of fractional steps*. Springer, Berlin

APPENDIX A : WAVE ENERGY DISSIPATION IN THE BOTTOM BOUNDARY LAYER

A.1 INTRODUCTION

Dissipation of wave energy due to wave-bottom interactions can occur due to many mechanisms. A review is given by e.g. Shemdin et al. (1978), who consider percolation, bottom motion (soft mud, vegetation) and bottom friction. For relatively fine sands as found in the North Sea, only bottom friction is important (Shemdin et. al., 1978; Weber et al., 1988).

The available literature on wave energy dissipation due to bottom friction is mainly concentrated on monochromatic waves with or without currents, and to a lesser extent on the spectral description of wave energy dissipation at the bottom boundary layer in cases without currents. In the following monochromatic and irregular waves are discussed separately.

A.2 GENERAL FORMULATION

A.2.1 Bottom shear stress parameterization

Bottom friction is commonly formulated in terms of a quadratic friction law. For pure waves (no current) and a pure current (no waves) the following formulations for bottom friction are often used.

$$\underline{\tau}_w = \tfrac{1}{2}\,\rho\, f_w\, \underline{u}_b |\underline{u}_b| \qquad \text{(A-1)}$$

$$\underline{\tau}_c = \tfrac{1}{2}\,\rho\, f_c\, \underline{U}\, |\underline{U}| \qquad \text{(A-2)}$$

where $\underline{\tau}_w$ is the instantaneous bottom shear stress for waves only, $\underline{\tau}_c$ is the bottom shear stress for current only, f_w and f_c are the corresponding friction factors, $\underline{u}_b$ is the near-bottom orbital velocity in absence of a boundary layer and $\underline{U}$ is the mean current velocity, averaged over depth.

If waves on currents are considered, two different parameterizations of the instantaneous bottom shear stress are frequently used. In the first, the bottom friction vector is related to the velocity due to both the current ($\underline{U}$) and the waves ($\underline{u}_b$, moving frame of reference), using a single friction factor f_{cw}:

$$\underline{\tau} = \tfrac{1}{2} \rho f_{cw} (\underline{U}+\underline{u}_b) |(\underline{U}+\underline{u}_b)| \qquad (A\text{-}3)$$

The friction factor f_{cw} is a function of both wave and current parameters (e.g. Grant and Madsen, 1979). In the second parameterization the instantaneous bottom friction vector consists of a mean friction, determined by the average current velocity, and a fluctuating component, determined by the near-bottom orbital velocity (Christoffersen, 1982) :

$$\underline{\tau} = \tfrac{1}{2} \rho f_c^* \underline{U}|\underline{U}| + \tfrac{1}{2} \rho f_w^* \underline{u}_b|\underline{u}_b| \qquad (A\text{-}4)$$

In this equation f_c^* and f_w^* are friction factors for the mean and the fluctuating motion respectively. Both friction factors incorporate wave and current influences. In the following, the approach leading to the first parameterization for the instantaneous bottom friction will be denoted as the integral approach; the second one will be denoted as the separate approach. Note that $f_c = f_{cw} = f_c^*$ in cases with currents only and that $f_w = f_{cw} = f_w^*$ in cases with waves only.

A.2.2 Energy dissipation

Independent of the parameterizations of the bottom shear stress, the average dissipation of energy E_d (per unit time and unit bed area) of the combined wave-current system is given as (e.g. Kajiura, 1968; Hasselmann and Collins, 1968) :

$$E_d = \langle \underline{\tau} . (\underline{U}+\underline{u}_b) \rangle \qquad (A\text{-}5)$$

where <.> denotes an average over time. In general the total dissipation can be divided in a mean current energy dissipation E_{dc} , and a wave energy dissipation E_{dw} (Christoffersen, 1982) :

$$E_d = E_{dc} + E_{dw} \tag{A-6}$$

$$E_{dw} = \langle \underline{\tau} . \underline{u}_b \rangle \tag{A-7}$$

$$E_{dc} = \langle \underline{\tau} \rangle . \underline{U} \tag{A-8}$$

Whereas the above division of the total energy dissipation in wave and current energy dissipation is generally applicable, expressions for E_{dw} (and E_{dc}) depend on the parameterization of the bottom friction as is shown below. To allow for a comparison with the expressions for a case without currents, such a case is considered first.

For cases without currents the mean wave energy dissipation can be determined directly from equations (A-1) and (A-7) as (Putman and Johnson, 1949) :

$$E_{dw} = \frac{2}{3\pi} \rho f_w u_{bm}^3 \tag{A-9}$$

where u_{bm} is the maximum near-bottom orbital velocity of the waves. This equation was derived assuming that the orbital velocity $\underline{u}_b$ varies sinusoidal in time and that $\underline{u}_b$ and the fluctuating part of the bottom friction $\underline{\tau}$ are in phase. The same assumptions will be used below.

Using a separate approach for waves on currents, the mean wave energy dissipation can be determined directly from equations (A-4) and (A-7) (Christoffersen, 1982) :

$$E_{dw} = \frac{2}{3\pi} \rho f_w^* u_{bm}^3 \tag{A-10}$$

This expression is similar to that for waves only (equation (A-9)), the only difference being the friction factor (f_w^* or f_w). Hence all current influences are gathered in the friction factor f_w^* and effects of currents on wave energy dissipation can be assessed simply by comparing the friction factors f_w^* for cases with currents with the friction factor f_w for cases without currents.

In the integral approach the wave energy dissipation E_{dw} is calculated indirectly as $E_{dw} = E_d - E_{dc}$ using equations (A-3) and (A-5) through

(A-8). Following the deduction of Brevik and Aas (1980) and Brevik (1980) the mean wave energy dissipation becomes :

$$E_{dw} = \frac{1}{2} \rho f_{cw} U^3 f(\gamma) \quad , \quad \gamma = U / u_{bm} \qquad \text{(A-11)}$$

where $f(\gamma)$ is a function of γ only, accounting for the time averaging (see e.g. Brevik and Aas, 1980, page 168). Expressions for $f(\gamma)$ depend on the value of γ :

$$\left.\begin{aligned} f(\gamma) &= \frac{4}{3\pi} \gamma^{-3} && \text{for} \quad \gamma = 0 \\ f(\gamma) &= \frac{1}{\pi}\left[\gamma^{-2}\arccos\left[1-2\gamma^2\right] + \tfrac{2}{3}\left[\gamma^{-1}+\gamma^{-3}\right]\left[1-\gamma^2\right]^{\frac{1}{2}}\right] && \text{for} \quad 0 < \gamma < 1 \\ f(\gamma) &= \gamma^{-2} && \text{for} \quad \gamma > 1 \end{aligned}\right\} \qquad \text{(A-12)}$$

For cases without currents (i.e. $\gamma = 0$) equations (A-11) and (A-12) are equivalent to equation (A-9), since $f_{cw} = f_w$ in such cases. In cases with currents effects of currents on the wave energy dissipation arise both explicitly in equation (A-11) through U and $f(\gamma)$ and implicitly through f_{cw}. Using the integral approach, the effects of currents on wave energy dissipation can only be assessed by considering the ratio of E_{dw} of equations (A-11) (integral approach) and (A-9) (waves only), which equals :

$$\frac{\frac{3}{4}\pi \gamma^3 f(\gamma) f_{cw}}{f_w} \qquad \text{(A-13)}$$

In many publications however (e.g. Grant and Madsen, 1979; Simons et al., 1988), only the relation between f_{cw} and f_w is assessed instead of the relation between $\frac{3}{4}\pi \gamma^3 f(\gamma) f_{cw}$ and f_w; this is obviously misleading with respect to the influence of currents on wave energy dissipation. Note that the ratio (A-13) simply equals f_w^*/f_w since equations (A-10) and (A-11) show that

$$f_w^* = \tfrac{3}{4}\pi \gamma^3 f(\gamma) f_{cw} \qquad \text{(A-14)}$$

A.3 FRICTION FACTORS FOR MONOCHROMATIC WAVES

A.3.1 Introduction

Extensive research has been performed on friction factors for monochromatic waves. In the literature, situations with and without currents are considered, both from a theoretical and an experimental point of view. In the following the theory for waves without currents is reviewed first to illustrate the behaviour of f_w as a function of wave conditions. Secondly, available theories for boundary layers and friction factors for monochromatic waves on currents are reviewed briefly. In papers on laboratory experiments for such cases, the friction factor f_{cw} of the integral approach is usually assessed. As shown in the previous section this is misleading with respect to the effects of a current on wave energy dissipation due to bottom friction. Therefore available measurements are re-analyzed to obtain friction factors f_w^* of the separate approach.

A.3.2 Theories for wave bottom boundary layers

The type of flow in a wave bottom boundary layer depends on the bottom amplitude Reynolds number and is rough turbulent for most practical conditions (e.g. Kamphuis 1975, 1978; Jonsson 1966a, 1978, 1980). In the rough turbulent regime the wave friction factor is independent of the Reynolds number and is a function of relative amplitude a_b/k_N only, where a_b is the near-bottom excursion amplitude and k_N is the roughness length scale of the bottom. Many theoretical and empirical expressions for the relation between the relative amplitude and the friction factor have been presented. Reviews of early work are given by Kamphuis (1975, 1978) and Jonsson (1966a, 1978, 1980). Early expressions for friction factors were mainly empirical, or based on time-invariant eddy viscosity models. The most consistent and detailed theory of this type is probably given by Kajiura (1968), who used a time-invariant three layer eddy viscosity model. For the rough beds Kajiura obtained :

$$\frac{1}{4.05\sqrt{f_w}} + \log_{10}\left[\frac{1}{4\sqrt{f_w}}\right] = -0.254 + \log_{10}\left[\frac{a_b}{k_N}\right] \qquad \text{(A-15)}$$

This expression is similar to the semi-empirical expression of Jonsson (1963, 1966a) and Jonsson and Carlsen (1976), which is often used in literature (cf. equation (2-33)) :

$$\frac{1}{4\sqrt{f_w}} + \log_{10}\left[\frac{1}{4\sqrt{f_w}}\right] = -0.08 + \log_{10}\left[\frac{a_b}{k_N}\right] \qquad \text{(A-16)}$$

The above theories are only valid for a_b/k_N larger than approximately 1. If a_b/k_N becomes smaller, the application of a constant value of f_w is suggested by several authors ($f_{w,max}$= 0.30 by Jonsson, 1978; $f_{w,max}$= 0.25 by e.g. Kajiura, 1968 and Grant and Madsen, 1982). The critical value of a_b/k_N is determined from $f_{w,max}$ and the actual expression for $f_w(a_b/k_N)$.

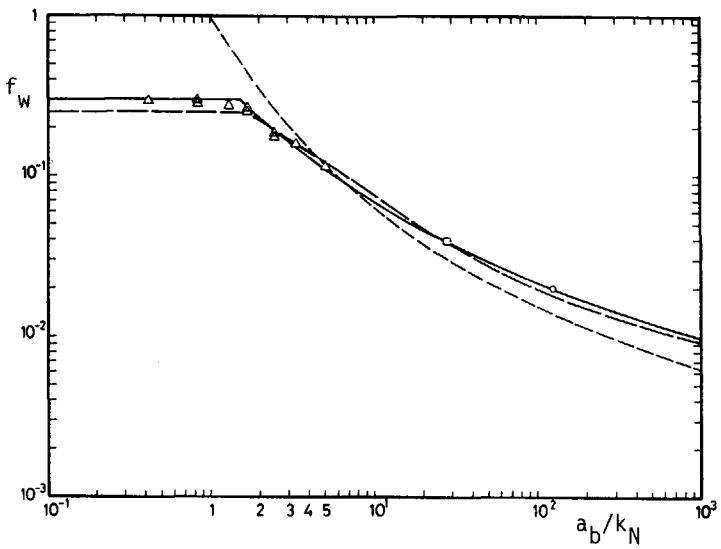

Fig. A-1 Friction factors: —— Jonsson (1963, 1966a) semi empirical, eq. (A-16); – – Kajiura (1968) theoretical, eq. (A-15); --- Kamphuis (1975, empirical); △, Bagnold (1946); ○, Jonsson (1963, test no. 1); □, Carlsen (1967, test no. 2). (Source: Jonsson, 1980)

To illustrate the behaviour of f_w and to illustrate differences between some well known expressions and measurements, f_w is presented in figure A-1 as a function of a_b/k_N (source : Jonsson, 1980). This figure shows a good agreement between calculated and measured values, both with respect to the application of a maximum value of f_w and with respect to equation (A-16). More recent measurements (Kamphuis, 1975; Kemp and Simons, 1982, 1983) show somewhat smaller friction factors, closer to equation (A-15) of Kajiura.

In spite of the close relation between measured and computed friction factors, the physics of the wave bottom boundary layer are still not completely understood. Recently more sophisticated models have been proposed including time varying eddy viscosity models (e.g. Fredsøe, 1984; Justesen, 1988). Such models, however, lead to qualitatively similar relations between f_w and a_b/k_N, as is shown by e.g. Justesen (1988), his figure 4 (not presented here).

Since reasonably accurate expressions for the wave friction factor f_w are available, the major problem in obtaining values of friction factors for practical situations is the estimation of the roughness length scale k_N of the bottom, in particular when movable beds such as the sandy bottom of the North Sea are considered. Due to ripple formation the bottom roughness k_N varies dramatically and the friction factor f_w can vary by an order of magnitude or more (Grant and Madsen, 1982; Graber and Madsen, 1988). Since ripple formation is expected to occur in the (southern) North Sea under storm conditions (e.g. Shemdin et al., 1978; Weber et al., 1988, Weber, 1989), the estimation of the bottom roughness has a potentially much larger impact on the calculated friction factors than the selection of the actual expression to calculate f_w from a_b/k_N.

A.3.3 Theories for wave-current bottom boundary layers

Bottom boundary layers, friction factors and energy dissipation for a combined wave-current system have been studied extensively in the last decades. A review of the early publications is given by Peregrine and Jonsson (1983), their section II.6. The most elaborate theories are those of Grant and Madsen (1979) (integral approach), Christoffersen

(1982) and Christoffersen and Jonsson (1985) (separate approach). The above theories are based on time-invariant two layer eddy viscosity models. The two layers represent a highly turbulent wave boundary layer, which is relatively thin compared to the depth, and a less turbulent current boundary layer (entire depth). The above theories use different sets of expressions to describe the eddy viscosity distribution over the depth, resulting in slightly different friction factors. The theories in general result in complicated expressions for wave frictions factors where approximately ten equations have to be solved simultaneously using iterative procedures (expressions not given here).

The behaviour of wave friction factors of such models is illustrated by Christoffersen and Jonsson (1985). A significant increase of the current friction factor f_c^* (equation (A-4)) occurs if waves are superimposed on currents. Furthermore these models show an increase of the wave friction factor f_w^* with increasing relative current velocity γ and with increasing relative amplitude a_b/k_N (for following currents).

Besides these rather complex theories, a simple interpolation formula for the wave-current friction factor f_{cw} of the integral approach has been suggested by Jonsson (1966b) :

$$f_{cw} = \frac{f_w + \gamma f_c}{1 + \gamma} \qquad \text{(A-17)}$$

in which f_w is determined ignoring the current using e.g. equation (A-16), and f_c is determined ignoring the waves using e.g. :

$$\sqrt{2/f_c} = \frac{1}{\kappa} \ln \frac{11d}{k_N} \qquad \text{(A-18)}$$

where κ (= 0.4) is the Von Karman constant. Using equations (A-14) and (A-12) the corresponding friction factor f_w^* of the separate approach can be determined.

The above theories have not been validated thoroughly, due to the limited availability of boundary layer data for waves on currents. Furthermore, to the knowledge of the present author, the validity of

the models has been checked using friction factors f_{cw} of the integral approach only. As discussed above, the effects of currents on wave energy dissipation and the validity of expressions for friction factors is more correctly assessed using the friction factor f_w^* of the separate approach. Therefore the available data have been re-analyzed in the following section to obtain friction factors f_w^* of the separate approach.

A.3.4 Measurements of attenuation of waves on currents

Wave friction factors in experiments are usually assessed by considering measured wave height attenuation rates. Several problems occur in such measurements. Usually attenuation rates are small, which makes the relative uncertainty (and therefore the spread) in the results large. This uncertainty is enhanced by the occurrence of reflected waves and by the contribution of the side wall friction to the wave height attenuation. Finally most available measurements consider conditions for which the Reynolds number is in the transition zone from smooth turbulent to rough turbulent flow, which also hampers the interpretation of the results.

Wave friction factors can be derived from the wave height attenuation rates by applying the linear wave theory in a wave energy balance equation assuming a stationary and homogeneous current, as in

$$E_{dw} = \frac{2}{3\pi} \rho f_w^* u_{bm}^3 = - \frac{d}{dx}\left[(c_g+U) \tfrac{1}{8}\rho g H^2\right] \qquad \text{(A-19)}$$

which gives

$$f_w^* = - \tfrac{3}{8}\pi \, g \, (c_g + U) \, u_{bm}^{-3} \, H \, \frac{dH}{dx} \qquad \text{(A-20)}$$

Some authors (e.g. Simons et al. 1988) have calculated values for f_w and f_{cw} using an approach equivalent to the use of equations (A-20), (A-14) and (A-12) and using measured values of H dH/dx and u_{bm}. An other approach (e.g. Brevik, 1980) is to substitute the linear theory expression for u_{bm} in equation (A-20), which after further elaboration results in :

$$f_w^* = 3\pi g \, (c_g + U) \left[\frac{\sinh kd}{\sigma}\right]^3 \frac{d}{dx} H^{-1} \qquad \text{(A-21)}$$

The latter approach is more suitable for use in this study than the former, since the friction factor thus is calculated using a method which is analogous to the way in which wave energy dissipation due to bottom friction is expressed in terms of wave heights in numerical wave models. Therefore observed friction factors as presented below have been calculated using equation (A-21) from observed wave height attenuation rates.

Note that in particular for the data of Simons et al. (1988) (discussed below) the choice of the method has a distinct influence on resulting values for frictions factors, since their (measured) velocities u_{bm} deviate strongly from similar velocities calculated from wave heights using the linear theory.

Measurements of attenuation of waves on currents are presented by Brevik and Aas (1980), Brevik (1980), Kemp and Simons (1982, 1983) and Simons et al. (1988). Of these data the smooth bed results of Brevik and Aas (1980) are not of interest for this study, since smooth beds are not expected to occur in natural shelf sea conditions. All other publications consider friction factors f_{cw} for rough beds. Before the data are re-analyzed, the quality of the available data will be discussed.

Brevik (1980) presents friction factors (f_{cw}) for four cases, including cases with waves propagating with or against the current. Brevik (1980) claims that the errors in the friction factors are less than 10~20 %. However, the large scatter in the observed wave heights (Brevik figure 8) makes the determination of wave height attenuation rates rather arbitrary. Kemp and Simons (1982, 1983) consider three current conditions, with waves on following currents, on opposing currents or without currents (T_a = 1.0 s, H = 40 ~ 60 mm, d = 200 mm). The following current cases show a large scatter in observed wave heights compared to the wave height decay. The opposing current cases show good quality results (see e.g. Kemp and Simons 1983, figure 5). Simons et al. (1988) present data for several cases with waves on following currents (T_a = 0.7 s or 1.0 s, H = 10 ~ 50 mm, d = 300 mm).

The quality of these data for T_a= 0.7 s deteriorates with the increase of the current velocity (see Simons et al. 1988, figure 4). The quality of the data for T_a= 1.0 s cannot be assessed from data presented in the paper. Simons et al. find extremely high wave friction factors (f_w = O(10)) for a small relative amplitude (a_b/k_N = O(0.1)) for cases without currents. Whereas these factors show good agreement with Jonsson's formula (equation (2-33)), they are suspicious since they are far out of the range of applicability of Jonssons formulation as discussed in section A.3.2. and since they are in conflict with previous data of e.g. Bagnold (1946) (see figure A-1).

Considering the above, the re-analysis will be limited to the opposing current cases of Kemp and Simons (1982, 1983) (henceforth denoted as KS), the following current cases of Simons et al. (1988) (henceforth denoted as S88) and all corresponding cases without currents.

Friction factors for the experiments of KS and S88 are (re-)calculated to assess the influence of currents on wave energy dissipation and to assess the quality of theoretical models for the wave-current boundary layer with respect to wave energy dissipation (see section A.3.3). The wave friction factor f_w^* is calculated using equation (A-21) and measured wave heights and attenuation rates as tabulated by KS and S88. Furthermore the wave-current friction factor f_{cw} is (re-)calculated for a comparison with f_w^*, using the above value of f_w^* and equations (A-14) and (A-12).

In figure A-2 friction factors f_{cw} and f_w^* for the experiments of KS and S88 are presented. The behaviour of the friction factor f_{cw} of the integral approach (figure A-2a) suggests a strong influence of currents on wave energy dissipation (as concluded by S88). As discussed above, this friction factor does not incorporate all effects of currents on the local wave energy dissipation, unlike f_w^* of the separate approach. Values of f_w^* as presented in figure A-2b show much smaller influences of currents than f_{cw}. Consequently the effects of the currents on wave energy dissipation are much smaller than suggested by f_{cw} so that the use of f_{cw} is obviously misleading with respect to the influence of currents on wave energy dissipation due to bottom friction.

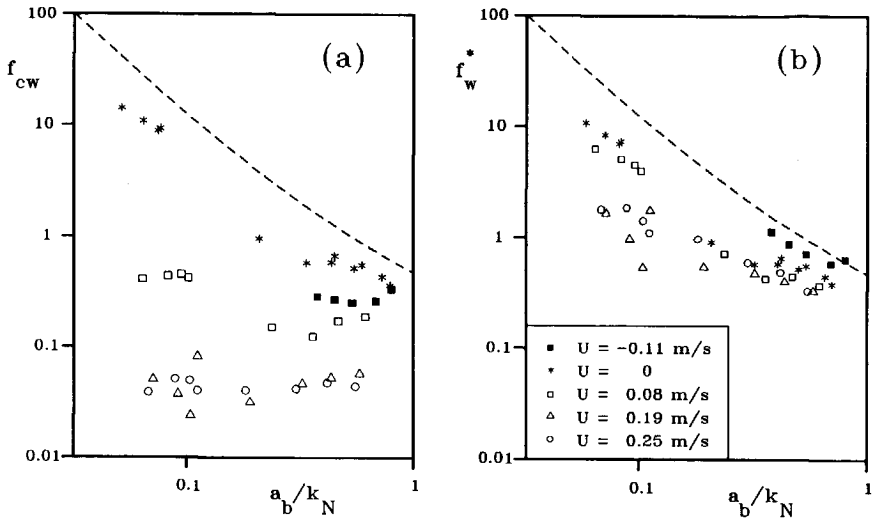

Fig. A-2 Friction factors for (a) the integral approach and (b) the separate approach as recalculated from the data of Kemp and Simons (1982, 1983) and Simons et al. (1988). --- : equation (A-16) without limitation of f_w for small relative amplitudes a_b/k_N.

Compared to the zero-current case, f_w^* is larger for opposing currents and smaller for following currents (see figure A-2b). For the following current cases with $a_b/k_N < 0.12$ the decrease of friction factor seems to become more distinct with increasing current velocity, whereas for the following current cases with $a_b/k_N > 0.12$ such a conclusion cannot be drawn. Note that the attenuation rates for the waves with $a_b/k_N < 0.12$ (i.e. S88 with $T_a = 0.7$ s) and U > 0.08 m/s as well as the corresponding friction factors incorporate a large uncertainty (Simons et al. figure 4), which might explain (part) of the factor of 2 to 4 between the friction factors for U = 0.08 m/s and U > 0.08 m/s ($a_b/k_N < 0.12$).

To assess the quality of theoretical models for wave-current boundary layers with respect to wave energy dissipation, theoretical friction factors have been calculated using two models. The first is the model of Grant and Madsen (1979), reformulated by Christoffersen (1982)

(expressions not given here). This model is fairly representative for two-layer time-invariant eddy viscosity models (see e.g. Christoffersen and Jonsson, 1985); it results in friction factors f_w^*. The second is the simple interpolation formula of Jonsson (1966b) (equation (A-17)), resulting in friction factors f_{cw}. Values for f_{cw} for the first model and f_w^* for the second model are calculated using equations (A-14) and (A-12).

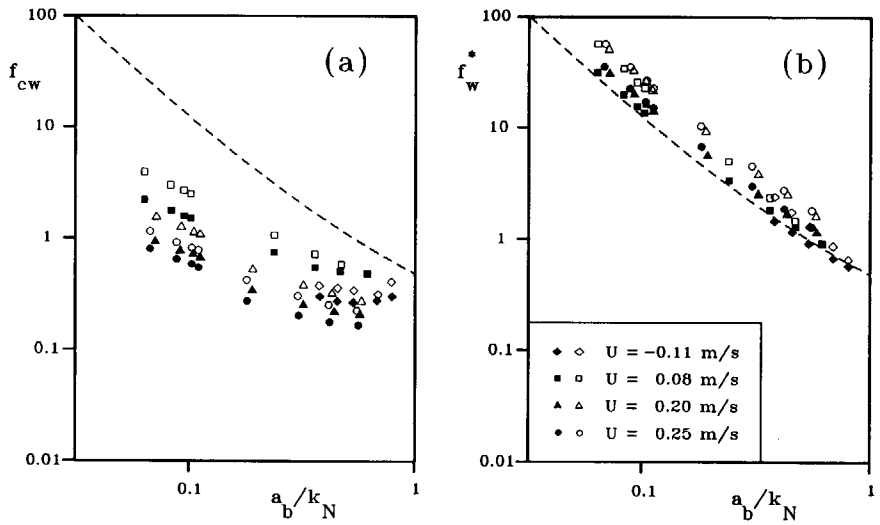

Fig. A-3 Friction factors for the experimental conditions of Kemp and Simons (1982, 1983) and Simons et al. (1988) as predicted by the theories of Grant and Madsen (Christoffersen, 1982; solid symbols) and by Jonsson's interpolation formula (equation (A-17); open symbols). --- : equation (A-16) without limitation of f_w for small relative amplitudes a_b/k_N.

In figure A-3 friction factors for the experimental conditions of KS and S88 as calculated with the above two models are presented (note that this figure contains theoretical results only and not data points). A comparison of panels a and b of this figure again shows the completely different behaviour of f_{cw} and f_w^*. The quality of the models can be assessed by comparing the predicted friction factors

f_w^* of figure A-3b with the observed friction factors of figure A-2b. Figure A-3b shows that both models considered here predict an increase of the friction factor f_w^* compared to the zero-current cases (f_w, dashed line) for following currents and a decrease for opposing currents. The observed friction factors of figure A-2b show exactly the opposite behaviour, so that the models predict current influences on the wave energy dissipation with the wrong trend.

Since the theoretical models mentioned above show a systematically wrong trend of the effects of the currents on wave energy dissipation, better results are obtained by calculating f_w^* according to equation (A-16), which does not contain explicit contributions of the current. Note that this approach does incorporate current influences on E_{dw} since currents affect wavenumbers, wave frequencies and wave heights, and thus influence f_w (through a_b/k_N) and u_{bm}; for this reason it is called "the moving frame approach". The fact that this approach is feasible indicates that the low-intensity turbulence of the mean current has only a small effect on the highly turbulent wave boundary layer.

Considering the above, the moving frame approach seems presently the best approach available (of the models considered here) to describe the observed current influences on wave height attenuation. On the one hand one should be careful with such a (general) conclusion, since it is mainly based on the results of Simons et al. (1988), which are in an extreme range of both a_b/k_N and f_w or f_w^*. On the other hand these data consider severely current dominated conditions ($1 < U/u_{bm} < 20$ for S88). If currents have a small influence on the wave boundary layer in severely current dominated conditions, this can be expected to be even more so for wave dominated conditions. In practical conditions the wave energy dissipation will be important only when the waves are in relatively shallow water, for which situation near-bottom orbital velocities are usually thus large that conditions are not severely current dominated.

A.4 ENERGY DISSIPATION IN SPECTRAL MODELS

A.4.1 Introduction

For cases without currents several spectral energy dissipation formulations are available (see section A.4.2). For cases with currents practically no such formulations are available. For such cases experience with monochromatic waves can be used to extend formulations for cases without currents to cases with currents (section A.4.3). To the knowledge of the author no laboratory data or accurate field data of wave energy dissipation for cases with irregular waves on currents are available.

In all formulations available the spectral source term for the wave energy dissipation due to bottom friction is based on the spectral density of the near-bottom velocity, which is linearly related to the spectral density of the surface elevation, with a proportionality factor given by $(\sigma/\sinh kd)^2$. This factor can be represented in many equivalent ways, since :

$$\frac{\sigma^2}{g^2 \sinh^2 kd} = \frac{k^2}{\sigma^2 \cosh^2 kd} = \frac{2k}{g \sinh 2kd} = \frac{2}{gd}\left[n - \frac{1}{2}\right]$$

The first three expressions are often used in the literature. The fourth expression is a logical extension of the third; it is elegant as it directly shows the effects of both the depth d and the relative depth through n. To simplify an intercomparison of different formulations for the bottom friction source terms, all expressions from the literature as presented below have been reformulated in terms of the rightmost term of the above equality.

A.4.2 Waves without currents

The most simple approach available to describe the spectral wave energy dissipation due to bottom friction is based on the results of the JONSWAP experiment (Hasselmann et al., 1973). In this approach a

linear relation between the variance density spectrum and the dissipation source function is assumed. The expression is closed using a constant Γ, which has the dimension of L^2T^{-3}, e.g. :

$$S_b(\underline{k}) = \frac{2\Gamma}{gd}\left[n - \frac{1}{2}\right] F(\underline{k}) \qquad \text{(A-22)}$$

Using the results of the JONSWAP experiment $\Gamma = -0.038\ m^2s^{-3}$ was found (Hasselmann et. al, 1973, swell), whereas numerical experiments of Bouws and Komen (1983) resulted in $\Gamma = -0.067\ m^2s^{-3}$ (wind seas).

Using a rigorous theoretical treatment, Hasselmann and Collins (1968) derived a quasi-linear spectral expression for the spectral dissipation of the following form (c_w of original paper replaced by $f_w/2$, following the definition of the friction factor as used in this appendix) :

$$S_b(\underline{k}) = -\ f_w\ \frac{1}{d}\left[n - \frac{1}{2}\right] u_{b,s}\ F(\underline{k}) \qquad \text{(A-23)}$$

where $u_{b,s}$ is a measure for the near-bottom orbital velocity and f_w is a friction factor assumed representative for the entire spectrum. Hasselmann and Collins suggest the use of a single universal friction factor for all wave conditions. Since $u_{b,s}$ is related to the entire spectrum of near-bottom velocities, this dissipation is not linear in wave energy. For the near-bottom velocity $u_{b,s}$ several formulations have been suggested. In the original paper a tensor-type expression was given, which results in a velocity which varies with the direction θ (Hasselmann and Collins, 1968, reformulated by e.g. Collins, 1972, and Graber, 1984). More simple approaches using a single representative near-bottom velocity for all directions were suggested by Collins (1972) and Graber (1984). (Notice that Collins' equation (13) is incorrect (see Graber), as is his equation (11), in which a Jacobean transformation was incorrectly used.)

A formulation similar to the one of Hasselmann and Collins (1968) is derived by Madsen et al. (1988a, 1988b) :

$$S_b(\underline{\iota}) = - \frac{8}{3\pi} f_w \frac{1}{d} \left[n - \frac{1}{2} \right] u_{b,r} F(\underline{\iota}) \qquad (A\text{-}24)$$

with

$$u_{b,r}^2 = 2 \iint \frac{\sigma^2}{\sinh^2 kd} F(\underline{\iota}) \, d\underline{\iota}$$

where the different symbols are defined as in equation (2-32). This equation differs from equation (A-23) of Hasselmann and Collins in the way the friction factor f_w and the representative near velocities ($u_{b,s}$ and $u_{b,r}$ respectively) are determined. Unlike proposed by Hasselmann and Collins, the friction factor f_w varies dynamically with the wave conditions, using the following form of equation (A-16) for irregular waves :

$$\frac{1}{4\sqrt{f_w}} + \log_{10}\left[\frac{1}{4\sqrt{f_w}} \right] = m_f + \log_{10}\left[\frac{a_{b,r}}{k_N} \right] \qquad (A\text{-}25)$$

with

$$a_{b,r}^2 = 2 \iint \frac{1}{\sinh^2 kd} F(\underline{\iota}) \, d\underline{\iota}$$

With the inclusion of the constant $8/3\pi$, equation (A-24) degenerates to the energy dissipation formulation for monochromatic waves (equation (A-9)) if only one spectral component is considered. In Madsen et al. (1988b) the constant $8/3\pi$ is replaced by the constant 1.

Recently Weber (1989) developed an eddy viscosity model for the description of the bottom friction source term. The model results in a directionally dependent representative friction velocity, which is comparable to the representative near-bottom velocity as originally derived by Hasselmann and Collins (1968), and in energy losses at the boundary layer. A dynamically adjusted friction factor (e.g. equation (2-33)) can be interpreted as a parameterization of such an eddy viscosity model. Consequently Weber's model can be interpreted qualitatively as a mixed form of the original Hasselmann and Collins model and the model of Madsen et al.. Since the use of friction factors makes a comparison with data more straightforward than the use of an eddy viscosity model, Weber's model is not considered in the comparison.

Of the three remaining approaches, the JONSWAP approach is not further considered here since a single constant in this model cannot be used to describe energy losses for both swell and wind seas (see above), and since nonlinear models show qualitatively better results when applied in the WAM model (Cavaleri et al., 1989).

The two remaining theories are similar with respect to the higher order relation between dissipation and spectral density and with respect to the use of a single friction factor for the entire spectrum (the applicability of a constant friction factor for the entire spectrum has recently been verified by Madsen and Rosengaus, 1988). There are two basic differences in the formulations; the estimation of the representative near-bottom velocity and the treatment of the friction factor f_w. The differences are discussed below.

The directional variation of the representative near-bottom velocity as proposed by Hasselmann and Collins (1968) has only a second order effect on the total energy dissipation compared to a situation with a constant velocity. Since it is furthermore rather sophisticated compared to the representation of the effects of e.g. surface breaking on wave energy dissipation, such a complex approach does not seem to justify the (numerical) effort invested.

Unlike the choice of the representative near bottom velocity, the use of friction factor which is dynamically adjusted to the local wave conditions (through a_b) has a direct impact on the total energy dissipation. Furthermore the use of a single friction factor independent of the local wave conditions is strange in view of the experience with friction factors for monochromatic waves. Recent research with spectral wave models for practical North Sea conditions (Weber, 1989) indicates that a constant friction factor cannot describe the differences in energy dissipation between swell and wind waves. Consequently a dynamically adjusted friction factor seems preferable.

A.4.3 Waves on currents

No specific theory for friction factors of irregular waves on currents is known to the author except for Hasselmann and Collins (1968) and an application of this theory by Hasselmann et al. (1973). In the first paper an effectively integral approach is used. However, the total energy dissipation as assessed by such an approach is not corrected

for the mean current energy dissipation to obtain the wave energy dissipation (e.g. equation (A-5)). Therefore the expression derived is applicable in cases without currents only.

Applying a separate approach to the bottom friction for irregular waves on currents, the expressions for spectral energy dissipation in cases with or without currents become identical. As in the spectral approach without currents, it seems logical to estimate a single wave friction factor for the entire spectrum. Considering the re-analysis of the available data for monochromatic waves on currents, a moving frame approach probably describes the effects of currents best.

A.5 DISCUSSION AND CONCLUSIONS

The review of available literature as presented in this appendix shows that wave energy dissipation due to bottom friction is extensively investigated, but still poorly understood, in particular when waves on currents are considered. For monochromatic waves without currents the theory is fairly well established. For irregular waves without currents, a spectral description of the energy dissipation with a single friction factor for the entire spectrum seems applicable, although there is little experimental verification for the application of a single wave friction factor for the entire spectrum.

For cases with waves on currents, theory shows that a separate approach with separate contributions to the bottom shear stress and the energy dissipation due to the current and waves respectively is preferable to an integral approach with a single term for both. Formulations for wave energy dissipation according to the separate approach allow a direct assessment of current influences on wave energy dissipation, in contrast to the integral approach. Furthermore assessing the combined wave-current friction factor f_{cw} of the integral approach is misleading with respect to the suggested effects of currents on wave energy dissipation.

Theories and (laboratory) measurements for waves on currents are available for monochromatic waves on (homogeneous and stationary)

currents only. A re-analysis of the available data shows that current-induced variations of wave energy dissipation at the bottom boundary layer are presently best described by a moving frame approach. In such an approach the friction factor is determined in a frame of reference which moves with the mean current velocity, whereas the effects of the current on the wave boundary layer are neglected (i.e. $f_w^* \approx f_w$).

For irregular waves on currents the model of Madsen et al. (1988a) seems presently the most suitable model, in particular since it describes influences of currents on wave energy dissipation (qualitatively) due to the use of the dynamically adjusted friction factor.

As stated in the first paragraph of this section much research on the effects of currents on wave energy dissipation at the bottom boundary layer remains to be done. The present conclusions with respect to the moving frame approach need to be verified further, since the measurements used to come to these conclusions are in an extreme range of a_b/k_N and f_w. Furthermore the present theories do not describe these data correctly, which should be investigated theoretically. Finally a major problem in the estimation of friction factors remains the determination of the bottom roughness length scale. In view of the large impact of the poorly understood process of ripple formation on the bottom roughness and corresponding friction factors, this subject is deemed to deserve the main attention in future research.

APPENDIX B : TESTING AND CALIBRATION OF WAVEWATCH

B.1 INTRODUCTION

In this appendix some results of test and calibration calculations for the numerical wave model WAVEWATCH are presented. The results presented here are a selection of the results as presented by Tolman (1989). They pertain to several propagation and generation tests and to the calibration of the minimum upstream fraction α_{min} and of the bottom roughness length scale k_N. Due to the use of the concepts of the WAM model (WAMDI group, 1988), no calibration of other constants in the source terms is needed (i.e. values of such calibration constants are obtained directly from the WAM model). In this appendix the results of various tests are presented. The features of the model and values for α_{min} and k_N as used in this study are discussed in section 3.4.

In the test cases selected for presentation in this appendix, a distinction is made between tests for wave propagation and generation. Since tests and calibration are closely related, especially where α_{min} is considered, a distinction between test and calibration cases will not be made explicitly.

B.2 PROPAGATION

B.2.1 Introduction

Propagation tests serve two main purposes: (a) to establish the behaviour of (combinations of) numerical schemes and (b) to assess the representation of various physical mechanism by the numerical model for practical numerical and physical conditions.

The first purpose mainly bears upon propagation in the $\underline{x}$ space. In this space the effect of minimum upstream fraction α_{min} has to be established, for which one-dimensional propagation tests suffice. Furthermore two-dimensional propagation in the $\underline{x}$ space has to be

considered for two reasons. First the propagation properties for propagation under an angle with the grid axes has to be established, secondly the behaviour of the boundary point scheme in the $\underline{x}$ space has to be assessed. Propagation in the ω and θ spaces are much more straightforward from a numerical point of view. Tests for propagation in these spaces are presented by Tolman (1989).

The physical mechanisms to be tested are propagation in the $\underline{x}$ space, (depth and current) shoaling, (depth and current) refraction and propagation over instationary depths and currents.

To achieve the above objectives, the following five test cases will be considered here :

- One-dimensional deep water propagation.
- Two-dimensional deep water propagation along a coast.
- Plane beach refraction (depth shoaling and depth refraction).
- Current shoaling in a one-dimensional situation. (Note that current refraction is identical to depth refraction from a numerical point of view.)
- Propagation over a one-dimensional current field which is instationary but homogeneous.

Most of these tests deal with situations which have a direct relation to physical problems, such as plane beach refraction. Tests of a more academic nature (such as tests for all terms in the propagation module separately) are presented by Tolman (1989).

In several tests monochromatic unidirectional waves are considered. In the spectral model such waves are obtained when only one spectral bin is considered, since every spectral bin is described using a single frequency and direction. The total energy E for monochromatic unidirectional waves with frequency ω_1 and direction θ_1 then becomes :

$$E = \rho g \frac{N(\omega_1, \theta_1)}{\sigma} \Delta\omega \, \Delta\theta \qquad \text{(B-1)}$$

Similarly monochromatic short-crested waves and irregular long-crested waves are described by a single discrete frequency ω_1 or a single

discrete direction θ_1 respectively, where the corresponding total energies are calculated as :

$$E = \rho g \, \Delta\omega \, \frac{1}{\sigma} \int N(\omega_1, \theta) \, d\theta \qquad \text{(B-2)}$$

and

$$E = \rho g \, \Delta\theta \int \frac{N(\omega, \theta_1)}{\sigma} \, d\omega \qquad \text{(B-3)}$$

In the one-dimensional propagation tests the spatial coordinate will be denoted as x (without suffix). In such test cases propagation along the x_1 axis was considered.

B.2.2 One-dimensional propagation

In the one-dimensional propagation test monochromatic unidirectional waves with an initial Gaussian energy distribution in space are propagated along the x axis (no currents). Propagation without source terms is considered, and equation (3-7) is replaced by $|\alpha| = \alpha_{min}$, so that $\alpha = 0$ can also be tested (for the propagation tests only; note that the minimum value of $|\alpha|$ as given by equation (3-7) equals 0.1). Since this test is used to establish the effects of α_{min}, several tests have been performed in which the resolution, Courant numbers and α_{min} have been varied. Both a situation with a relatively small and a relatively large initial spread spr_x compared to the mesh size Δx are considered ($spr_x = 2.0 \, \Delta x$ and $7.5 \, \Delta x$ respectively, E given by equation (B-1)). The mean position and spread of the instantaneous energy distribution along the x axis are defined as

$$x_m = m_1 / m_0 \qquad \text{(B-4)}$$

and

$$spr_x = m_2/m_0 - x_m^2 \qquad \text{(B-5)}$$

where

$$m_n = \int x^n \, E \, dx \qquad \text{(B-6)}$$

Results of calculations with relatively high Courant number (0.94) are presented, since the highest values for α are expected to be needed for such conditions (since the ICN scheme shows largest negative action for such conditions). The analytical solution to this problem consists of convection with velocity c_g without changing the spatial shape of the distribution.

Results for various upstream fractions α (= α_{min}) are shown in figure B-1. The total wave energy in the model (i.e. the local total energy (B-1) integrated over space) is very nearly conserved (changes less than 0.1 %), as long as no action crosses the physical boundaries of the numerical model. In table B-1 test results for integrated parameters other than the total action are presented. Presented are the mean x_m and the spread spr_x, both relative to the mesh size Δx.

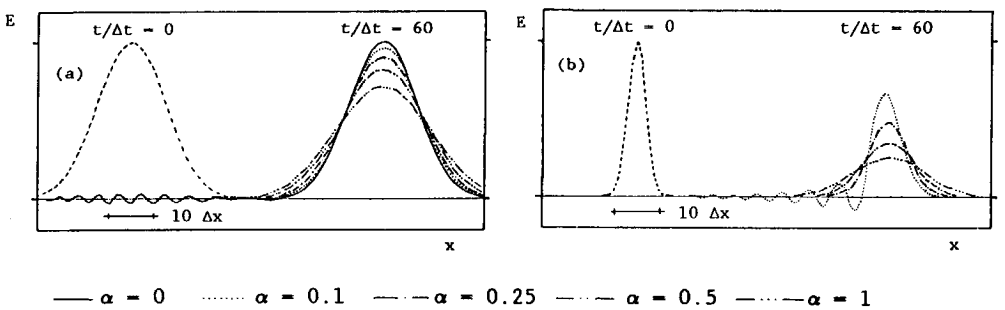

Fig. B-1 One-dimensional deep water propagation without currents for various upstream fractions α (Courant number 0.94). (a) large initial spread (spr_x = 7.5Δx) (b) small initial spread (spr_x = 2.0Δx)

Figure B-1a and the first columns of table B-1 show that only a small upstream fraction (e.g. α = 0.10) is needed to remove the tail of the action density distribution, if the mesh size in the model is small enough to represent the spatial action distribution well. Errors in x_m and spr_x as introduced by such values of α are small. For smaller Courant numbers the ICN scheme with upstream fraction α shows comparable errors in x_m and spr_x, however, less tail forming occurs (test results not presented here).

Table B-1 Results of one-dimensional deep water propagation tests without currents. Courant number 0.94, 60 time steps.

	large initial spread		small initial spread	
α (-)	$x_m/\Delta x$ (-)	$spr_x/\Delta x$ (-)	$x_m/\Delta x$ (-)	$spr_x/\Delta x$ (-)
0.00	77.24	7.36	[1]	[1]
0.10	77.22	7.73	77.21	3.12
0.25	77.20	8.31	77.22	4.25
0.50	77.12	8.92	77.22	5.67
1.00	76.90 [2]	10.09 [2]	77.18	7.71
anal.	77.21 [3]	7.50	77.21 [3]	2.00

[1] Unstable model behaviour
[2] Small part of action distribution has passed through the downstream model boundary
[3] Initially 21.00

In a situation with small initial spread (figure B-1b), right hand side of table B-1) the ICN scheme with $\alpha = 0$ shows unstable behaviour (case $\alpha = 0$ not shown in the figure). A small upstream fraction ($\alpha = 0.05$ to 0.10) is sufficient to stabilize the scheme, but will not remove the tail and negative action. In the case considered here an upstream fraction $\alpha = 0.25$ was needed to remove all negative action, introducing significant diffusion (error in spread) but no significant error in the mean convection velocity (offset x_m).

These results indicate that the smallest value of α as given by equation (3-7) (i.e. $\alpha = 0.10$) suffices to stabilize the numerical scheme and to remove all negative action for increments Δx smaller than approximately $\frac{1}{5} spr_x$. For larger increments Δx, the minimum upstream fraction α_{min} has to be chosen larger than 0.10 (e.g. $\alpha_{min} \approx 0.25$ for $\Delta x \approx \frac{1}{2} spr_x$). Note that negative action occurring due to a (locally) poor resolution will be removed by the conservative elimination algorithm (see figure 4), although this algorithm is meant to eliminate negative action as caused by the numerical scheme for the propagation in the θ space only.

B.2.3 Two-dimensional propagation along a shore

In the test of two-dimensional deep water propagation without currents monochromatic unidirectional waves with an initial two-dimensional Gaussian energy distribution in space are propagated parallel to a coast under an angle with the grid axes. This test is mainly meant to investigate whether the numerical scheme has good propagation properties for propagation under and angle with the grid axes, and whether the scheme for the boundary points in the $\underline{x}$ space behaves satisfactorily. Only a single test case is considered here, for waves propagating under and angle of 45° with the x_1 axis. Mesh sizes in x_1 and x_2 spaces are equal (Δx). Propagation takes place over about 9 meshes in the x_1 and x_2 direction with a Courant number 0.79. A case is considered where the initial spatial spread of the wave energy (equation (B-1)) is relatively large ($spr_x = 5.33\ \Delta x$ in x_1 and x_2 direction, equation (B-5)). To illustrate the behaviour of the ICN scheme itself, an upstream fraction $\alpha = 0$ is used, for which equation (3-7) is replaced by $|\alpha| = \alpha_{min}$ (as in the one-dimensional propagation test). The analytical solution consists of convection without changes in the shape of the spatial distribution of the total action of the waves.

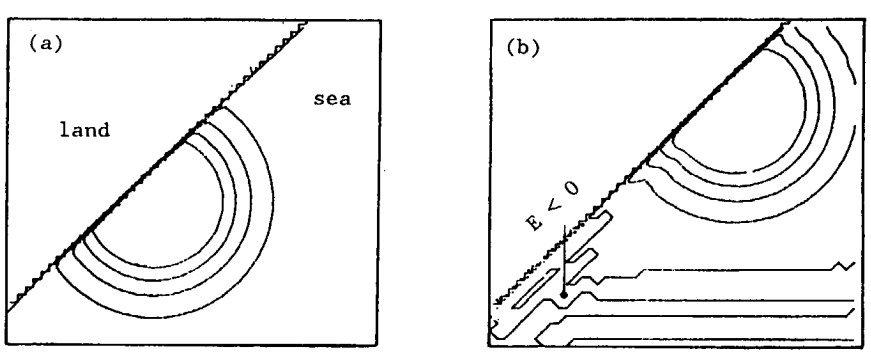

Fig. B-2 Two-dimensional deep water propagation along a coast. Propagation under 45° with the x_1 axis. Courant number 0.79 (two-dimensional). (a) initial distribution of energy (E) (b) situation after 24 time steps. Contours $\frac{1}{8}$, $\frac{1}{4}$ and $\frac{1}{2}$ times E_{max} of initial spatial distribution and at $E = 0$.

The results of the numerical model are shown in figure B-2. The maximum value of the spatial action density distribution changes less than 0.3%. Mean errors in the propagation velocity of the top are less than 5%. Negative action occurs in large areas, but in absolute value it is always smaller than 0.5% of the maximum positive action density. Near the coast some diffusion can be recognized, as expected when using an upstream scheme for boundary points.

B.2.4 Plane beach refraction

The plane beach refraction test is mainly meant to illustrate the numerical representation of refraction and shoaling in practical (numerical and physical) conditions. Therefore a single beach is considered, which has a slope in the x_1 direction only and which is described in the model with increment Δx_1 = 5 km and a depth range from 50 m to 5 m ($\partial d/\partial x_1 = -10^{-3}$). Depth contours are parallel to the x_2 axis. The directional step $\Delta\theta$ = 15°, the time step Δt = 5 min and the upstream fraction α = 0.4. A relatively large upstream fraction is chosen since larger upstream fractions are expected to show worse results of the numerical model than smaller upstream fractions. To represent the relatively narrow directional distribution of swell and the relatively broad directional distribution of wind seas, two cases have been considered (both with a wave period of 10 s). Case I concerns a small spread ($\cos^{12}(\theta-\bar{\theta})$) and strongly oblique incidence ($\bar{\theta}$ = 45°) at the deep water boundary. In case II a situation is considered with a large spread ($\cos^{2}(\theta-\bar{\theta})$) and near-normal incidence ($\bar{\theta}$ = 15°) at the deep water boundary. The mean direction $\bar{\theta}$ is given by equation (4-23), whereas the directional spread spr_θ is given as :

$$spr_\theta = \left[2 - \frac{2}{m_0}\sqrt{a^2+b^2}\right]^{\frac{1}{2}} \qquad \text{(B-7)}$$

where

$$m_0 = \iint F(\omega,\theta)\ d\omega\ d\theta$$

(Kuik et al.,1988; a and b are defined as in equation (4-23), a/m_0 and b/m_0 are the first two Fourier components of the directional distribution).

For the simple geometry of a plane beach, semi-analytical solutions for the action density distribution as a function of the local depth d are available. Considering a situation with a bottom slope in x_1 direction only, the angle as a function of depth is calculated using Snel's[1] law :

$$\frac{\sin \theta}{c} = \text{constant} \qquad \text{(B-8)}$$

where the constant is determined from the (deep water) boundary conditions. Using this analytical solution for the directions, which is a function of the direction at the (deep water) boundary and the local depth, a semi-analytical solution for the directional distribution as a function of depth can be obtained. When the distribution at the deep water boundary is known at intervals $\Delta\theta'$ ($\Delta\theta' \ll \Delta\theta$, grid counter j), the analytical solution can be estimated as :

$$F(\theta_j) = F(\theta_{o,j}) \frac{2\Delta\theta'}{\theta_{j+1} - \theta_{j-1}} \left[\frac{c_{g,o} \cos \theta_{j,o}}{c_g \cos \theta_j} \right] \qquad \text{(B-9)}$$

where the suffix o indicates known parameter values at the deep water boundary.

Results for both cases are shown in figures B-3 and B-4. In case I (small initial spread) the mean direction $\overline{\theta}$ and total energy E as obtained from the numerical model show good agreement with the semi-analytical solutions ($\Delta\theta' = 1°$). The directional spread spr_θ, however, is represented badly. This can be explained by the extremely small directional spread compared to the directional increment $\Delta\theta$ (the spread spr_θ is even smaller than the directional increment $\Delta\theta$). Case II, in which much larger spreads occur, shows good agreements between numerical and analytical results.

---

1. Willebrordus Snel van Royen lived and worked in the low countries (1580-1626). In his scientific publications, he used the Latinized name Snellius. In English literature his Latinized name is generally used in the incorrectly de-latinized form of Snell.

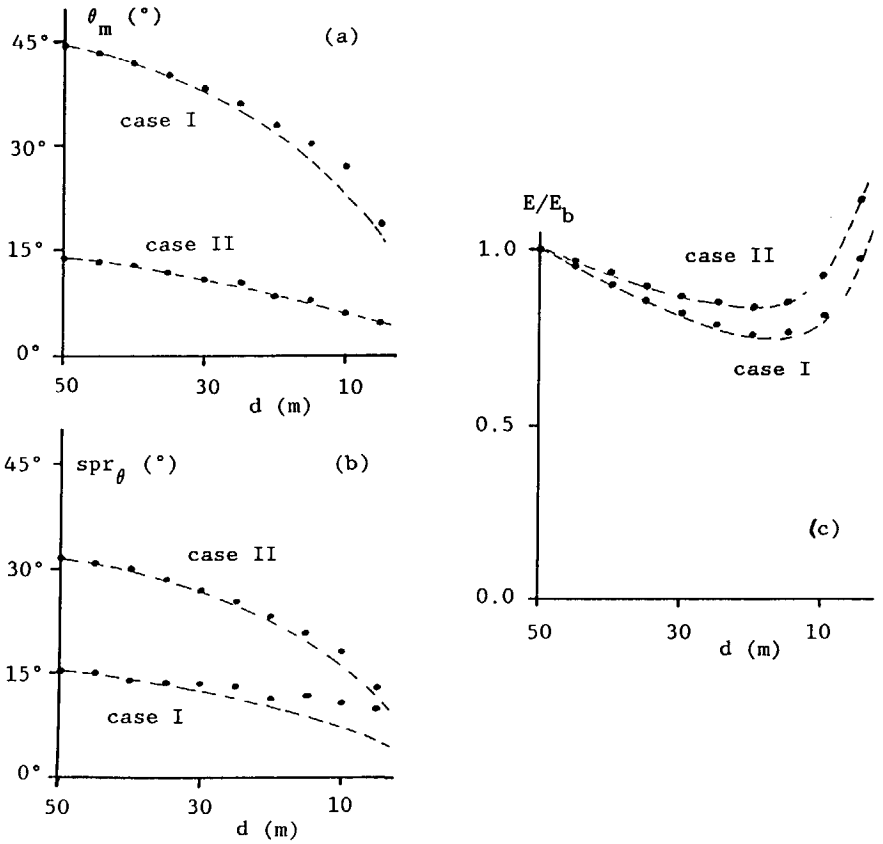

Fig. B-3 Depth refraction on a plane beach, integral parameters. (a) mean direction $\overline{\theta}$, (b) directional spread spr_θ, (c) total energy E, normalized with total energy at the boundary E_b. --- : semi-analytical solution, • : numerical results.

B.2.5 Current shoaling

The current shoaling test is mainly meant to illustrate the numerical representation of current shoaling in practical currents conditions. Therefore only two similar test with either opposing or following currents are considered, where the total situation is one-dimensional. The (absolute) period of the monochromatic waves is 10 s. The current velocity has a constant gradient in the x direction. At the input boundary the current velocity is zero. Cases with both a following and

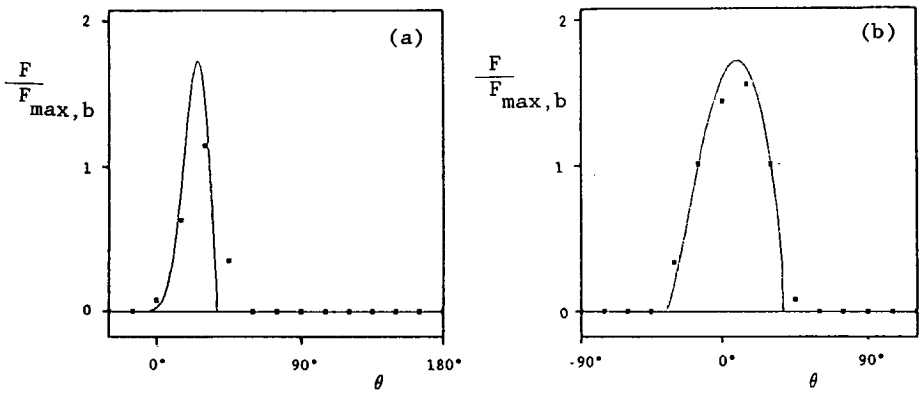

Fig. B-4 Depth refraction on a plane beach, directional distribution at 10 m, (a) case I, (b) case II

an opposing current with velocities up to 3.25 m/s have been considered. The analytical solution for the wave energy in such a case is given as (e.g. Longuet-Higgins and Stewart, 1960; Phillips, 1977) :

$$\frac{E}{E_0} = \frac{c^2}{c(c+2U)} \quad , \quad \frac{c}{c_0} = \frac{1}{2} + \frac{1}{2}\left[1 + 4\frac{U}{c_0}\right]^{\frac{1}{2}} \qquad \text{(B-10)}$$

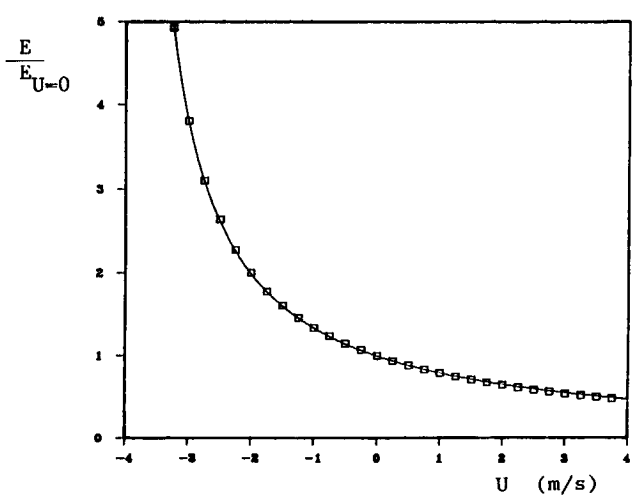

Fig. B-5 One-dimensional current shoaling in deep water, —— : analytical solution, □ : numerical model.

in which U indicates the current velocity and the index o refers to a situation where U = 0. The test results are presented in figure B-5. They show an excellent behaviour of the numerical model.

B.2.6 One-dimensional propagation over a homogeneous instationary current

The test with an instationary current is mainly meant to illustrate the numerical representation of variations of the absolute frequency, for which purpose a single academic situation is considered. In this test irregular waves travel in water of constant depth (both in space and time) over a homogeneous current which varies in time. The total situation is one-dimensional. Waves in extremely shallow water are considered; these are non-dispersive, since the propagation velocity of all spectral components becomes equal to $\sqrt{gd}$. Therefore changes in spectral shape occur due to the instationarity, but not due to dispersion in the x space. In such homogeneous current conditions with homogeneous and stationary depth both the wavenumber k and the relative frequency σ remain constant (equations (2-14) and (2-15)). The total action (of the spectrum) is conserved during propagation since equations (2-19) and (2-17) show that dA/dt = 0. Furthermore the total energy is conserved since there is a zero exchange of energy between waves and currents in homogeneous fields.

A situation is considered with a depth of 1 m and a current velocity which is zero at t = 0 and goes to 1 m/s in 30 h. The change in time of the current velocity is described by the function 1-cos(t/T), where T = 60 h. After 30 h the current velocity remains constant. Initially the action density has a Gaussian distribution in the frequency space with a mean frequency of 0.1 Hz and a spread of 0.07 Hz (equation (B-7)). This results in a poor resolution in the frequency space, which is worse than expected in natural conditions. The total energy (equation (B-3)) has an intial Gaussian distribution in space with $spr_x = 5.0\Delta x$ (equation (B-5)). This results in a good resolution in the x space. The spatial increments are 25 km and the time step is 1.5 h.

Since the energy is conserved during propagation and the waves are non-dispersive, the total energy (equation (B-3)) is convected in the x space without changes in the shape of the distribution in this space. The ability of the numerical model to do so is illustrated in figure B-6, which shows the spatial distribution of the total energy at t = 0 and at t = 30 h ($t/\Delta t = 20$). The agreement between the exact solution and the results of the numerical model is excellent. Also shown in this figure are the results as obtained with the numerical model when $c_\omega = 0$, i.e. when changes of absolute frequency due to the instationary current are neglected. The differences between the results so obtained and the results as obtained with the full numerical model ($c_\omega \neq 0$) show the importance of the change in absolute frequency in situations as considered here.

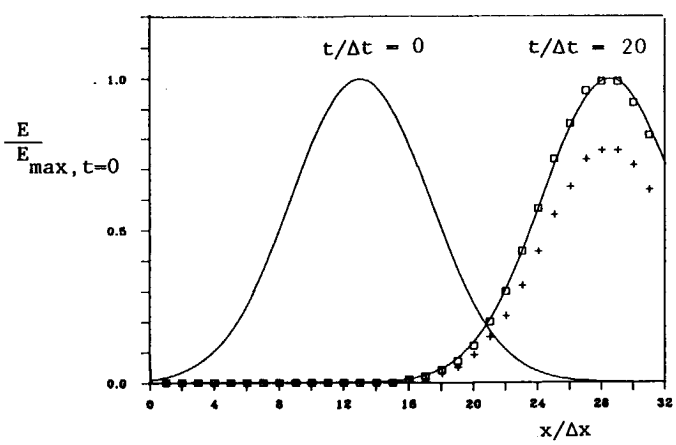

Fig. B-6 Spatial distribution of normalized total energy in the test with a homogeneous and instationary current. —— : analytical solution, □ : numerical model with $c_\omega \neq 0$, + : numerical model with $c_\omega = 0$.

Finally figure B-7 shows normalized frequency spectra as a function of either absolute frequency f_a or relative frequency f_r both for the initial situation at x = 300 km and after 30 h at x = 700 km. Figure B-7a shows a significant change of the shape of the absolute frequency spectra, whereas figure B-7b shows only small variations in the shape of the relative frequency spectrum. Considering the poor resolution in

the frequency space, the numerical results as presented in the latter figure shows a good agreement with the analytical solution (i.e. no change in the shape of $F(f_r)$). For increasing resolution in the frequency space the numerical results show better agreement with the above analytical solution for $F(f_r)$ (results not presented here).

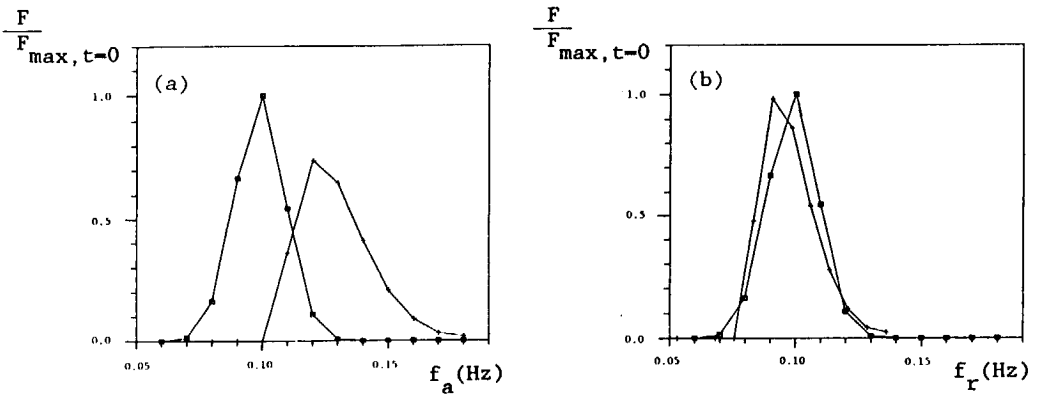

Fig. B-7 Normalized frequency spectra in the test with a homogeneous and instationary current, (a) absolute frequency spectrum, (b) relative frequency spectrum. □ : t = 0, x = 300 km , + : t = 30 h, x = 700 km

B.3 GENERATION

B.3.1 Introduction

Wave generation tests are performed to compare growth characteristics of WAVEWATCH with those of other wave models and data, and to calibrate the bottom roughness length scale k_N in the source term for dissipation due to bottom friction (equations (2-32) and (2-33)). In the intercomparison of wave models and in the comparison of wave models with data, it is common practice to compare growth curves for the non-dimensional energy and the non-dimensional peak frequency for time-limited, fetch-limited and depth-limited situations (e.g. SWAMP group, 1985; SWIM group, 1985)

Time and fetch-limited growth curves are mainly used to illustrate the model behaviour of WAVEWATCH. Time-limited growth curves are

calculated assuming homogeneous conditions (usually deep water). Since the corresponding results of WAVEWATCH are practically identical to those of WAM (Tolman, 1989; deep water), such results will not be presented here. In fetch-limited situations both wave generation and propagation are essential. Fetch-limited growth curves (stationary wind and wave conditions) can be determined for deep water (e.g. SWAMP group, 1985) or for limited water depths (e.g. SWIM group, 1985; uniform water depth). In this appendix only deep-water fetch-limited growth curves are considered, to illustrate the corresponding behaviour of WAVEWATCH (section B.3.2)

Depth-limited growth is assessed here to calibrate the bottom roughness length scale k_N. Depth-limited situation are most economically assessed in homogeneous conditions (i.e. depth and time-limited growth). Such cases are considered in section B.3.3.

B.3.2 Fetch-limited growth curves

Fetch-limited calculations have been performed to compare the fetch-limited growth characteristics of WAVEWATCH with those of other models presented in literature (e.g. SWAMP group, 1985), in particular with the WAM model (WAMDI group, 1988) and with the numerical model EXACT-NL (Hasselmann and Hasselmann, 1985b). To the authors knowledge, WAM and WAVEWATCH are presently the only published third generation models for arbitrary situations. EXACT-NL is a third generation model which uses a much more rigorous treatment of the source functions than WAM or WAVEWATCH. However, it can only be used for calculations in one dimension, i.e. in time for homogeneous conditions or for calculations in a one-dimensional space for stationary conditions. This makes EXACT-NL from a numerical point of view completely different from WAM or WAVEWATCH. It has nevertheless also been incorporated in the following comparison since it uses a third generation approach to the physics.

Following SWAMP test II, a situation is considered with a wind (U_{10} = 20 m/s) blowing perpendicular across a straight coastline over deep water. The non-dimensional energy $\tilde{E}$ (integrated over the spectrum) and the non-dimensional peak frequency $\tilde{f}_p$ are considered as a function of the non-dimensional fetch $\tilde{x}$:

$$\tilde{E} = g^2 \int_0^{2\pi} \int_0^{\infty} F(\omega,\theta)\, d\omega\, d\theta \;/\; U^{*4} \qquad \text{(B-11)}$$

$$\tilde{f}_p = U^* f_p / g \qquad \text{(B-12)}$$

$$\tilde{x} = gx/U^{*2} \qquad \text{(B-13)}$$

where U^* is the wind friction velocity. In the SWAMP study $C_d = [U^*/U_{10}]^2$ is assumed to be a constant ($C_d = 1.83\ 10^{-3}$), whereas C_d in equation (2-24) is a function of the wind speed U_{10}. In the calculations with the numerical model C_d of equation (2-24) is used, whereas $C_d = 1.83\ 10^{-3}$ (SWAMP) is used in the normalization of the non-dimensional parameters.

The discretization of the spectrum and the value of constants used in this test are identical to those used in the North Sea hindcasts (see table 1), except for the spatial increment, which was set to Δx = 24 km. Note that the spectral discretization is identical to that of the WAM model, except for the angular increment (where WAM uses $\Delta\theta = 30°$). Empirical constants in the description of wind input, dissipation due to whitecapping and non-linear interactions are identical to those of the WAM model (values as presented in chapter 2 and section 3.3.3).

Non-dimensional fetch-limited growth curves for $\tilde{E}$ and $\tilde{f}_p$ are shown in figure B-8. The results of WAM, SWAMP (several wave models) and JONSWAP (measurements) as presented in this figure are taken from the WAMDI group (1988), whereas the results of EXACT-NL are taken from the SWAMP group (1985).

The agreement between the non-dimensional energy $\tilde{E}$ of WAM (solid lines) and WAVEWATCH (dashed lines) for small fetches ($\tilde{x} \approx 10^6$) is poor, whereas the agreement for larger fetches ($\tilde{x} \approx 10^7$) is good. The agreement with respect to peak frequency $\tilde{f}_p$ is good for small fetches, but poor for larger fetches. Although some differences between WAM and WAVEWATCH could be expected in view of the different propagation schemes used, differences as large as those presented in figure B-8 are not likely caused by the differences in the propagation scheme only. Further investigations into the differences between WAM and

WAVEWATCH are beyond the scope of this study, but nevertheless interesting.

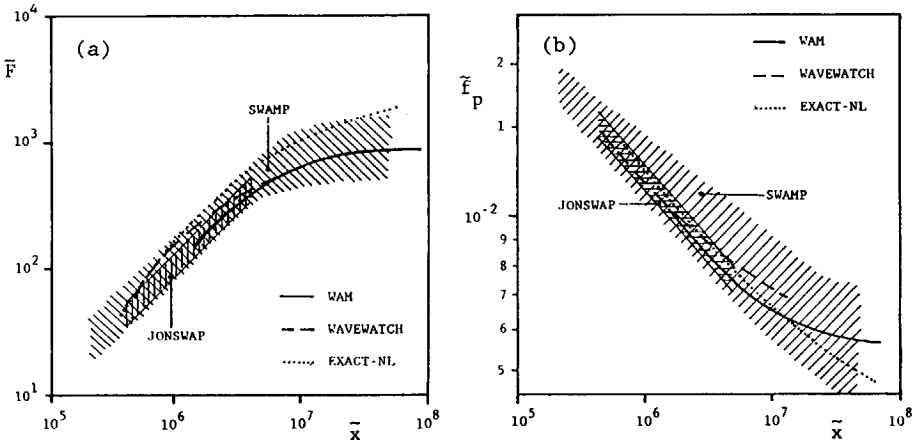

Fig. B-8 (a) Non-dimensional energy $\tilde{E}$ and (b) peak frequency $\tilde{f}_p$ as a function of the non-dimensional fetch $\tilde{x}$ (U_{10} = 20 m/s). Shaded areas represent JONSWAP data and results of the models of the SWAMP study.

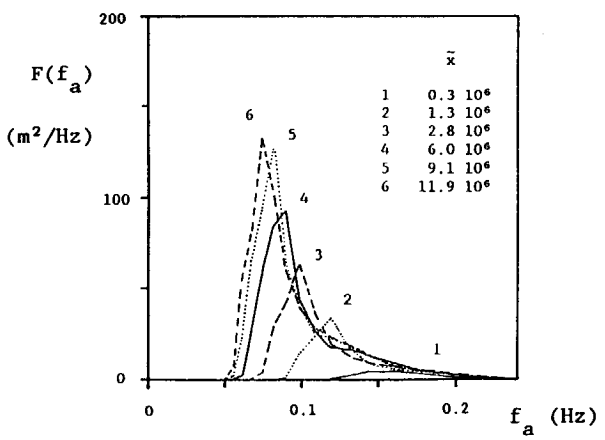

Fig. B-9 Fetch-limited spectra for U_{10} = 20 m/s (WAVEWATCH).

Growth curves for EXACT-NL are also presented in figure B-8 (dotted lines). Compared with EXACT-NL, WAVEWATCH also shows large differences, but the results of WAVEWATCH are in general closer to those of EXACT-NL then the results of WAM. In view of the differences between WAM and EXACT-NL, the results of WAVEWATCH for fetch-limited conditions are acceptable.

Spectra for several non-dimensional fetches are shown in figure B-9. In these spectra an overshoot is present. The overshoot is somewhat larger than that of WAM (WAMDI group, 1988, figure 5), but less pronounced than that of EXACT-NL (SWAMP group, 1985, figure 7.3d).

B.3.3 Depth-limited growth curves

To calibrate the bottom roughness length scale k_N in the bottom dissipation source term (equations (2-32) and (2-33)) a homogeneous situation without currents is considered with wind speed U_{10} = 20 m/s. For several depths d (7.5 m, 15 m, 30 m, 60 m and 120 m) and roughness scales k_N (see figure B-10) the equilibrium wave height H_∞ and wave period T_∞ have been calculated (the suffix ∞ indicating an "infinite" integration time). For a comparison with data in figure B-10, the following dimensionless variable have been defined :

$$\tilde{d} = g\, d \,/\, U_{10}^2 \qquad \text{(B-14)}$$

$$\tilde{H}_\infty = g\, H_\infty \,/\, U_{10}^2 = \frac{4\, g}{U_{10}^2} \left[\int_0^{2\pi} \int_0^{\infty} F_\infty(\omega,\theta)\, d\omega\, d\theta \right]^{\frac{1}{2}} \qquad \text{(B-15)}$$

$$\tilde{T}_\infty = g\, T_\infty \,/\, U_{10} = g \,/\, (f_{p\infty}\, U_{10}) \qquad \text{(B-16)}$$

Also shown in figure B-10 is the envelope of observations reviewed by Holthuijsen (1980). A comparison with Holthuijsen (1980) shows that results for values of k_N of approximately 0.05 m show excellent agreement with several recent analytical expressions for $\tilde{H}_\infty$ and $\tilde{T}_\infty$ as a function of $\tilde{d}$ (e.g. Bretschneider, 1973; Krylov, 1976; Groen en Dorrestein, 1976). As illustration the relation of Krylov (1976) is plotted in figure B-10.

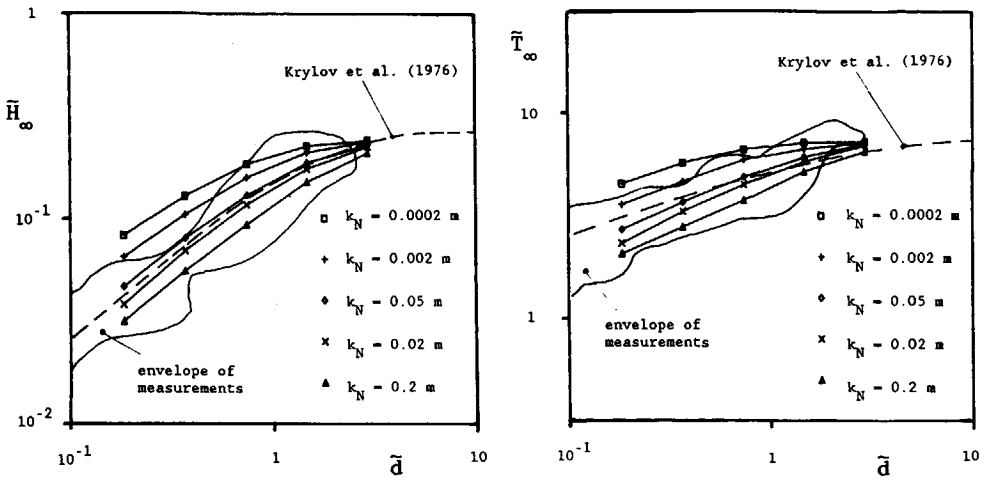

Fig. B-10 Non-dimensional wave height $\tilde{H}_\infty$ and wave period $\tilde{T}_\infty$ as a function of the non-dimensional depth $\tilde{d}$ for different roughness scales. Full curves : WAVEWATCH results for various values of k_N. Envelope of measurements from Holthuijsen (1980).

The test cases with homogeneous shallow water conditions show that the model for energy dissipation due to bottom friction with a constant bottom roughness results in a good agreement between numerical results and measurements (or analytical expressions) for $\tilde{H}_\infty$ and $\tilde{T}_\infty$ if k_N is approximately 0.05 m.

C : SETUP OF MODEL CALCULATIONS

C.1 INTRODUCTION

To perform numerical calculations with WAVEWATCH, a bottom grid, wind fields, depth and current fields and wave boundary conditions at upwind model boundaries are required. Some information on the models for the calculation of depth and current fields, wave boundary conditions and on WAVEWATCH is presented in sections C.2 through C.4. Wind fields are described in section C.5, whereas the overall grid dimensions are discussed in section C.6. Finally section C.7 deals with the start-up times of the separate models.

C.2 DEPTH AND CURRENT

Currents and water levels are calculated using the numerical model DUCHESS, which solves the depth integrated shallow water equations on a plane grid. For the calculations a bottom schematization for the North Sea on an 8 km × 8 km plane grid was obtained from Rijkswaterstaat (figure 13, section 5.1). The grid consists of 134 × 142 grid points in the E-W direction and the N-S direction respectively and is constructed using a Mercator projection. The origin of the map (i.e. the point of the map which touches the earth and in which the N-S axis is parallel to the meridian, grid point (64,80)) is located at 4°E 55°N (see Voogt, 1985).

The model is driven by wind stresses and by water level boundary conditions at the open boundaries derived from tidal constituents. At the northern boundary the deep water components O1, K1, N2, M2, S2 and K2 were applied. At the southern boundary the shallow water components MS4 and M4 were added to the above deep water components. At the Baltic Sea a closed boundary was applied. The bottom friction was modelled using a constant Chezy coefficient C = 65 $m^{0.5}/s$ (cf. Voogt, 1985).

C.3 WAVE BOUNDARY CONDITIONS

Wave boundary conditions were calculated using the numerical ocean wave model DOLPHIN. DOLPHIN is a deep-water spectral wave model for the hindcasting of spectra at selected locations and times using a ray backtracking method (Holthuijsen and De Boer, 1988). The values of calibration constants as used in the calculation of the wave boundary conditions for WAVEWATCH are gathered in table C-1 (i.e. the default settings after the first calibration of DOLPHIN). These calibration constants were determined for DOLPHIN to fit fetch limited growth curves from literature (i.e. SWAMP test II).

Table C-1 Calibration constants of DOLPHIN

growth :	c_1 = 188	dissipation :	c_5 = 250.
	c_2 = 4		
	c_3 = 0.59	limiting form :	c_6 = 0.0023
	c_4 = 0.12		c_7 = -0.223

For the meaning of the constants reference is made to Holthuijsen and de Boer (1988)

C.4 WAVEWATCH

For the North Sea calculations with WAVEWATCH a spectral discretization, grid and time steps as gathered in table 1 (section 3.3) have been used. Values for the minimum upstream fraction α_{min} and the bottom roughness length k_N are selected in section 3.3.2 and are also given in table 1. All calibration constants for the source functions for wind input, nonlinear interaction and wave breaking at the surface (S_{in}, S_{nl} and $S_{ds,s}$ respectively) are taken directly from the WAM model (the WAMDI group, 1988; see chapter 2 and section 3.2.3). A bottom schematization for WAVEWATCH with a mesh size of 24 km × 24 km was obtained from the above grid for the depth and current calculations by simply considering every third point in both grid directions only.

Since WAVEWATCH only incorporates an exponential growth term, no waves will be generated if there is no initial wave energy in the model. Therefore an initial situation, consisting of equilibrium PM spectra with the mean wave direction in the direction of the wind and a $\cos^2$ directional distribution is calculated from the first wind field of the hindcast period.

C.5 INPUT WIND FIELDS

Wind fields (U_{10}) for the cases considered were obtained from KNMI, and consisted of the UK6 wind fields of the fine mesh atmospheric model of the British Meteorological Office (BMO). The wind fields were delivered by KNMI at three-hour intervals on a 1°× 1° spherical grid. Wind fields for 0000 GMT and 1200 GMT are so-called nowcasts, and consist of calculated wind fields, improved with observations, whereas the other wind fields are forecasts calculated starting from the most recent nowcast.

C.6 GRID DIMENSIONS

To minimize calculational efforts the overall dimensions of the spatial grid for WAVEWATCH has been chosen differently for the SW winds (case I) and NW winds (cases II and III).

For the SW winds of case I the grid includes the Channel and the Dover Straits, and has a northern boundary at approximately 57°N (see figure C-1). The Dover Straits are included in the model since some wave energy is expected to enter the North Sea here. The northern North Sea is not included in the model since significant currents mainly occur in the central and southern North Sea and since waves generated in the Northern North sea will not reach the southern North Sea for SW wind conditions. No wave energy is assumed to enter the model through either the western or the northern model boundaries. For SW storms wave energy mainly travels out of the model area at the northern boundary, so that the above assumption is valid there (except for jan. 3 and 4, see e.g. wind directions at AUK, figure 18). At the western

boundary, however, significant wave energy is expected to enter the model area, so that the above assumption is not valid. However, for waves on the southern North Sea, only the wave energy entering through the Dover Straits is of importance. For SW winds such energy is mainly generated in the part of the Channel now included in the model, so that the results in the southern North Sea are not expected to be influenced by the wrong boundary conditions at the western model boundary. Obviously results for the Channel itself will be influenced by the boundary conditions. Note that the poor resolution of the Dover Straits in a 24 km × 24 km grid likely causes larger errors in the southern North Sea than the closed western boundary.

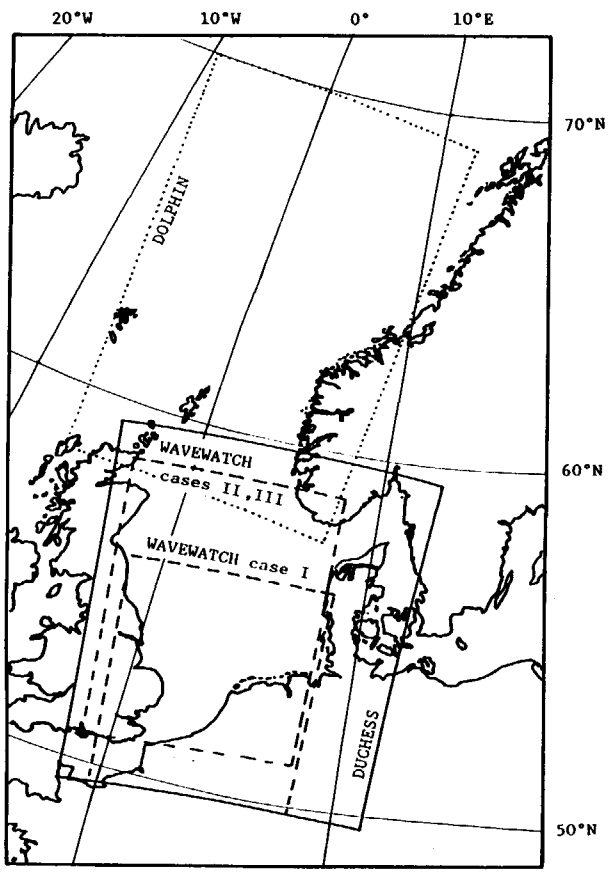

Fig. C-1 Grids sizes for different cases and models

For the NW storm cases a grid was used, ranging from approximately 51°30'N to 58°30'N (see figure C-1). Since waves do not enter the southern North Sea through the Dover Straits for NW wind conditions, this grid does not incorporate the Channel. Furthermore no boundary conditions are calculated for the western boundary. At the northern boundary significant wave energy will enter the model for both NW storm cases considered here (see section 5.2). Therefore the grid for WAVEWATCH incorporates the major part of the Northern North Sea; moreover boundary conditions (two-dimensional variance action spectra) were generated for the northern model boundary using the deep water wave model DOLPHIN (Holthuijsen and De Boer, 1988). The (wind) grid of DOLPHIN, which was defined on a 55.5 km × 111 km grid (Mercator projection) is shown in figure C-1.

C.7 START-UP TIMES

Since all numerical models used in this study start calculations from an arbitrary initial situation, a start-up period is needed to damp start-up effects in the numerical results.

For the depth and current model (DUCHESS), which starts calculation from a situation without currents and a with a horizontal mean water level, a two day start up period is used, cf. Voogt (1985). Hence tidal calculations start two days earlier than the calculations with WAVEWATCH.

The start up times of the wave models depend on wind and wave conditions in the days preceding the hindcast and on the travel time of waves through the area considered. Startup times of the wave models are presented in figures C-2 through C-4 and are discussed below.

For case I SW winds occurred over the (southern) North Sea for several days preceding the hindcast period. Although a severe NW storm blows in the Norwegian Sea near Iceland, no swell from NW directions is observed in the available data for location AUK (data not presented here). In particular for the southern North Sea fetches are small (order of 250 km), which makes a one day start up period for WAVEWATCH sufficient (see figure C-2, DOLPHIN not used here.)

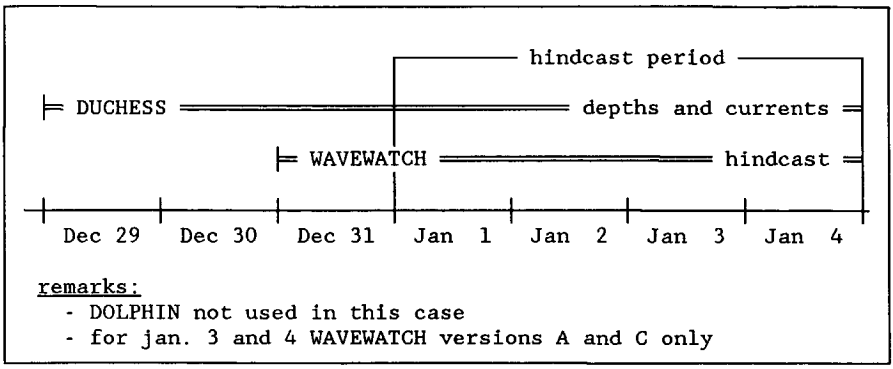

Fig. C-2 Model runs for case I, December 1987 and January 1988

For case II weak SW winds occurred over entire North Sea in the period preceding the actual hindcast. Significant NW winds develop in the Norwegian Sea approximately 1-2 days before the hindcast period. To incorporate all effects of these NW winds in the wave models, calculations with DOLPHIN start two days before the actual hindcast period. The results of DOLPHIN (not presented here) show that significant wave energy starts to enter the North Sea through the northern boundary at approximately 24 h before the actual hindcast, at which time calculations with WAVEWATCH start (see figure C-3).

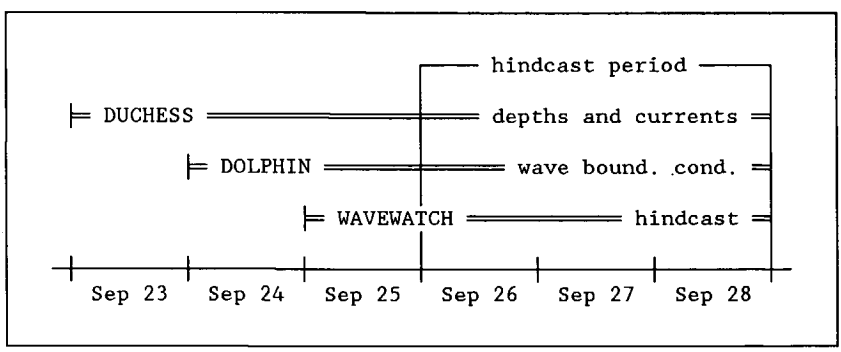

Fig. C-3 Model runs for case II, September 1987

For case III NW winds occurred over the Norwegian Sea and the North Sea for several days prior to the actual hindcast period. To assure

that waves generated in the Norwegian Sea are fully present in the model, a two day start up period for WAVEWATCH is used, whereas calculations of the wave boundary conditions again start one day before the calculations of WAVEWATCH start (see figure C-4).

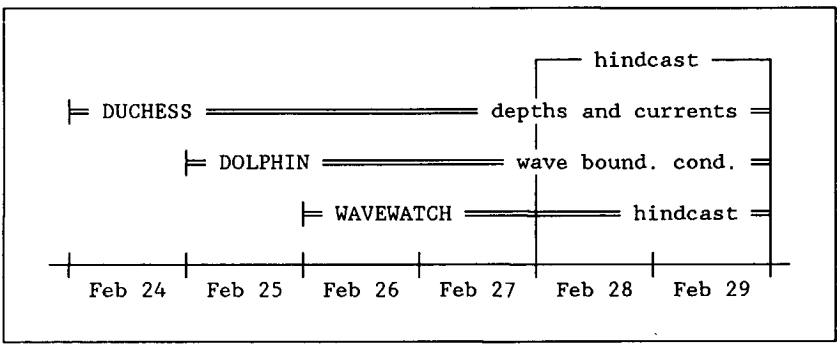

Fig. C-4 Model runs for case III, February 1988

Wind wave propagation in tidal seas

ERRATA

p. 113, lines 4 and 5

"($\Delta T_{a,o}$, solid lines)"	should be	"($\Delta T_{a,o}$, dashed lines)"
"($\Delta T_{a,c}$, dashed lines)"	should be	"($\Delta T_{a,c}$, solid lines)"

p. 122, line 10

"12.5 h and 3 h"	should be	"15 h and 9 h"

P. 125, 2nd line from below

"of 12.5 h and less"	should be	"comparable to those of the tides"